(2)

ESL-TR-89-47

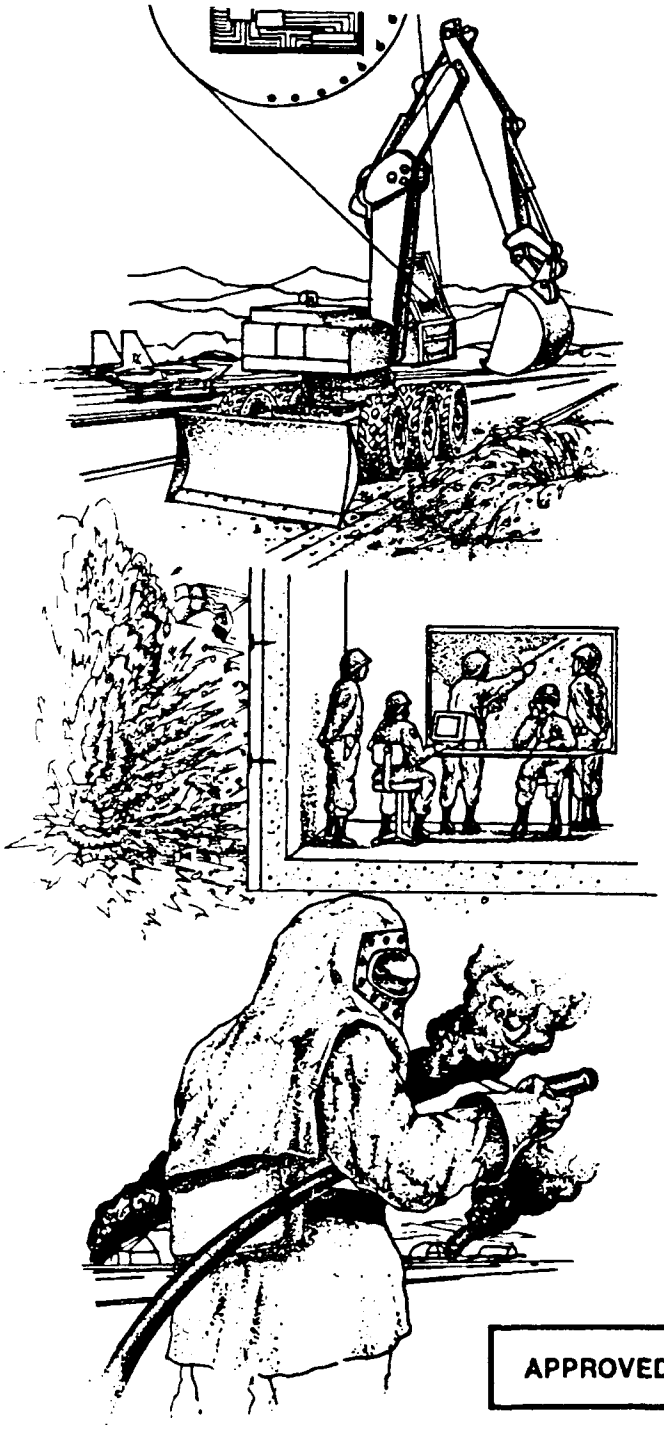

DYNAMIC TESTING OF LATERALLY CONFINED CONCRETE

L.E. MALVERN AND D.A. JENKINS

AEROSPACE ENGINEERING,
MECHANICS AND ENGINEERING
SCIENCE DEPT.
UNIVERSITY OF FLORIDA
GAINESVILLE FL 32611-2031

SEPTEMBER 1990

FINAL REPORT

JULY 1988 — AUGUST 1989

APPROVED FOR PUBLIC RELEASE: DISTRIBUTION UNLIMITED

ENGINEERING RESEARCH DIVISION
Air Force Engineering & Services Center
ENGINEERING & SERVICES LABORATORY
Tyndall Air Force Base, Florida 32403

NOTICE

PLEASE DO NOT REQUEST COPIES OF THIS REPORT FROM HQ AFESC/RD (ENGINEERING AND SERVICES LABORATORY). ADDITIONAL COPIES MAY BE PURCHASED FROM:

NATIONAL TECHNICAL INFORMATION SERVICE
5285 PORT ROYAL ROAD
SPRINGFIELD, VIRGINIA 22161

FEDERAL GOVERNMENT AGENCIES AND THEIR CONTRACTORS REGISTERED WITH DEFENSE TECHNICAL INFORMATION CENTER SHOULD DIRECT REQUESTS FOR COPIES OF THIS REPORT TO:

DEFENSE TECHNICAL INFORMATION CENTER
CAMERON STATION
ALEXANDRIA, VIRGINIA 22314

REPORT DOCUMENTATION PAGE

Form Approved
OMB No 0704-0188

1a REPORT SECURITY CLASSIFICATION: UNCLASSIFIED	1b RESTRICTIVE MARKINGS
2a SECURITY CLASSIFICATION AUTHORITY	3 DISTRIBUTION/AVAILABILITY OF REPORT: Approved for Public Release. Distribution Unlimited
2b DECLASSIFICATION/DOWNGRADING SCHEDULE	
4 PERFORMING ORGANIZATION REPORT NUMBER(S)	5. MONITORING ORGANIZATION REPORT NUMBER(S): ESL-TR-89-47
6a. NAME OF PERFORMING ORGANIZATION: Aerospace Engineering, Mechanics and Engineering Science Dept. / 6b OFFICE SYMBOL (If applicable)	7a. NAME OF MONITORING ORGANIZATION: Headquarters, Air Force Engineering and Services Center
6c. ADDRESS (City, State, and ZIP Code): University of Florida, Gainesville, Florida 32611-2031	7b. ADDRESS (City, State, and ZIP Code): HQ AFESC/RDCM TYNDALL AFB, FL 32403-6001
8a. NAME OF FUNDING/SPONSORING ORGANIZATION: AIR FORCE ENGINEERING & SERVICES CENTER / 8b. OFFICE SYMBOL (If applicable): AFESC	9 PROCUREMENT INSTRUMENT IDENTIFICATION NUMBER: F08635-88-C-0194
8c. ADDRESS (City, State, and ZIP Code): TYNDALL AFB, FL 32403-6001	10 SOURCE OF FUNDING NUMBERS: PROGRAM ELEMENT NO 6.1 / PROJECT NO 0100 / TASK NO 8322 / WORK UNIT ACCESSION NO N/A

11 TITLE (Include Security Classification)
DYNAMIC TESTING OF LATERALLY CONFINED CONCRETE (UNCLASSIFIED)

PERSONAL AUTHOR(S)
MALVERN, LAWRENCE E. and JENKINS, DAVID A.

13a. TYPE OF REPORT	13b. TIME COVERED	14. DATE OF REPORT (Year, Month, Day)	15. PAGE COUNT
	FROM 880701 TO 890831	September 1990	81

16. SUPPLEMENTARY NOTATION

Availability of this report is specified on reverse of front cover.

17. COSATI CODES			18. SUBJECT TERMS (Continue on reverse if necessary and identify by block number)
FIELD	GROUP	SUB-GROUP	CONCRETE, MECHANICAL PROPERTIES, DYNAMIC TESTING, RATE EFFECTS, CONFINEMENT EFFECTS, HOPKINSON BAR

19 ABSTRACT (Continue on reverse if necessary and identify by block number)

For investigating the effects of deformation rate in confined deformation of concrete, a hydraulic pressure cell has been designed and installed on the 3-inch diameter Split-Hopkinson Pressure Bar (SHPB) system at the University of Florida. Plain concrete specimens were tested in axial dynamic compression while subjected to moderate lateral confining pressure. A simple design of a small cell supported by an O-ring near the specimen end of each of the two pressure bars was produced. The specimen is protected by a latex membrane that overlaps the pressure bar ends but does not extend to the O-rings. Water is used as the hydraulic fluid.

The cell was designed for a maximum pressure of 3000 psi (20.7 MPa). It has been used in 21 dynamic axial compression tests at initial lateral confining pressures from 485 to 1500 psi (3.3 to 10.3 MPa) on concrete specimens prepared at the U.S. Army Waterways Experiment Station (WES). (continued overleaf)

DISTRIBUTION/AVAILABILITY OF ABSTRACT: ☐ UNCLASSIFIED/UNLIMITED ☒ SAME AS RPT ☐ DTIC USERS	21 ABSTRACT SECURITY CLASSIFICATION: UNCLASSIFIED
22a NAME OF RESPONSIBLE INDIVIDUAL: Lt. Steven Kuennen	22b TELEPHONE (Include Area Code): (904) 283-6298 / 22c OFFICE SYMBOL: HQ AFESC/RDCM

DD Form 1473, JUN 86 *Previous editions are obsolete.*

BLOCK 19. ABSTRACT (continued)

The lateral pressure is not constant during a test, because of the lateral expansion of the specimen. A small amount of air was trapped in the cell before the water was introduced, so that further compression of the trapped air would accomodate the specimen expansion. The pressure rise was held to less than 50 percent in most of the tests on the WES specimens.

The confined axial dynamic stress-strain responses differ markedly from the unconfined response. The unconfined SHPB tests usually show a peak stress followed by rapid strain-softening; the specimen is usually reduced to many small fragments, and there is no elastic recovery at the end of the SHPB loading time of about 300 micro-seconds. In contrast, all 21 of the confined tests showed an apparent elastic recovery at the end of the loading period, although many of them exhibited extensive cracks and damage after the test. Five of them had been fractured into two pieces by a diagonal crack, and two showed even greater fragmentation. The others were recovered intact but showing crack traces on their surface.

A few of the confined stress-strain curves showed a peak followed by a slowly declining stress, but at the end of the loading period the specimens still carried at least 97 percent of the peak stress. In others the peak is replaced by a plateau or a peak followed by a short dip and then hardening again to the end of the loading period, where the stress was frequently the maximum stress reached during the loading. This second hardening regime may be related to the lateral pressure rise that occured during the test.

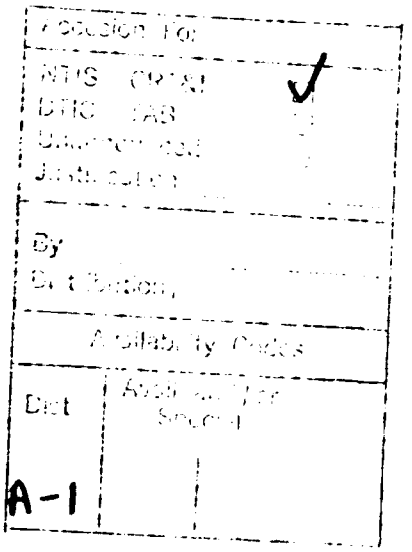

PREFACE

This report was prepared by the Department of Aerospace Engineering, Mechanics, and Engineering Science, University of Florida, Gainesville, Florida, 32611-2031, under Contract No. F08635-88-C-0194, for the Engineering and Services Laboratory, Headquarters, Air Force Engineering and Services Center (HQ AFESC/RDCM), Tyndall AFB, Florida.

This report summarizes the work done between 1 July 1988 and 31 August 1989. The principal investigators at the University of Florida were L. E. Malvern, PhD and D. A. Jenkins, PhD, Department of Aerospace Engineering, Mechanics and Engineering Science, 231 Aerospace Engineering Building, Gainesville, Florida 32611-2031. Capt S. T. Kuennen served as the project officer for HQ AFESC/RDCM.

This report has been reviewed by the Public Affairs Office and is releasable to the National Information Service (NTIS). At NTIS it will be available to the general public, including foreign nationals.

This report has been reviewed and is approved for publication.

STEVEN T. KUENNEN, Capt, USAF
Project Officer

NEIL H. FRAVEL, Lt Col, USAF
Chief, Engineering
Research Division

LOREN M. WOMACK, GM-14
Chief, Air Base Structural
Materials Branch

FRANK P. GALLAGHER III, Col, USAF
Director, Engineering and
Services Laboratory

(The reverse of this page is blank.)

TABLE OF CONTENTS

LIST OF FIGURES

List of Tables

SECTION I

INTRODUCTION

A. OBJECTIVE

The major objective of this investigation was to design and fabricate a hydraulic pressure cell for use in confined compressive testing of concrete in a Split Hopkinson Pressure Bar (SHPB) system and to demonstrate its use. A second objective was to carry out a confined compressive testing program on specimens of one particular type of concrete provided by the sponsor, the Air Force Engineering and Services Center (AFESC), Tyndall, AFB, Florida.

B. SCOPE

A background literature survey was conducted, as reported in Subsection IC. This report presents the results of the investigation and an account of how some problems had to be overcome before the two objectives were attained. For example, when the pressure cell was completely filled with liquid before pressurization, a large pressure rise occurred during the tests, to as much as 5.5 times the initial pressure. The pressure increase was greatly reduced by trapping air in the pressure cell to accommodate the lateral expansion of the deforming specimen.

Section II describes the experimental equipment and procedures. It begins with a brief description of the SHPB system at the University of Florida, followed by two subsections describing the new pressure cell and peripheral equipment, using water as the hydraulic fluid, and the testing technique.

Section III describes the dynamic testing program carried out to meet the second objective and gives some typical test results as well as the results of some multilinear regression analyses that summarize the trends observed in the results. Additional details on the individual tests are given in the appendix.

Conclusions and recommendations are given in Section IV and Section V. The appendix contains five tables of data and 31 figures, including 30 figures which graphically present the results of 30 tests (9 unconfined and 21 confined). All these curves are drawn to the same scale to facilitate visual assessment of the pressure effects.

C. BACKGROUND

1. Early Dynamic Tests not with a Split-Hopkinson Pressure Bar

Early work on rate effects in concrete was reviewed in a 1956 ASTM symposium, Reference 1. At stress loading rates from 1 to 1000 psi (6.895 to 6895 kPa) per second in testing machines, compressive strength was reported to be a logarithmic function of the loading rate with recorded strength increases up to 109 percent of the strength reported at "standard rates", 20 to 50 psi (140 to 345 kPa) per second. By using cushioned impact tests, Watstein (Reference 2) obtained strengths 185 percent of the standard. Watstein also reported rate effects on the measured secant modulus of elasticity, energy absorption (up to 2.2 times the static value), and strain to failure.

Dynamic elastic properties of concrete bar specimens have been studied by Goldsmith and his colleagues (References 3 and 4) by analyzing longitudinal wave propagation induced by impacting the end of a long bar with a steel sphere. Dynamic tensile strengths have been measured in similar longitudinal impacts with small projectiles by Birkimer and Lindemann (Reference 5) and at the University of Florida by Griner et al. (References 6 and 7) and by Sierakowski et al. (Reference 8).

Read and Maiden (Reference 9) surveyed the state of knowledge on the dynamic behavior of concrete at high stress levels in 1971. At the higher stress levels the most extensive experimental data then available were those of Gregson (Reference 10), who used a gas gun to provide flyer plate impacts against thin concrete plates and determine the uniaxial strain response at pressures from 40 to 8,000 ksi.

Watstein's "cushioned impact" tests used a 140-pound (63.6 kg) hammer striking a specimen set in plaster of paris atop a dynamometer mounted on a 3200-pound (1455-kg) anvil (Reference 2). The specimen was capped by a steel plate. Green (Reference 11) and Hughes and Gregory (Reference 12) used a ballistic pendulum with a 25 pound (11.4-kg) hammer having a 1-inch (25.4-mm) diameter face, which impacted one face of a 4-inch (101.6-mm) cube specimen mounted against an anvil. The anvil was also suspended as a pendulum to measure retained kinetic energy. Atchley and Furr (Reference 13) used a drop tester with drop heights up to 20 feet (6.1 meters) and found dynamic strengths up to more than 1.6 times the static strengths. Seabold (Reference 14) represented the rate effects on unconfined compressive strength in concrete up to strain rates of about $5\ s^{-1}$ by an empirical formula containing both a linear term and a logarithmic term in the strain rate.

Hughes and Gregory (Reference 15) have used a drop tester with a 48.2-pound (21.9-kg) hammer falling through a height of up to more than 6 feet (1.82 meters). The specimens were mainly

4-inch (101.6-mm) cubes, although some 4 by 4 by 8 inch (101.6 by 101.6 by 203.2 mm) prisms were tested. Specimens were fitted with metal plates on top and bottom and mounted atop a steel load column fitted with strain gages to record the transmitted force. The load column was not of uniform diameter, and it was too short to avoid reflected waves during the recording, but by using a simple bar-wave theory they estimated transient stresses and concluded that the impact strengths averaged about 1.92 times the static compressive strength. This is comparable to the dynamic strength increases reported by Watstein in 1953. For some of their "strong concretes" dynamic compressive strengths about 260 MPa (37.7 ksi) were found by Hughes and Gregory (Reference 15). Hughes and Watson (Reference 16) used a similar test technique and concluded that the percentage increase in compressive strength in dynamic tests over the static strength was greater for low-strength concrete than for high-strength concrete.

2. Unconfined Tests with the Split-Hopkinson Pressure Bar

The compressive Kolsky bar or Split-Hopkinson Pressure Bar (SHPB), introduced by Kolsky (Reference 17) is widely used for determining material properties in the strain-rate range from about 10^2 to 10^4 s^{-1}; see, e.g., Lindholm (Reference 18), Lindholm and Yeakley (Reference 19), and Nicholas (Reference 20) for examples of its use with metals and details of instrumentation of the system and of elastic wave analyses in the pressure bars. Bertholf and Karnes (Reference 21) made a two-dimensional numerical analysis of the SHPB system and concluded that, with lubricated interfaces, the one-dimensional elastic-plastic analysis was reasonable if limitations are imposed on strain rate and rise time in the input pulse and if specimen length to diameter ratio is about 0.5.

Geotechnical materials and concrete have been investigated with Hopkinson bar systems. Lundberg (Reference 22) investigated energy absorption in dynamic fragmentation of Bohus granite and Solenhofen limestone specimens of 25-mm diameter and 50-mm length in a compressive system at striker bar speeds from 2.5 to 20 m/s. Specimen strain rates were not reported, but general fracture of the specimens occurred when the stress was about 1.8 times the static strength for Bohus granite and about 1.3 times the static strength for Solenhofen limestone.

Bhargava and Rehnström (Reference 23) found unconfined dynamic compressive strengths of 1.46 and 1.67 times the static strength in plain concrete and fiber-reinforced and polymer-modified concrete. Their failure strengths were identified as the maximum amplitude of short-pulse stresses that could be transmitted through the specimen and were more associated with the onset of failure than with complete crushing of the 100-mm diameter by 200-mm length cylinders. Their vertical bar apparatus was 36 meters high, and the 250-mm-long striker bar could be dropped through heights up to 10 meters to impact the 2-meter-long input bar. Their short striker bar gave a loading

pulse duration only about twice the transit time through an elastic specimen.

At the University of Florida, Sierakowski et al.* found dynamic compressive strengths around 26.4 ksi (182 MPa) in 3/4-inch (19.05 mm) diameter SHPB specimens of fine-grained concrete. This was 1.93 times the static compressive strength of 13.7 ksi (94.5 MPa). These specimens had been aged 4 years in laboratory storage in a dry place. They were cut from some of the same bars previously tested by Sierakowski et al. (Reference 8), who had found dynamic strengths around 9.0 ksi (62 MPa) as compared with static strengths of 7.9 ksi (54.5 MPa) for 28-day concrete. The static strengths of the 4-year concrete were measured on small specimens of 3/4-inch (19.04-mm) diameter. A more extensive program by Tang et al. (Reference 24), testing 28-day mortar specimens in the same small-bar system, showed a linear dependence of maximum stress on the strain rate at the maximum stress at rates up to 800 s^{-1}. Malvern et al. (References 25 and 26) described the large SHPB system used for concrete tests in the present investigation and reported some of the results on unconfined high-strength concrete.

Since then, the accuracy of the results obtained with the 3-inch (76.2-mm) diameter SHPB has been improved by correction for the shape changes produced in the elastic pulses in the pressure bars of the system by the elastic wave dispersion in the bars (References 27 and 28). The dispersion correction routine uses a Fast Fourier Transform (FFT) frequency analysis and is programmed in FORTRAN for use on a high-speed personal computer. This gives much faster execution than a Fourier series method previously tried following the methods used by Felice (Reference 29) and by Follansbee and Frantz (Reference 30).

Few other applications of SHPB technology to concrete have been made. Kormeling et al. (Reference 31) adapted it for dynamic tensile tests. They reported dynamic tensile strengths of more than twice the static value at strain rates of approximately 0.75 s^{-1}. A 2-inch (50.8-mm) diameter system at the U.S. Air Force Engineering and Services Laboratory has also been adapted to tensile testing, as well as for compressive testing of concrete and compressive testing of soil confined by steel jackets (Reference 32).

Malvern et al. (Reference 33) have recently reported research in which unconfined SHPB tests of concrete specimens were stopped after various amounts of axial deformation by a loose steel collar slightly longer than the specimens, to permit micrographic examination of various stages of the developing crack configurations.

---

* R. L. Sierakowski, L. E. Malvern and H. Doddington, "Hopkinson Bar Tests of Three-Fourths Inch Diameter Concrete Specimens," University of Florida, Gainesville, Florida (unpublished), 1981.

Ross et al. (Reference 34) have measured dynamic tensile strengths with direct tension specimens in a tensile SHPB and by splitting-tensile tests of a transversely mounted cylinder in a compressive SHPB. They found dynamic strengths (at strain rates of 10 to 100 s^{-1}) around three times the static tensile strength. A numerical inelastic analysis of their splitting-tensile test was reported by Tedesco et al. (Reference 35).

Suaris and Shah (Reference 36) have surveyed mechanical properties of materials subject to impact and rate effects in fiber-reinforced concrete. Many investigators have found significant increases in impact tensile strength in fiber-reinforced concrete over that of plain concrete (Reference 37).

Radial inertia effects in geotechnical materials, which may be mistaken for strain-rate effects, have been discussed by Glenn and Janach (Reference 38). They observed high radial accelerations, which they attributed to dilatancy in their granite specimens, and suggested that the lateral confinement induced by this radial inertia causes the core of the cylinder to be more nearly in a state of uniaxial strain than uniaxial stress. Their tests involved direct impact of the striker against the specimen at such high speeds that failure occurred during the first transit of the wave through the specimen.

Young and Powell (Reference 39) investigated lateral inertia effects in SHPB tests on Solenhofen limestone and Westerly granite. They used embedded wire loops and an externally applied longitudinal magnetic field to measure radial velocities, determine radial accelerations, and calculate radial-stress confinement in tests with loading pulse lengths of 50 microsec in specimens of length 46 to 52 mm. The impact speeds used (29.9 to 61.4 m/s) apparently caused failure during the first passage of the stress wave through the specimen. They concluded that the induced radial stress field can produce a confining pressure sufficient to account for increases of compressive strength observed in SHPB experiments.

Measurements of the surface motion by circumferential strain gages have shown (Reference 26) that the radial inertia confinement at the lower impact speeds in the SHPB tests at the University of Florida was not significant, but that it is significant at higher speeds.

3. Confined Testing

There is an extensive literature on quasistatic confined testing of concrete, which will not be discussed in detail here. D. W. Hobbs (Reference 40) has reviewed various kinds of quasistatic multiaxial tests in his discussion of failure criteria for concrete. These include cube tests where the applied forces are independently controlled in three orthogonal directions (see, for example, Reference 41) and cylinder tests with lateral hydraulic pressure. A common

procedure in the cylinder tests is to increase the axial loading and the lateral pressure together to an initial state of hydrostatic stress, after which the lateral pressure is held constant during the subsequent axial loading in a testing machine (Reference 42).

Dynamic tests of concrete specimens with a controlled lateral confinement, such as those reported in this research, are extremely rare. A few tests have been reported at varying strain rates and confining pressures in a testing machine.

Takeda et al. (Reference 43) have performed triaxial tests on concrete cylinders loaded by compressive and tensile axial loads with axial straining rates of 2×10^{-5} s^{-1}, 2×10^{-2} s^{-1} and 2 s^{-1} after statically applied confining pressure up to 1.5 times the uniaxial compressive strength had been initially imposed. Plots of their results, in the form of octahedral shear stress versus octahedral normal stress, both normalized by dividing by the uniaxial compressive strength at the particular rate of straining, showed no significant differences among the relations at the three rates of strain.

Recently, Yamaguchi and Fujimoto (Reference 44) reported a similar triaxial testing program at axial compressive strain rates of order 10^{-6} to 10^{-1} s^{-1}. For unconfined uniaxial tests over this range of rates the maximum stress was increased by as much as 50 percent. In the triaxial tests, the lateral pressure supplied by the hydraulic pump could not be held constant during the high-rate axial compression but decreased during the test. The result was that the initial parts of the higher-rate axial stress-strain curves increased with strain rate (as did the initial modulus), but at the higher axial strains the increase was smaller and the high-rate curves often fell below the static curve at the same initial lateral pressure, because the lateral pressure was constant in the static test.

Gran et al. (Reference 45) devised a method to study the tensile failure of brittle geologic materials at strain rates from 10 to 20 s^{-1}. A cylindrical rod was loaded in triaxial compression; then the axial load was released rapidly, allowing rarefaction waves to propagate along the rod to interact at the center to form a tensile stress equal in magnitude to the initial static axial compression. They estimated that, for their concrete specimens, at axial strain rates of 10 to 20 s^{-1} the tensile strength with 10 MPa (1450 psi) lateral confining pressure was about 100 percent higher than the unconfined static splitting tensile strength and about 40 percent higher than the unconfined dynamic tensile strengths at the same rates.

Dynamic triaxial tests of high strength concrete were reported by Gran et al. (Reference 46) with both axial and lateral pressures applied by the venting of explosive gases. Their axial compressive strain rates varied from 0.5 to 10 s^{-1} and lateral confining pressures from zero to 124 MPa (18 ksi).

Little rate effect was noted at the lower rates, but at an axial compressive strain rate of 6 s^{-1}, the elastic modulus was about 60 percent higher and the unconfined compressive strength about 100 percent higher than the static values (at 10^{-4} s^{-1}). The triaxial compressive data established an approximate shear failure envelope, for strain rates between 1.3 and 5 s^{-1}, which was 30 to 40 percent higher than that for static loading.

Christensen et al. (Reference 47) used a compressive SHPB system to test nugget sandstone specimens under confining pressures up to 207 MPa (30 ksi). They also used truncated cone striker bars to spread out the rise time of the loading pulse to improve the accuracy and resolution of the initial portion of the stress-strain curves. Although it was only 17 inches (432 mm) long, the high-pressure cell enclosed all of the small SHPB except for the end of the incident bar, which protruded through an end of the cell where it was impacted axially by a striker bar. They concluded that the failure locus of the nugget sandstone at the high axial strain rate (around 500 s^{-1}) was 15 to 20 percent higher than in quasistatic tests for all values of the confining pressure. The main features of the stress-strain response were similar to those seen at low rates. In particular, the phenomenon of dilatancy was not significantly affected by the change from low rates to high rates, contrary to what had been conjectured.

Lindholm et al. (Reference 48) tested specimens of Dresser basalt under confining pressures up to 690 MPa (100 ksi) at strain rates up to 10^3 s^{-1} and considered also temperature. They found unconfined strength variation by a factor of 3 over the range of rate and temperature examined. The dependence of the ultimate strength on rate and temperature indicated that fracture was controlled by a thermal activation process. All the experimental data correlated well with a proposed thermal activation fracture criterion.

Some SHPB tests on concrete specimens passively confined by close-fitting steel or aluminum jackets were performed at the University of Florida (Reference 49). The confining pressure developed by the jacket in constraining the specimen expansion was estimated from strain-gage measurements of hoop strains on the outer wall of the jacket, assuming elastic response of the jacket. The pressure was not controllable, but increased during each test from zero to a maximum of from about 22 MPa (3.2 ksi) to 44 MPa (6.4 ksi) depending on the impact speed of the SHPB striker bar. What was lacking in these jacketed tests was both the ability to control the lateral pressure and to measure it accurately during the tests, which would make it possible to perform a series of tests with deformation rates and lateral confinement pressures independently varied. It was concluded that active confinement in a hydraulic pressure cell would be a step toward achieving that goal. Sections II and III describe the equipment and procedures of such an investigation.

SECTION II

EQUIPMENT

A. SPLIT HOPKINSON PRESSURE BAR

The large SHPB system at the University of Florida consists of two long strain-gaged pressure bars with a short specimen sandwiched between them. Analysis of the observed longitudinal elastic stress waves in the two pressure bars furnishes information about both the force and the displacement versus time at each of the two specimen interfaces. This record is used to determine the average stress and strain in the specimen. This facility, which utilizes 3-inch (76.2-mm) diameter bars, is the only one of its size in the United States. It has been used for unconfined dynamic compressive testing, with strain rates at failure from 5 to 200 per second, of five different kinds of high-strength concrete, prepared at Waterways Experiment Station, Terra-Tek Inc., and SRI International, and also for testing SIFCON (slurry-infiltrated fiber concrete) furnished by the New Mexico Engineering Research Institute for AFWAL.

As currently configured it provides a loading pulse lasting 300 microseconds, imparted by impact of the 30-inch (762 mm) striker bar against the incident pressure bar. The whole system, including gas gun, pressure bars and a shock absorber at the far end, is almost 30 feet (9.15 meters) long.

Figure 1 is a schematic of the pressure bar arrangement, with a Lagrange diagram above it illustrating the elastic wave propagation in the pressure bars. Figure 2 shows an example of the bar strains versus time recorded from the stored signals in a digital oscilloscope. Compressive strain is plotted upward. After the passage of the first incident pulse, there is a dwell time before the arrival of the reflected pulse from the specimen, which is recorded at the same gage station as the incident pulse. Another channel shows the pulse transmitted through the concrete specimen into the transmitter bar. Because the two gage stations are approximately equidistant from the specimen, the transmitted pulse arrives at the transmitter-bar gage station at about the same time as the reflected pulse arrives at the incident-bar station. Also shown are records from two strain gages (axial and hoop) mounted on the specimen.

For purposes of analysis, the pulses are time shifted, so that time zero coincides with the arrival at the first specimen interface, and corrected for wave dispersion in the pressure bars, using a procedure developed for AFESC/RDC, Tyndall AFB, Florida (Reference 27 and 28). The dispersion-correction procedure is similar to that used by Follansbee and Frantz (Reference 30) and Felice (Reference 29), except that it uses a more efficient Fast-Fourier Transform method instead of a Fourier series.

Although the corrected and uncorrected pulses appear similar, the differences in detail, especially for the incident and reflected pulses (which are added algebraically to obtain the pressure bar strain at the first specimen interface) lead to significant differences in the first interface stresses. Figure 3 shows corrected first and second interface stresses in the nominally 3-inch-long (76.2 mm) specimen. Figure 4 shows corrected and uncorrected stress-strain curves for the same specimen. The dispersion correction leads to much closer agreement of the two interface stresses, an approximate equilibrium of the two stresses before they have reached half the maximum stress in this case. The dispersion correction has also eliminated the oscillations previously reported in the first-interface stress-time recording in these tests of high-strength concrete with specimens of the same diameter as the pressure bars.

B. PRESSURE CELL DESIGN AND FABRICATION

The pressure cell used in this study is shown in Figures 5, 6 and 7, and a detailed shop drawing is provided in the appendix, Figure A-1. The main chamber and end caps are made of 17-4 PH stainless steel and have been left in condition "A." The chamber is designed for a maximum operating pressure of 3000 psi (20.7 MPa) with a safety factor of 10. The pressure cell is sealed at each end by rubber O-rings which are compressed between the chamber and the 3-inch SHPB bars by the two-piece end caps (Figure 7). The inner piece of each end cap is keyed by two steel dowel pins to prevent rotation during tightening, which is accomplished by using two specially made spanner wrenches. A latex membrane covers the specimen and a short length of each bar to allow the specimen and specimen interfaces to remain dry. The chamber is provided with four access ports spaced around the central region. One is used for the pressurized water inlet, one for an air bleed, one for the pressure transducer, and one is left blank.

Several peripheral systems are also required. An axial preload must be applied to the specimen to hold it in place and to prevent the latex membrane from being forced into the bar/specimen interfaces during pressurization. To this end, the loading device shown in Figure 8 was constructed. Axial force is applied to the transmitter bar through a shear pin by a simple jackscrew mechanism (a modified drill press vise). The shear pin, made of cylindrical phenolic stock, is designed to break away at a low axial load early in the test and cause no further interference with the motion of the transmitter bar. The magnitude of the axial force initially applied is measured by an instrumented aluminum yoke which is connected to a dedicated conditioner and digital readout unit.

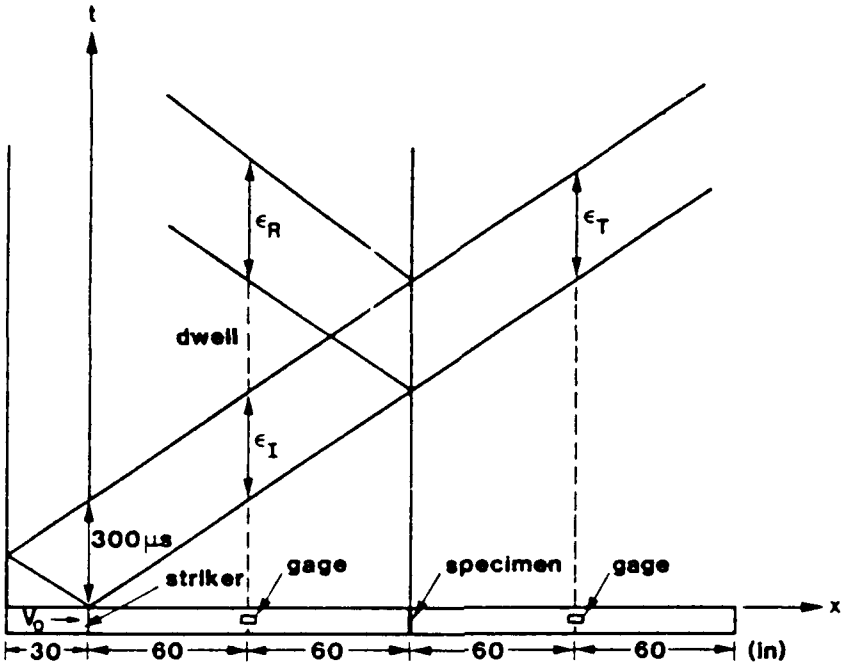

Figure 1. Schematic of SHPB Bars and Lagrange Diagram

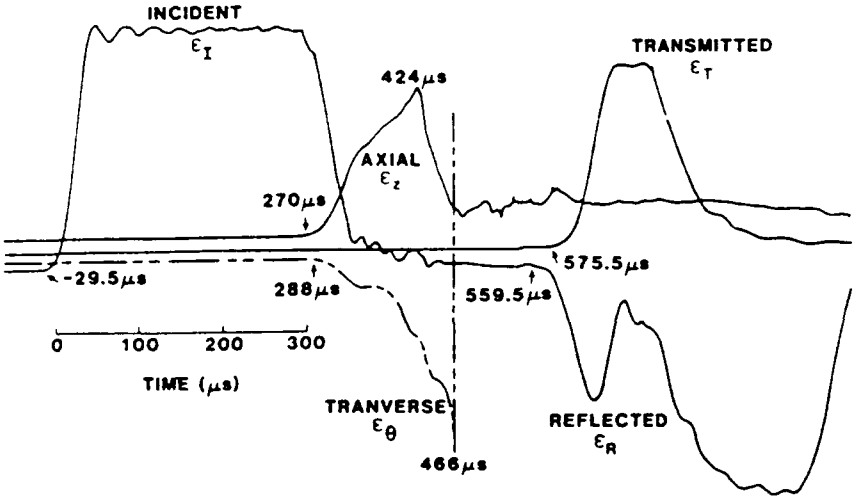

Figure 2. Strain Pulses in Pressure Bars and Axial and Transverse Specimen Surface Strains

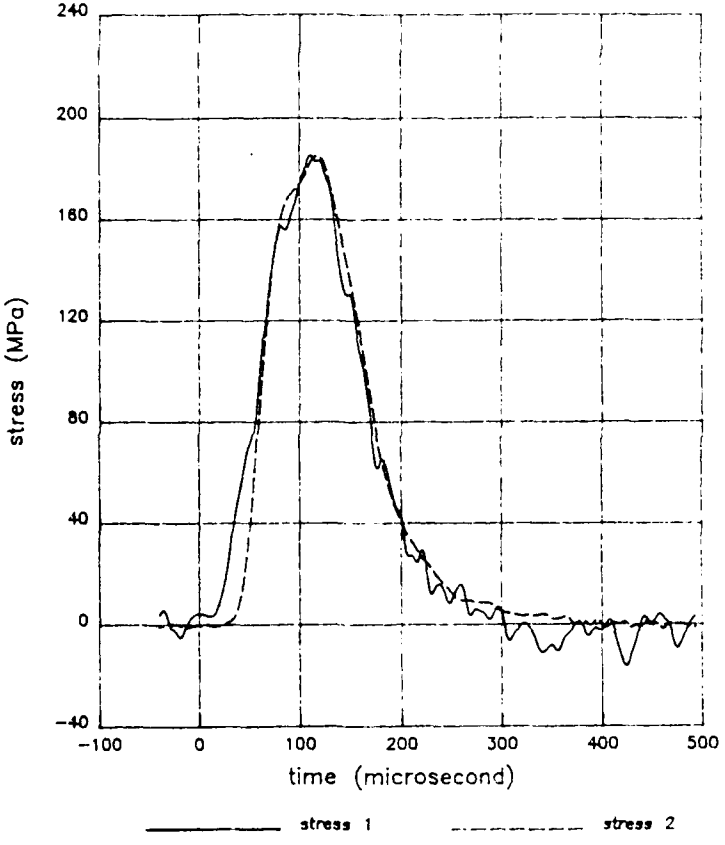

Figure 3. Corrected Stresses at Two Specimen Interfaces.

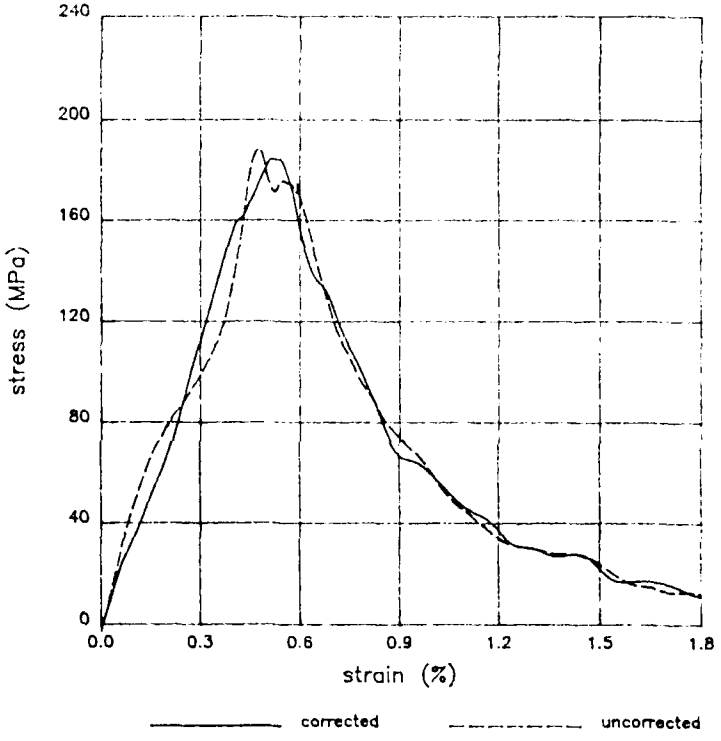

Figure 4. Corrected and Uncorrected Dynamic Stress-Strain Curves.

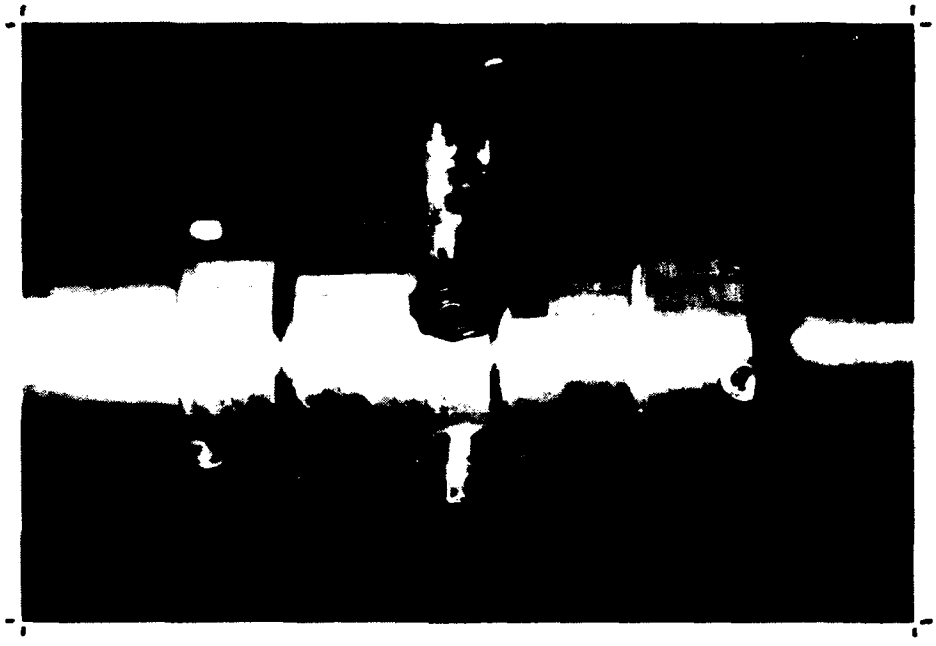

Figure 5. Confinement Pressure Cell Installed on 3-inch (76.2-mm) SHPB with Specimen in Place.

Figure 6. Confinement Pressure Cell. At the rear is the pressurized water feed line; the air bleed valve is at the top and the pressure transducer is at the front.

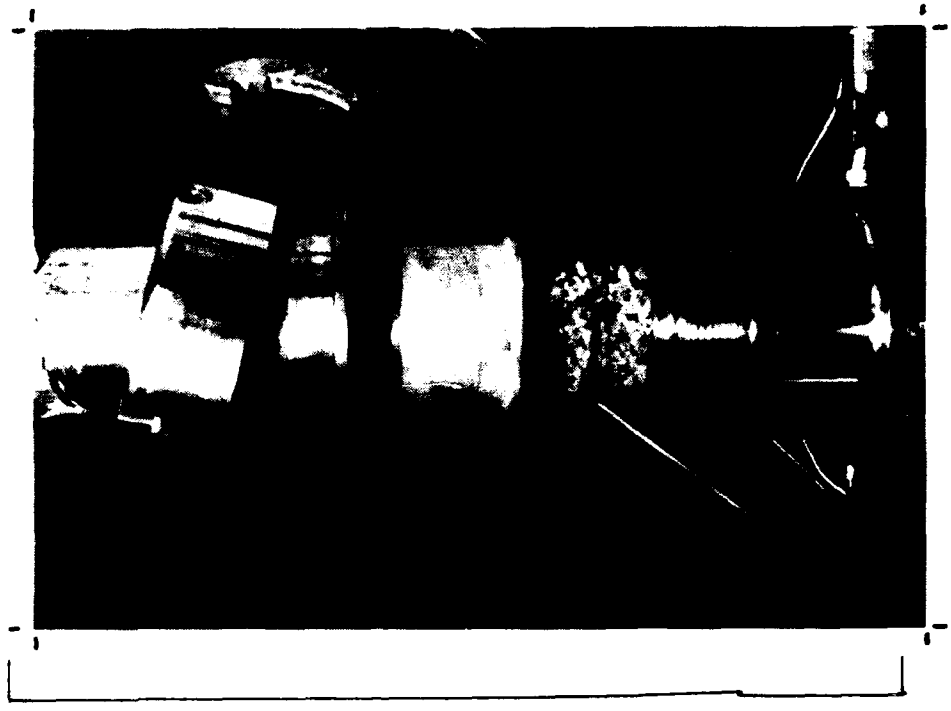

Figure 7. Disassembled Pressure Cell Showing the Separate Parts. To the left is the two-piece end cap and the rubber O-ring. A prepared specimen is shown in place between the bars with a latex membrane partially unrolled (no aluminum tape in this photo). Spanner wrenches shown in background.

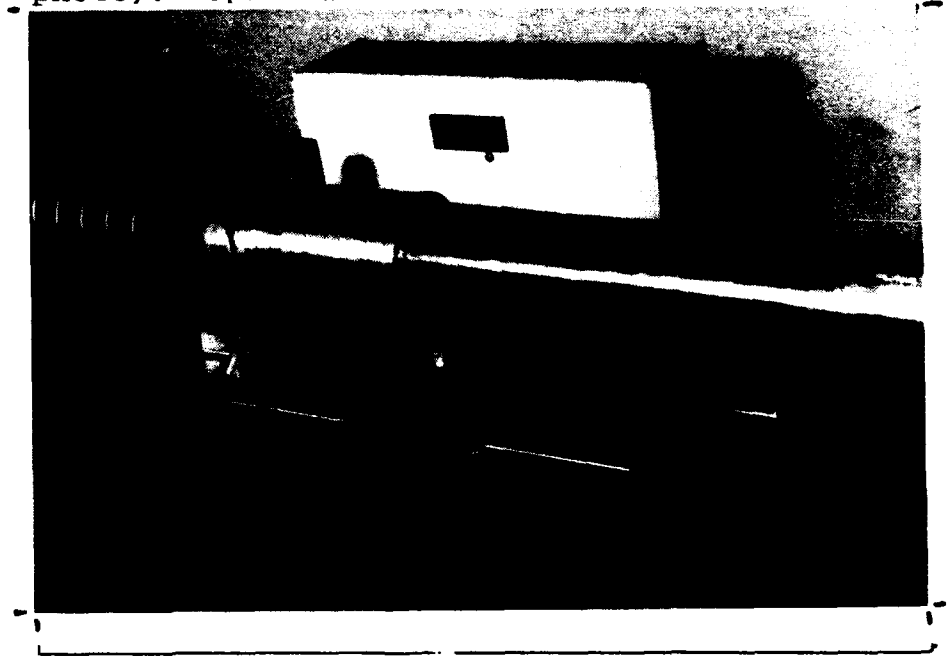

Figure 8. Axial Loading Device Installed at the Far End of the Transmitter Bar. Force is applied through a phenolic shear pin and measured using an instrumented aluminum yoke and the readout device shown in the background. The shock absorber is at the extreme left.

The incident pressure bar on the other end of the specimen is kept from moving by a simple mechanical stop (Figure 9) which can easily be passed (as when reloading the gas gun) by simply rotating the bar 90 degrees. The stops on the bar were attached with epoxy adhesive and dacron binding to avoid the need for drilling holes in the bar.

Pressurized water is supplied by a standard manually operated hydrostatic test pump with a 12,000 psi capacity (Richard Dudgeon, Inc., Model 7J). Low pressure water is delivered to the pump, Figure 10, through a common garden hose, while a 7000 psi (48.3 MPa) reinforced line connects the pump to the chamber. A large dial gauge on the pump provides a convenient reference for setting the initial pressure. A Kulite Semiconductor Model ETM-300-375-5000A pressure transducer attached to the chamber allows precise measurement of the water pressure throughout the conduct of the test. A schematic diagram of the complete system is shown in Figure 11.

C. TESTING TECHNIQUE

Early trials of the system uncovered problems with maintaining integrity of the latex seals during pressurization because of the presence of small voids at or near the specimen surface. As the pressure was increased, the latex was frequently cut, allowing water to be forced into the specimen/bar gap. A satisfactory remedy was developed and adopted as part of the standard test protocol. Each specimen was first ground on the ends to ensure parallel contact faces. A rapid-setting epoxy resin was spread onto the cylindrical surface, carefully filling any visible openings. After the resin was set, the surface was ground smooth using an abrasive disk grinder, with care taken to remove only the excess epoxy resin. The specimen was then placed in the SHPB between the bars, positioned, and the desired axial preload applied. One wrap of 4-inch-wide adhesive-backed aluminum foil tape was then applied over the specimen and part of the bars with a 1/2-inch (12.7 mm) overlap, and finally a latex membrane, Soiltest Inc. Triaxial Soil Membrane, 2.5 by 0.014 by 9 inches (63.5 by 0.356 by 229 mm), was unrolled over the taped specimen and bars. The soft aluminum tape apparently was capable of blunting the sharp edges of the pores, and most membranes survived, even at initial pressure up to 1500 psi (10.34 MPa).

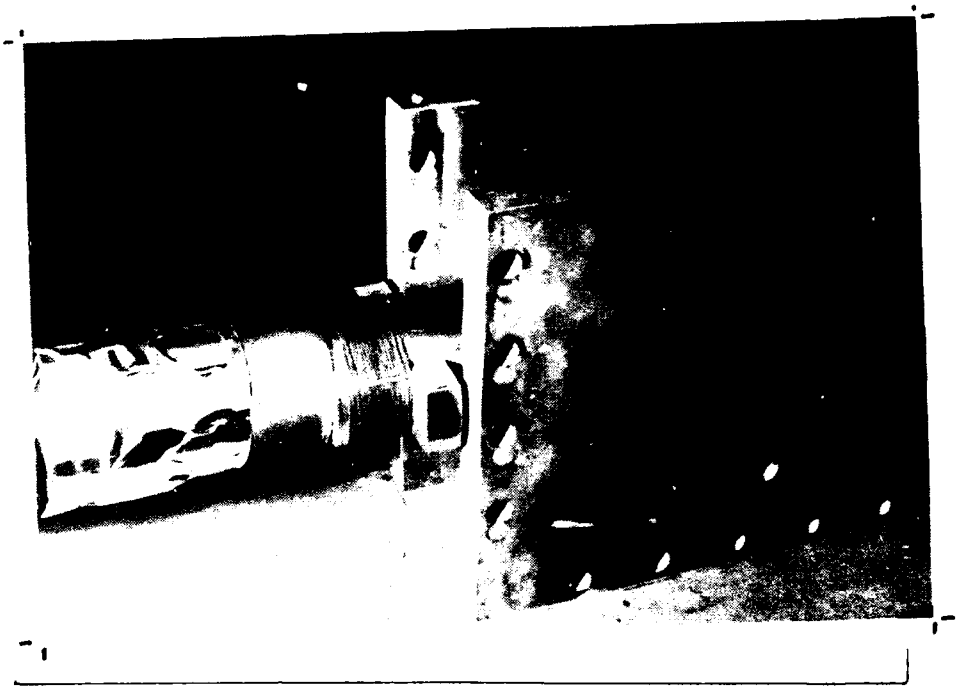

Figure 9. Axial Preloading Stop on Incident Pressure Bar. The two large triangular pieces are bolted to the SHPB framework, while the two small shaped blocks are bound and epoxied to the incident bar.

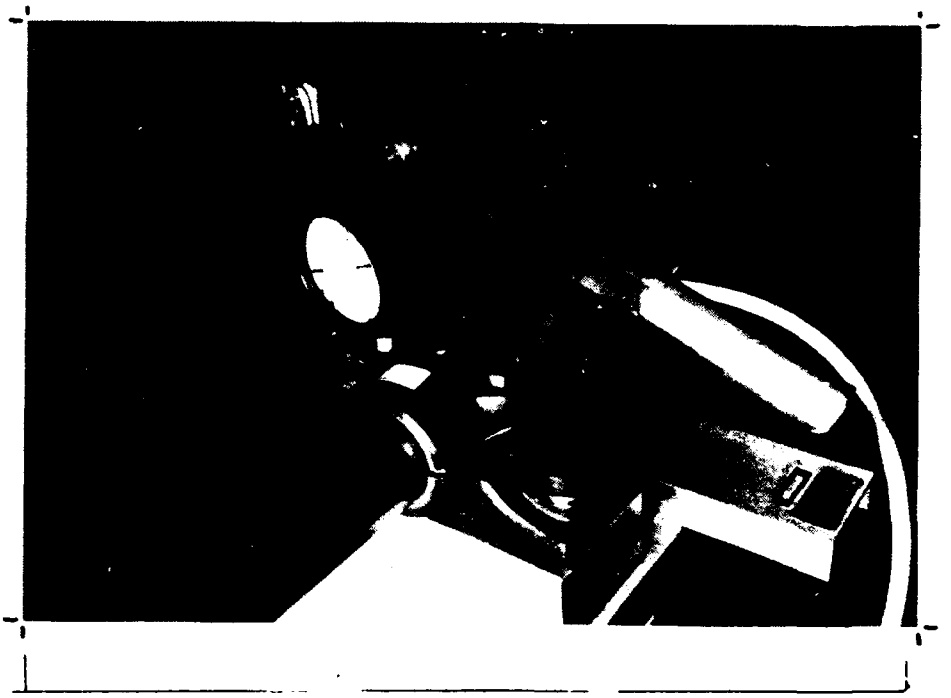

Figure 10. Hydrostatic Test Pump with Dial Gauge for Setting Initial Pressure.

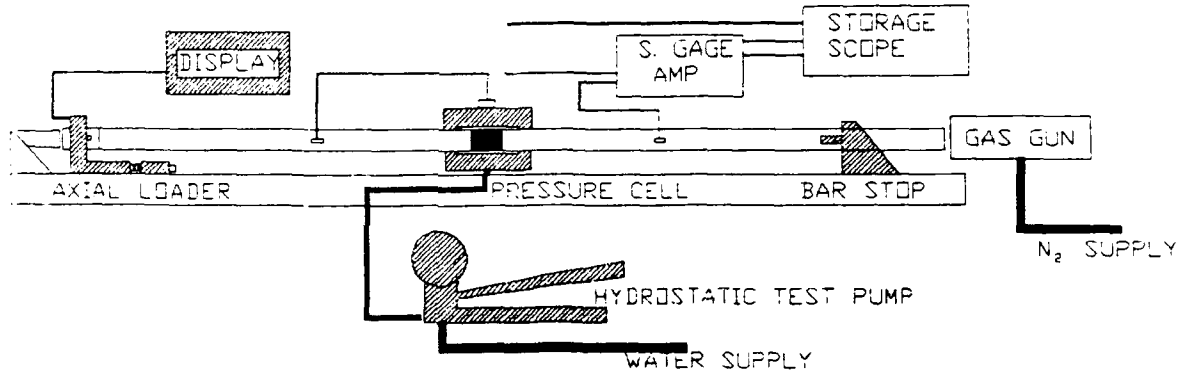

Figure 11. Schematic Diagram of the Complete System.

Tests were routinely conducted by closing the air-bleed screw and filling the chamber with pressurized water. The small amount of trapped air provided a slight accumulator action and reduced the increase in confinement pressure that occured as the test progressed and the specimen expanded. When the desired level of initial confining pressure was set, the SHPB test was initiated as for an unconfined test. The usual strain gage readings were recorded, as well as the output of the pressure transducer. Following the test, failed specimens could be removed and examined after taking off the two end caps and sliding the chamber to one side.

SECTION III

DYNAMIC TESTING PROGRAM OF LATERALLY CONFINED SPECIMENS

A. INTRODUCTION AND TEST MATRIX

The major emphasis of this investigation was on designing and fabricating the pressure cell and peripheral equipment. The initial objectives of the testing program reported here were (1) to demonstrate that the system worked properly, and (2) to investigate the effects of lateral confining pressure on the dynamic compressive response of one particular concrete at several different striker-bar impact speeds in the SHPB. The particular concrete was chosen by the sponsor, HQ AFESC, Tyndall AFB, Florida. Specimens were prepared at the U. S. Army Waterways Experiment Station (WES).

Before the WES specimens arrived, preliminary tests were made on concrete specimens prepared at the University of Florida (UF) Civil Engineering Department with the assistance of Mr. Daniel S. Richardson. The first test was made with an old 3-inch (76.2-mm) specimen to check the system at an initial lateral confining pressure of 3.1 MPa (450 psi). Because the pressure cell had been filled with water, forcing out all the air before the initial pressure was applied, there was a large pressure rise during the test. The maximum pressure recorded by the transient pressure transducer was about 5.5 times its initial value. The dynamic stress-strain curve resembled that of a work-hardening metal with elastic recovery after a maximum strain of about 1.1 percent. The maximum stress reached before unloading was about 110 MPa (16 ksi). The specimen was recovered intact, although both the maximum stress and maximum strain were greater than the failure values of stress and strain in earlier unconfined tests of the same material. This is qualitatively the kind of response that we would have expected at a constant confining pressure somewhat higher than the initial pressure.

In the next two tests, made on specimens from a new batch prepared at UF, a small amount of air was left trapped in the pressure cell. The lateral expansion of the specimen during these tests was accommodated by additional compression of the trapped air with a smaller pressure rise to a maximum pressure of about 2.5 to 3 times the initial pressure. The pressure records showed oscillations, which may have been associated with the spring action of the trapped air. The amount of trapped air was increased in subsequent tests. The entire initial air content of the pressure cell with the specimen and membrane in place, approximately 23.6 in^3 (387,000 mm^3), was trapped and compressed when the water was pumped in. At the highest initial confining pressure used with the WES specimens, it was estimated (based on adiabatic compression of dry air) that the trapped air volume was reduced to about 0.88 in^3, (14,400 mm^3) and that about 201 ft-lb (272 J) of work was required to compress the air. The energy

stored in this volume of compressed air constitutes a small, but finite, hazard that would be absent in an all-water system. A catastrophic failure of the pressure cell into several large pieces would still most likely be a harmless incident, since the energy imparted to the pieces would allow them to move only a short distance before they fell to the floor. Very small pieces could achieve lethal velocities, however, and caution is warranted. With this amount of trapped air the largest pressure observed during the tests on UF specimens was less than 1.6 times the initial pressure. This occurred for an initial pressure of 5.08 MPa (737 psi) at a striker-bar impact speed of 514 in/sec (13.1 m/s) which gave a maximum stress of about 150 MPa (21.8 ksi) in this concrete whose unconfined static strength was about 6 ksi. The specimen was recovered intact, although its surface showed two diagonal cracks, extending almost the entire length of the specimen. Similar cracks will be described and exhibited for the WES series. In the WES series the maximum pressure was approximately 1.8 times the initial pressure. This occurred for the test at the lowest initial pressure used in the series, 3.26 MPa (472 psi) and the striker-bar impact speed of 582 in/sec (14.8 m/s). In only six of the tests was the pressure rise more than 50 percent. The oscillations seen when only a small amount of trapped air was retained had essentially disappeared when the larger amount of air was trapped. Although the pressure was not constant during the WES tests, the pressure rises were small enough that a reasonable determination of the confining pressure effects could be made by testing at several different initial confining pressures.

Five different confining pressures were used in the test series on the WES concrete. A total of 21 confined dynamic tests were carried out in the SHPB system. Table 1 shows the test matrix.

TABLE 1. TEST MATRIX (confined WES specimens)

Nominal Initial Water Pressure (psi)/(MPa)	SPECIMEN NUMBERS FOR SHPB FIRING PRESSURES (psi)/(MPa)				
	250/ 1.724	300/ 2.07	400/ 2.76	500/ 3.45	600/ 4.14
500/3.45	A02	A03	A01 A09	A10	---
750/5.17	A05	A06	A04 A22	A07 A11	---
1000/6.90	---	A12	A18	A08	A25
1250/8.62	---	---	A24	A17	A23
1500/10.34	---	---	A13	A21	A20

At each level of nominal initial lateral pressure a sequence of tests was performed at increasing striker-bar impact speeds, governed by the SHPB gas gun firing pressures. As the results will show, the same firing pressure does not always give the same striker-bar impact speeds. Also the initial pressure in each group of tests was not exactly the same, and the pressure rise during the test varied.

Nine unconfined tests were also performed on specimens of the same material, over a range of SHPB firing pressures from 130 psi to 600 psi (0.90 MPa to 4.14 MPa) to give a baseline for assessing the effect of confining pressure. Typical test results will be presented and discussed in Subsection III B.

B. DESCRIPTION OF TEST RESULTS

1. Unconfined Tests of WES 7-ksi (48.3 MPa) Concrete

Nine unconfined tests are reported in the appendix, Figures A-2 to A-10. Each figure has two parts. Part (a) shows time plots of the two interface stresses, the specimen strain, and the specimen strain rate. Note that zero time on the abscissa is well before the beginning of the test. Part (b) gives the dynamic stress-strain curves and also strain rate versus strain.

The nine tests are for striker-bar impact speeds from 56.5 in/sec (1.45 m/s) up to 666 in/sec (16.9 m/s). A typical example is shown in Figure 12. The stress reaches a maximum of 92.4 MPa (13.4 ksi) at a strain of about 0.4 percent, where the strain rate was 51.6 s^{-1}, after which the stress decreases during the strain-softening regime. For the eight tests leading to failure the test results of maximum stress σ_m versus the strain rate $\dot{\epsilon}_m$ at the maximum stress were reasonably represented over the strain rate range reported by a linear regression

$$\sigma_m = A + B\,\dot{\epsilon}_m \qquad (1)$$

with $A = 56.4$ MPa and $B = 0.415$ MPa·s.

2. Confined Tests

The observed responses in the confined tests are quite different from those of the unconfined tests. Most of them do not show a peak stress followed by a continuously decreasing stress, even when post-impact examination shows that the specimen has been separated into two or more pieces. In some cases the maximum stress reached is at the end of the SHPB loading pulse,

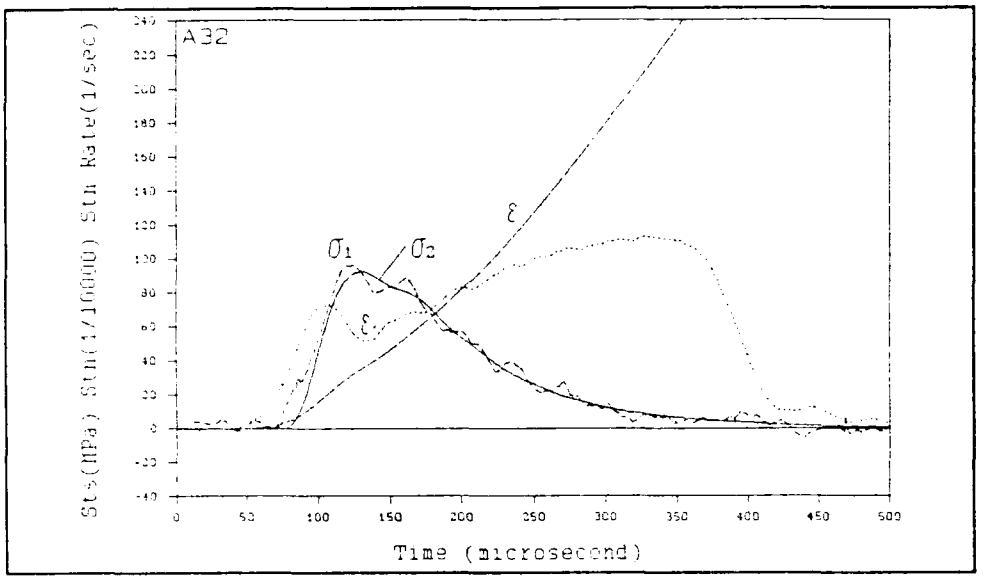

(a) Time Plots of Two Interface Stresses, Strain and Strain Rate.

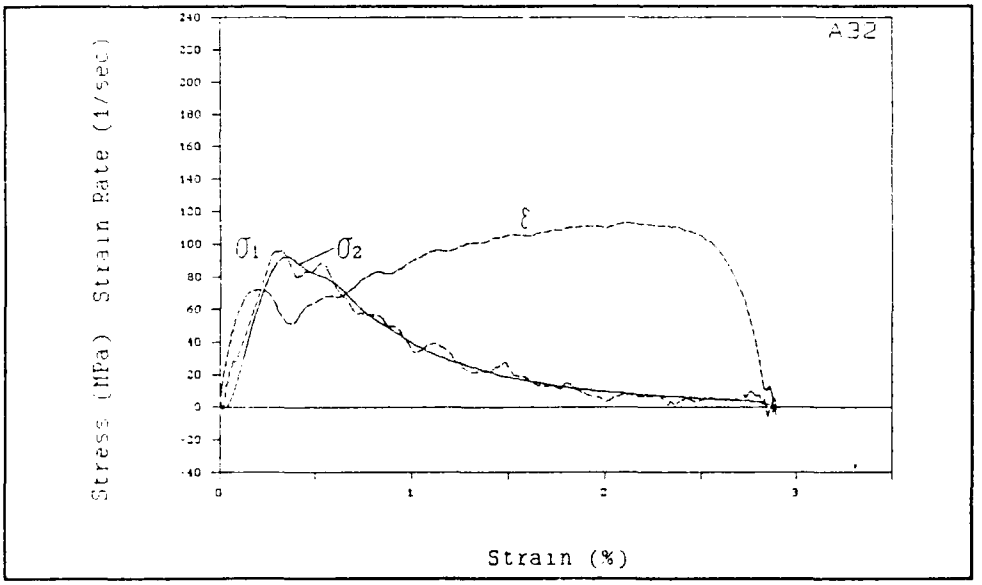

(b) Stress-Strain Curves and Strain Rate Versus Strain.

Figure 12. Unconfined Test of Specimen A32. Impact Speed 352 in/s (8.94 m/s).

and presumably the stress would have continued to rise for a longer time, if the striker bar had been longer, so that unloading did not occur. In other cases a peak occurs followed by a decrease or by a plateau and then the stress rises again. In a few cases at the lower confining pressures, the peak is in fact followed by a continuously decreasing stress; however, the stress decreases at a slower rate than in the unconfined tests, so that a substantial stress is still present at the end of the loading pulse. Accompanying the unloading, in all cases, the stress-strain curves show an apparent elastic recovery; that is, the unloading curve is roughly parallel to the initial loading slope. The observed stress-strain response and the condition of the surviving specimen now depend both on the amount of confining pressure and on the strain rate.

There is not a typical confined response. A few examples of the various types of response observed will be given here. Results of all 21 confined tests are given in the appendix, beginning with Figure A-11. All the figures (both confined and unconfined tests) are plotted to the same scale for convenient comparison.

An example of apparent strain softening behavior is shown in Figure 13 for specimen No. A03, from the lowest confining pressure group, loaded by a moderate striker-bar impact speed of 420 in/sec. (10.7 m/s). The peak stress of 124 MPa (18 ksi) occurs at a strain of about 0.7 percent at a strain rate of 59 s^{-1}. This strain rate is comparable to the value of 51.6 s^{-1} at the peak stress of 92.4 MPa in the unconfined test of Figure 12. However, the confined peak stress is about 35 percent higher, and the subsequent stress decrease before unloading is much smaller, less than 7 percent in the confined test.
Figure 13(a) shows that the confining pressure increased during the test from an initial value of about 3.32 MPa (482 psi) to a maximum of 4.7 MPa (653 psi). This confined specimen was recovered intact, although the surface showed prominent diagonal surface cracks reaching to the ends of the specimen, as well as some shorter cracks near the mid-length, inclined at about 25 degrees to the axial direction. By contrast, the unconfined specimen had been reduced to rubble.

Many of the higher-speed-impact confined specimens showed approximately parallel prominent diagonal surface cracks on two opposite sides; in some cases the recovered specimen was in two pieces, in others it was still coherent. Figure 14 shows the recorded curves for one of the most severely damaged but still coherent specimens, No. A20, which was impacted at 640 in/sec (16.3 m/s). The second interface stress reached a plateau value of about 179 MPa (26 ksi) at a strain of about 1.1 percent, where the strain rate was about 100 s^{-1}. The stress started increasing again at about 2 percent strain and reached about 195 MPa just before the unloading occurred. The recovered specimen was still coherent, but it was then manually separated into two pieces with bare hands. The lateral pressure increased from an initial value

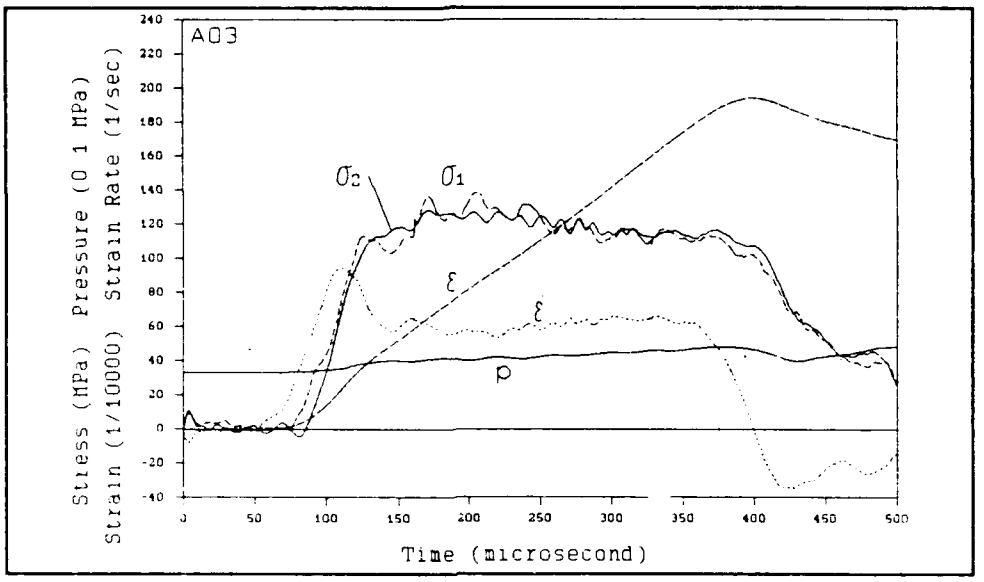

(a) Time Plots of Two Interface Stresses, Strain and Strain Rate and Confining Pressure.

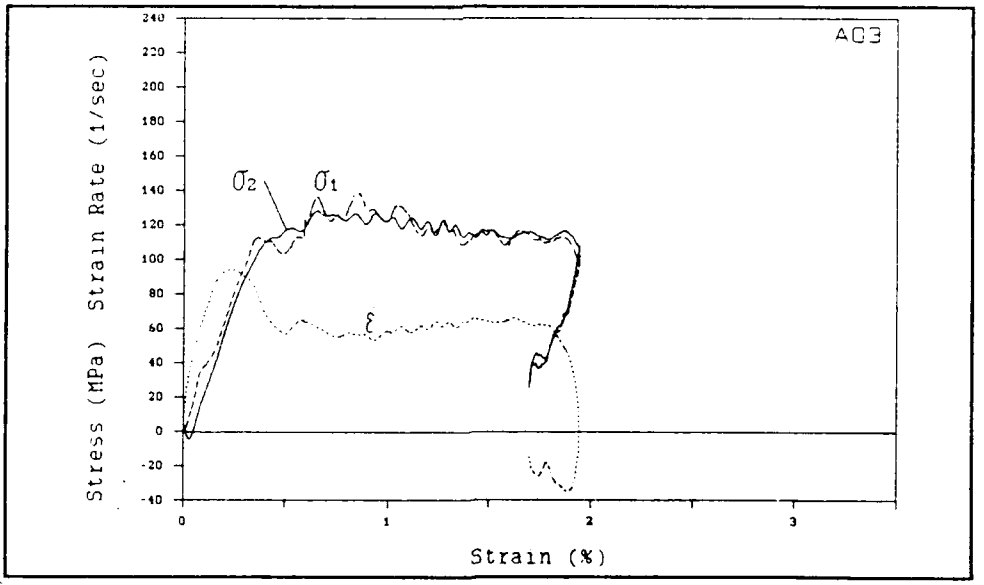

(b) Stress-Strain Curves and Strain Rate Versus Strain.

Figure 13. Test of Specimen A03 with Initial Confining Pressure 3.32 MPa and Impact Speed 420 in/s (10.67 m/s).

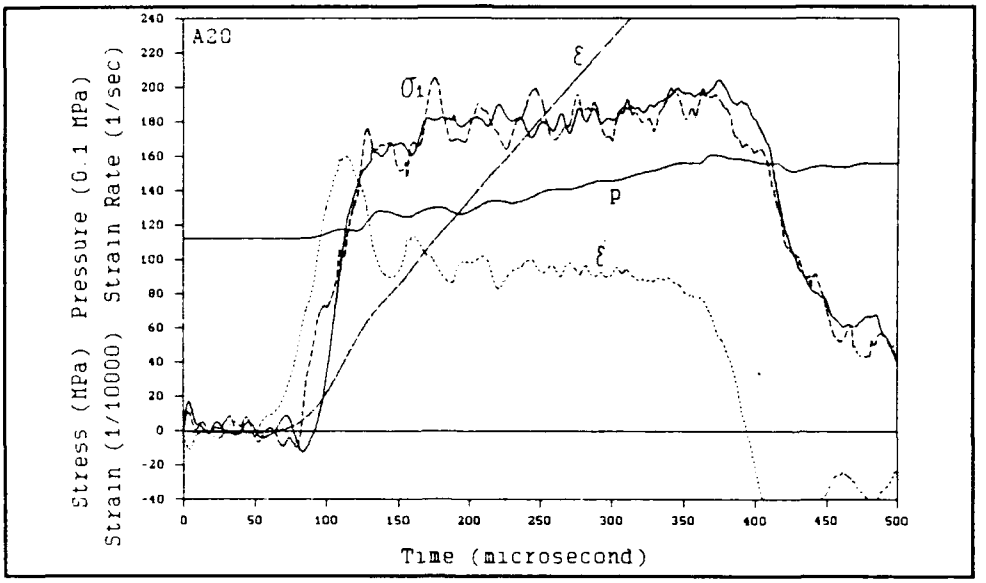

(a) Time Plots of Two Interface Stresses, Strain and Strain Rate and Confining Pressure.

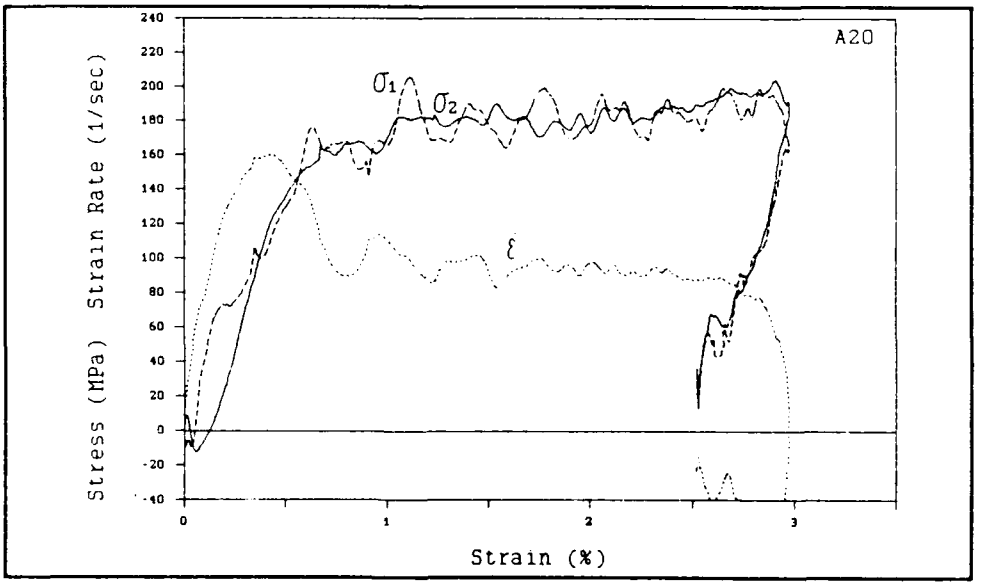

(b) Stress-Strain Curves and Strain Rate Versus Strain.

Figure 14. Test of Specimen A20 with Initial Confining Pressure 11.2 MPa and Impact Speed 640 in/s (16.26 m/s).

of 11.2 MPa (1620 psi) to a maximum of 16 MPa (2320 psi) during the test, an increase of 43 percent.

Figure 15, for specimen No. A23, shows similar behavior, except that the stress plateau is replaced by a decreasing stress interval before the stress started increasing again at about 2 percent strain, finally reaching a stress of about 185 MPa just before the unloading. In this case the specimen was recovered in two pieces, separated by the diagonal crack.

This diagonal crack pattern was exhibited by 15 of the 21 confined test specimens; of these, 5 were recovered separated into two pieces (curves in Figures A-13, A-14, A-20, A-25, A-28), and 10 were coherent (curves in Figures A-12, A-18, A-19, A-23, A-24, A-26, A-27, A-29, A-30, A-31). There does not seem to be a consistent difference between the types of curves obtained when the recovered specimens were coherent and those which were separated. All still showed an apparent elastic recovery upon unloading.

Examples of these diagonal cracks are shown in the photographs of Figures 16 to 19. Figure 16 shows two specimens, A09 on the left and A07 on the right. In each of these, the specimen was recovered in two pieces; it was reassembled for the photograph of Figure 16. Figure 17 shows the same two specimens each with the top piece removed, inverted and sitting to the left of the bottom piece. For specimen A07 (on the right) the crack is fairly flat and at approximately 45 degrees to the axial direction in the interior, but on the surface the crack angle is closer to 30 degrees near the middle, as may be seen in Figure 18. For A09 the crack surface is more curved, although there is a small fairly flat section near the center of the specimen. Figure 19 shows one view of the diagonal crack trace on the surface of specimen No. A13, which was firmly coherent after the test. When the crack approaches the end of the specimen it tends to assume a somewhat conical shape, so that its trace on the surface runs around the rim at the end instead of cutting across the end surface. This can be seen at the left end of Figure 19, and in Figures 16 to 18. Other shorter surface crack traces are usually present in addition to the main diagonal crack, although they do not show up in these photographs. Test recordings for these three specimens are given in the Appendix: Figure A-14 for Specimen A09, Figure A-20 for Specimen A07, and Figure A-29 for Specimen A13.

Two of the specimens showed greater damage. Specimen A10 was reduced to small fragments except for a blunted conical piece that survived at one end. This was for the highest speed impact in the lowest confining pressure group. Curves are given in the Appendix Figure A-15. The stress-strain curve shows an apparent elastic unloading at the end despite all the damage. Specimen A11 had two large pieces running the full length of the specimen, each with a flat portion on one end. A blunted conical piece survived at the other end and there were many smaller fragments.

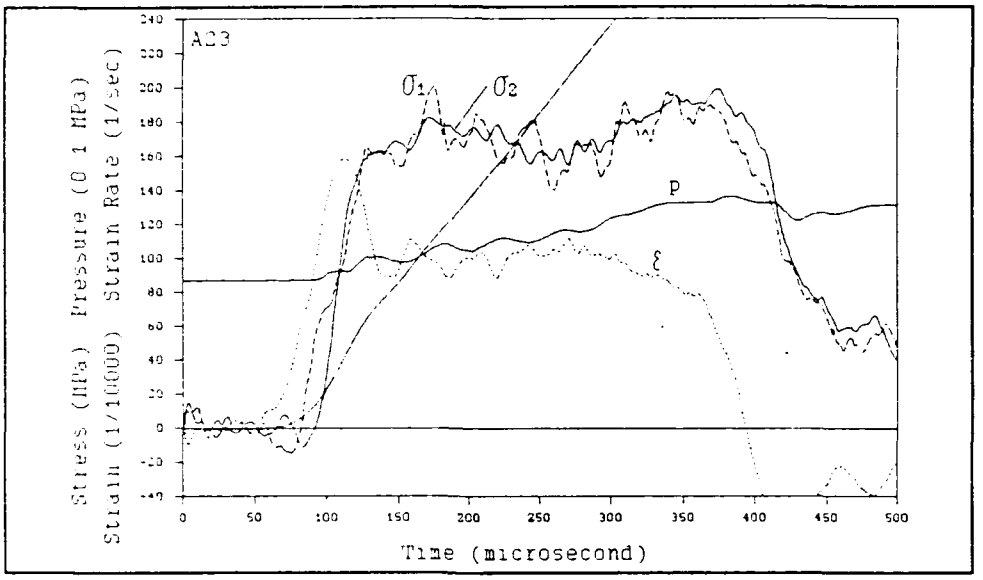

(a) Time Plots of Two Interface Stresses, Strain and Strain Rate and Confining Pressure.

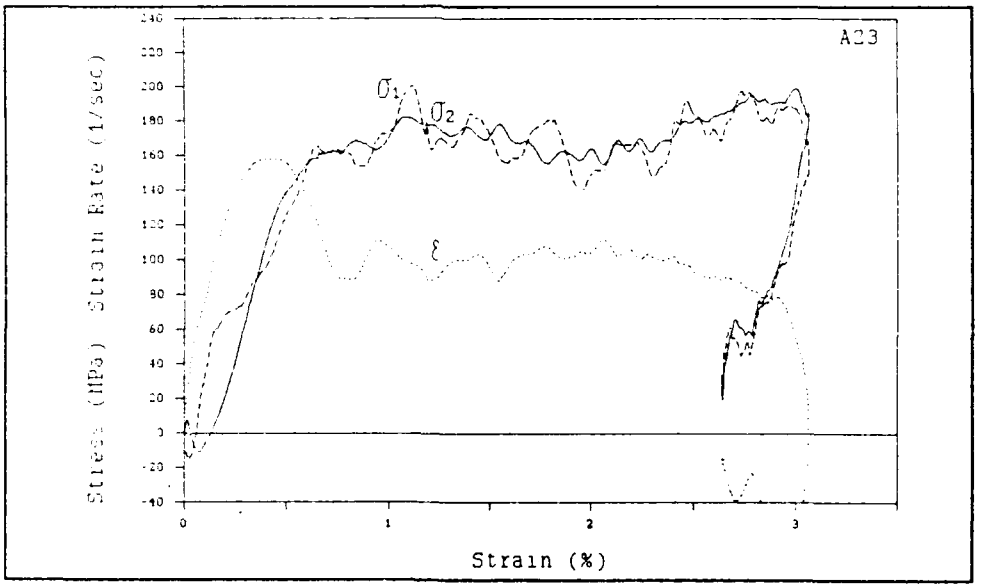

(b) Stress-Strain Curves and Strain Rate Versus Strain.

Figure 15. Test of Specimen A23 with Initial Confining Pressure 8.69 MPa and Impact Speed 641 in/s (16.28 m/s).

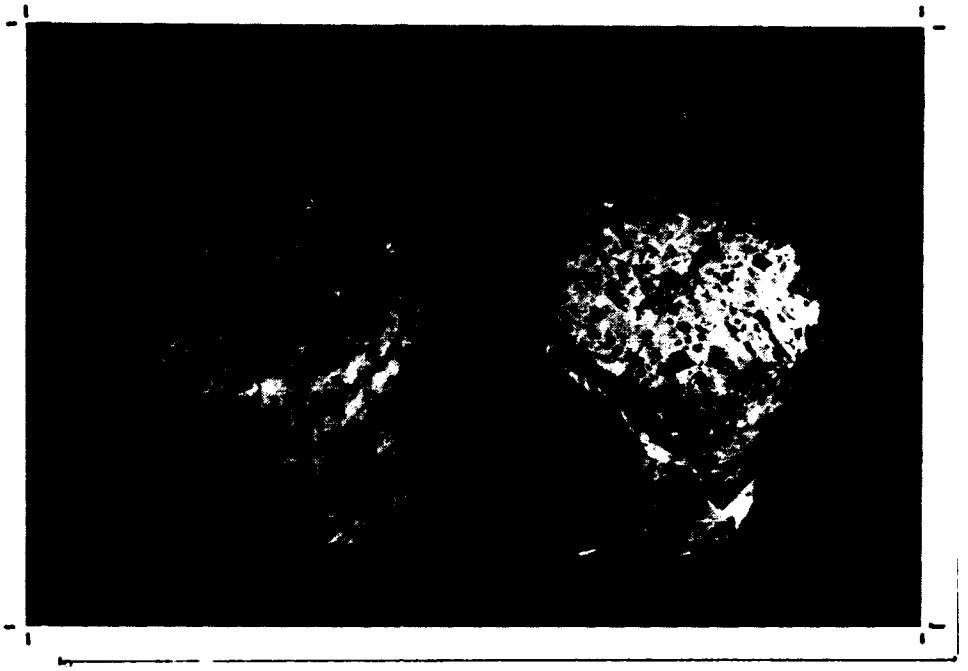

Figure 16. Reassembled Specimens A07 (on the Right) and A09 (on the Left) after Fracture by Diagonal Cracks.

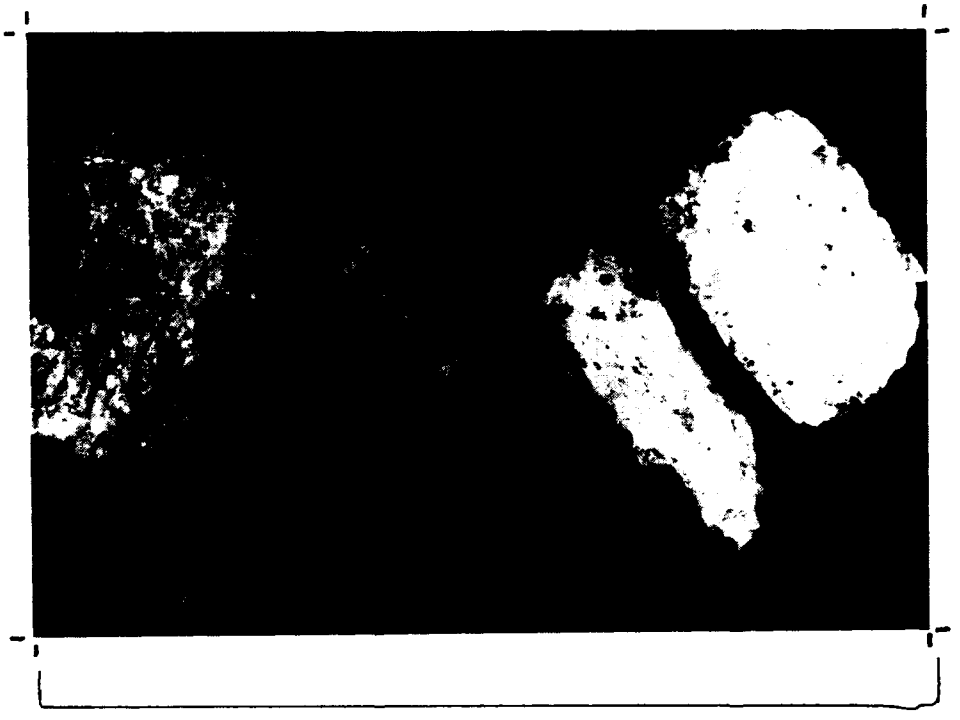

Figure 17. Fractured Specimens A07 (on the Right) and A09 (on the Left).

This was for the highest speed impact in the second-lowest confining pressure group. See Figure A-21. The stress-strain curve is comparable to that of Figure A-20 for specimen A07 where the recovered specimen showed fracture into two pieces by a diagonal crack. The initial failure may have been by a diagonal crack in both cases, with additional damage occurring before unloading in Specimen A11.

The other four confined specimens (A02, A05, A06, A12) were recovered intact with some cracks visible on the surface (longer cracks in A06 and A12 than in A02 and A05) but no apparent coalescence into a major diagonal crack.

Tables A-1 through A-5 at the end of the appendix list pertinent features for each of the 21 confined tests whose curves are given in Figures A-11 through A-31.

In the nine unconfined tests, one specimen (No. A33) was apparently undamaged (see curves of Figure A-2). Figure 20 shows the surviving hourglass shape of another specimen (No. A34), impacted at 200 in/sec. (5.08 m/s), with the fragments that had been split off from the part near the lateral surface shown at the left. Curves for this specimen (Figure A-3) show an apparent elastic recovery. In the other seven unconfined tests (Figures A-4 to A-10) no elastic recovery appears, and the specimens had been reduced to small fragments.

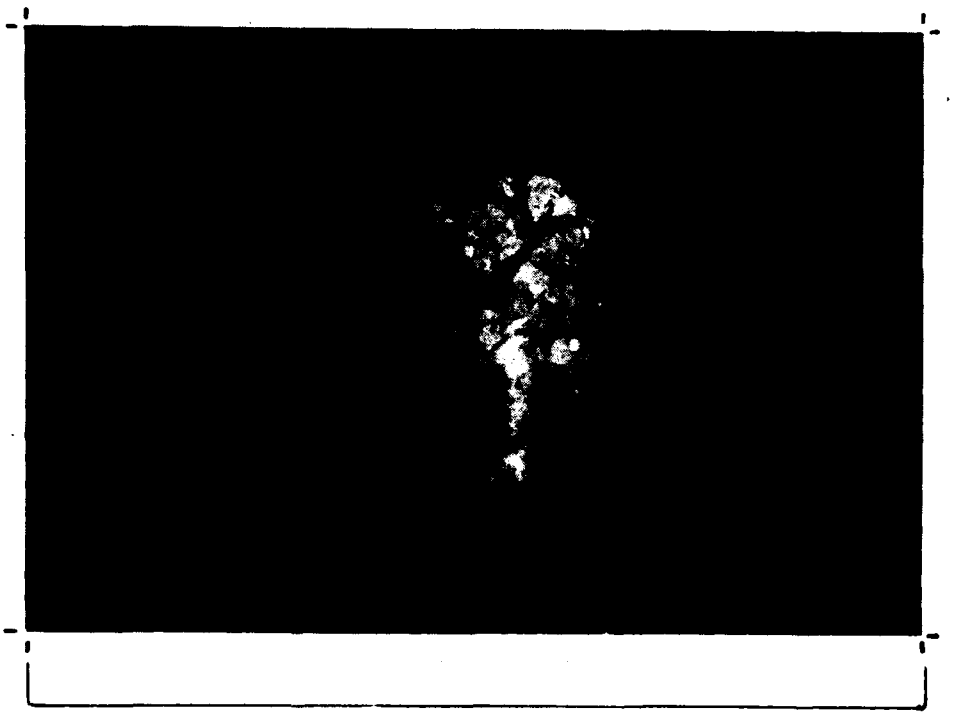

Figure 18. Side View of Fractured Specimen A07.

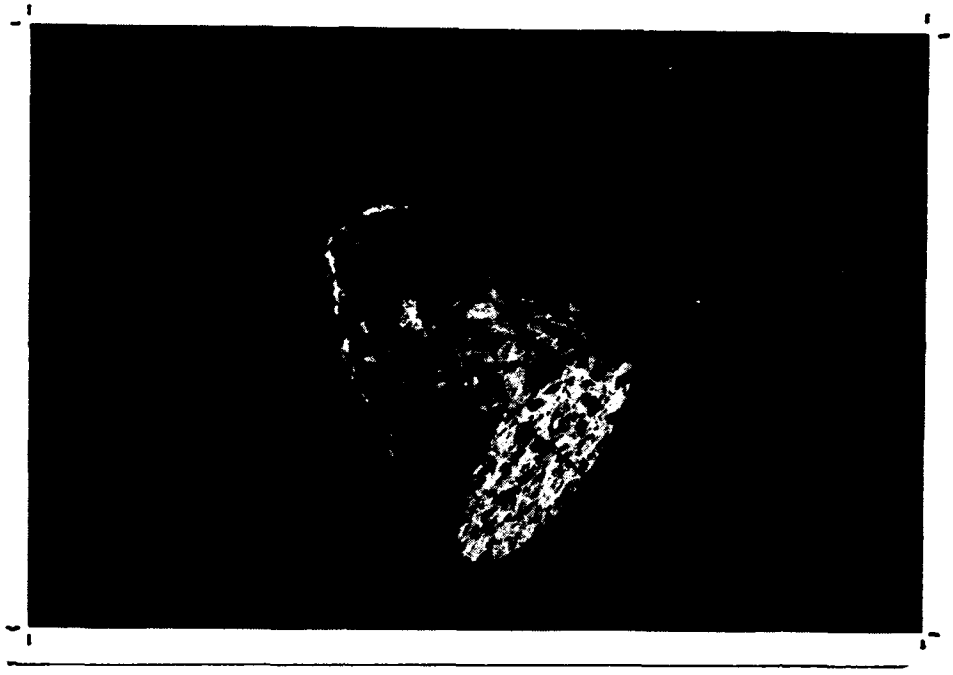

Figure 19. Diagonal Crack Trace on Surface of Coherent Specimen A13.

Figure 20. Partially Intact Unconfined Specimen A34 with Hourglass Shape.

3. Summary of Lateral Pressure Effects

Two different types of regression analyses were carried out to summarize the effects of lateral pressure and strain rate on these rather diverse mechanical responses,. The first type is similar to that of analyses of unconfined tests given in Equation (1) of Subsection III B1. For those 19 tests in which the stress-strain curve showed a first peak followed by a decrease or by a plateau, the second-interface stress at this first peak is taken as the failure stress, σ_f, analogous to the peak stress σ_m in the unconfined tests. A multilinear regression fit to an equation of the form

$$\sigma_f = A + B\,\dot{\epsilon}_f + C\,p_f \qquad (2)$$

with A=64.4 MPa, B=0.388 MPa·s, C=7.59

gave a good fit to the data of 27 tests, including 8 unconfined tests and 19 confined tests. The strain rate coefficient B is slightly smaller, but of the same order as in the fit to the unconfined tests in Equation (1). At the higher pressures, however, the relative importance of the rate effect is smaller.

For example, the equation obtained by assuming a constant pressure of 10 MPa would be

$$\sigma_f = 140 + 0.388\,\dot{\epsilon}_f\ , \qquad (3)$$

while for p = 0, the equation would be

$$\sigma_f = 64.4 + 0.388\,\dot{\epsilon}_f\ . \qquad (4)$$

The coefficients in Equation (4) are different from those in Equation (1) because they are obtained by the multilinear regression for the whole data set for the 27 tests, while Equation (1) was obtained with a linear regression for the data of only the 8 unconfined tests with apparent damage. Actually both Equations (1) and (4) give a good match to the results of the unconfined tests over the dynamic range of strain rates from 51.9 s^{-1} to 123 s^{-1} obtained in these tests. None of these linear fits should be extrapolated outside the range of the data on which they are based; in particular these equations should not be expected to extrapolate to the quasistatic unconfined strength of around 48 MPa (7 ksi). The data for the multilinear regression fit for Equation (2) is contained in Tables A-1 to A-5 at the end of the appendix. Data from Figures A-22 and A-29 were not included, because there was no identifiable first peak or plateau.

The second type of regression analysis looked at each of the stress-strain curves for the 21 confined tests at four selected values of strain, which appeared in all 21 curves, (0.005, 0.008, 0.011, 0.014) and attemped to fit a simple expression to all this data to summarize the trends in the rising parts of the curves (above the initial "knee"). A multilinear regression

$$\sigma = B_o + B_1 \epsilon + B_2 \dot{\epsilon} + B_3 p \qquad (5)$$

with $B_0 = 68.1$ MPa, $B_1 = 2110$ MPa,

$B_2 = 0.159$ MPa·s, $B_3 = 5.82$ (nondimensional)

for p and σ in MPa was fairly successful.

To examine the confining pressure effects on the strain and strain-rate dependence of the curves, the following form was fitted to the same data as for Equation (5).

$$\sigma = (A_0 + A_1 p) + (B_0 + B_1 p)\epsilon + (C_0 + C_1 p)\dot{\epsilon} \qquad (6)$$

with $A_0 = 63.36$ MPa $A_1 = 6.696$

$B_0 = 1023$ MPa $B_1 = 139.6$

$C_0 = 0.347$ MPa·s $C_1 = -0.02745$ s

for p and σ in MPa

obtained by multilinear regression. Thus, for example, increasing the pressure from zero to 10 MPa approximately doubles the first parenthesis in Equation (6), the "constant term." The hardening coefficient multiplying ϵ is more than doubled, while the rate-sensitivity coefficient is reduced by 21 percent. In fact the fitted expression predicts a negative coefficient of $\dot{\epsilon}$ for p greater than 12.46 MPa, a prediction that should be viewed with considerable caution. Such a multilinear regression fit to the various parts of curves where quite different deformation processes are occurring is questionable at best; it certainly is not intended to represent a constitutive model, but as the dashed curves fitted by it show in Figures 21 to 23, it does approximately fit the early rising parts of the experimental curves fairly well. It does not reproduce any strain softening regimes. The regression fit does gives a compact representation of the trends with confining pressure; in particular it indicates a reduced rate sensitivity with increasing pressure. Figure 21 is from the lowest confining pressure group at a low impact speed, Figure 22 is from an intermediate pressure group at an intermediate speed, and Figure 23 is from the highest pressure group. It may be remarked that the data used as input values of $\dot{\epsilon}$ to get these dashed curves was obtained by smoothing the $\dot{\epsilon}$ versus ϵ experimental records, so that the oscillation in the $\dot{\epsilon}$ versus ϵ experimental curves does not produce an oscillation in the fitted curves of σ versus ϵ.

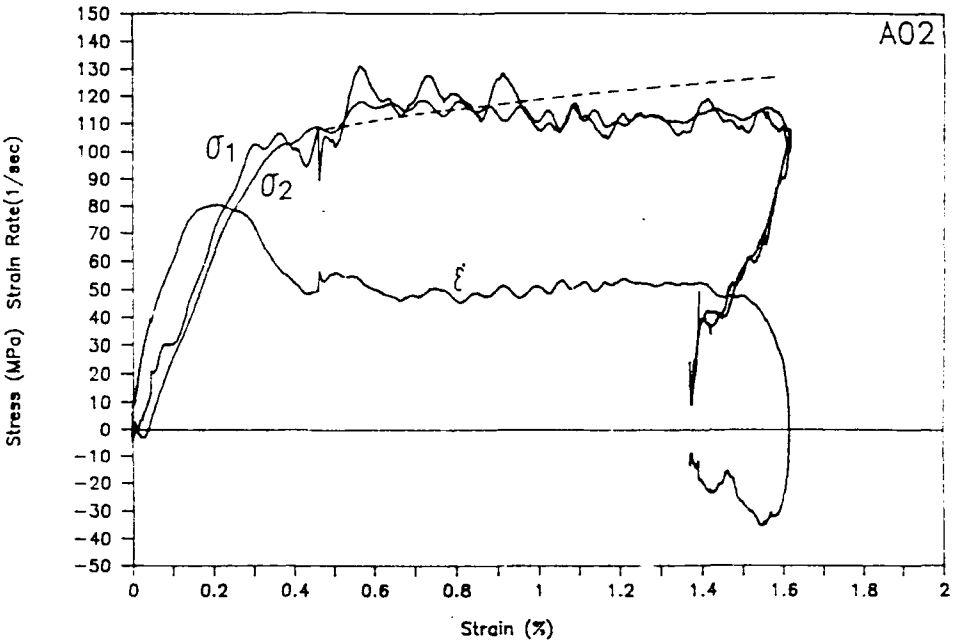

Figure 21. Example of Regression Fit by Equation (6) for Low Confining Pressure (Dashed Curve).

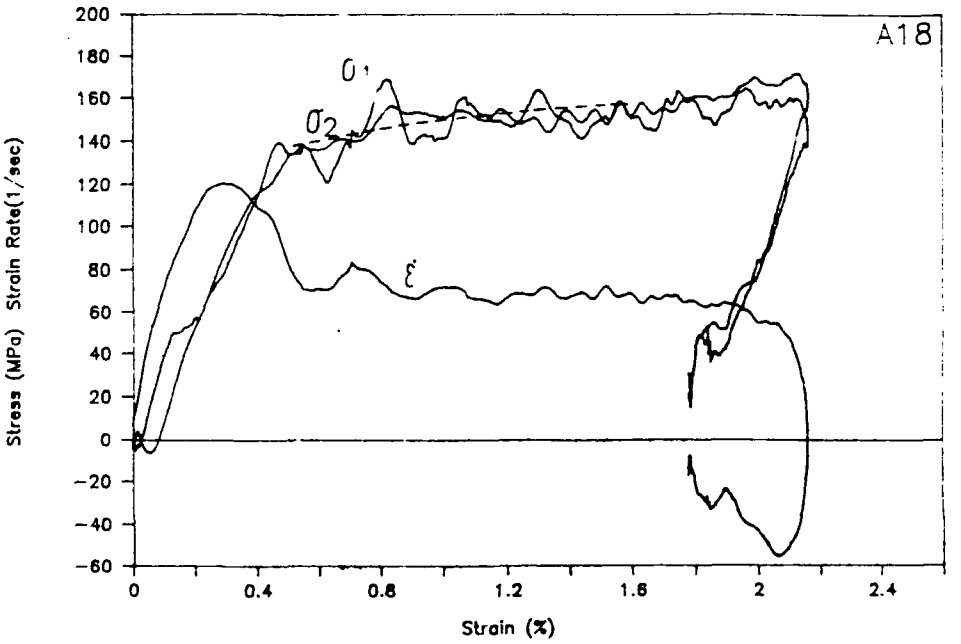

Figure 22. Example of Regression Fit by Equation (6) for Intermediate Confining pressure (Dashed Curve).

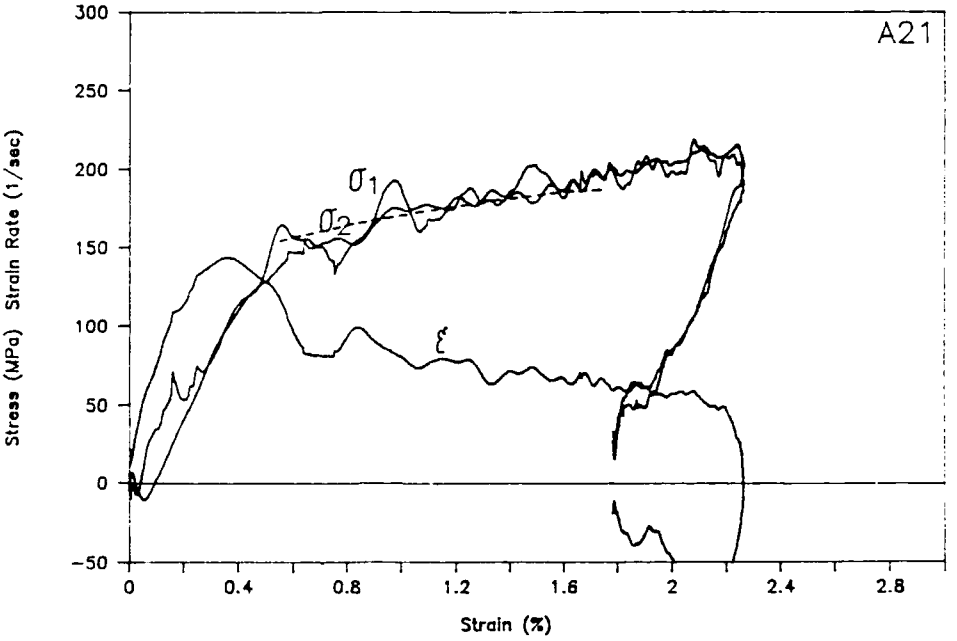

Figure 23. Example of Regression Fit by Equation (6) for Highest Pressure Group (Dashed Curve).

SECTION IV

CONCLUSIONS

A. DESIGN AND FABRICATION OF PRESSURE CELL

The principal objective of this investigation was to design and fabricate a hydraulic pressure cell and demonstrate that it would work satisfactorily for confined dynamic compressive testing of concrete in a Split Hopkinson Pressure Bar (SHPB) system. That objective was attained with a design that emphasized simplicity of fabrication and use. The pressure cell was designed for a maximum operating pressure of 3000 psi (20.7 MPa) with a factor of safety of 10. Water was chosen as the hydraulic fluid because of the possibility of spills and leakage in the dynamic testing environment. This choice had the added advantage of avoiding the chemical interaction of some hydraulic fluids with the latex membranes used to protect the specimen.

The peripheral systems included a device for applying and measuring a static axial preload to the specimen, a manually operated test pump with pressure gauge for setting the initial hydraulic pressure, and a semiconductor pressure transducer in the pressure cell to record the transient pressure rise during a test by means of a digital oscilloscope. The lateral pressure increases during a test because of the lateral expansion of the deforming specimen. By trapping the air initially in the pressure cell in order to accommodate the volume expansion of the specimen by further compression of the air, the maximum pressure reached during the test was held to less than 1.5 times the initial pressure in most tests, although in 7 of the 21 confined tests the maximum pressure was between 1.54 and 1.81 times the initial value.

B. CONFINED TESTS OF WES 7-ksi (48.3-MPa) CONCRETE

A total of 21 confined dynamic compressive tests were performed with five levels of initial lateral confining pressure, from 500 psi (3.45 MPa) to 1500 psi (10.34 MPa). The main objective of this testing program was to demonstrate that the new system worked and could furnish information about the confined dynamic response of concrete. That objective was attained.

The testing program was too limited to furnish definitive conclusions about the dynamic response, but some trends may be noted. As expected, the confined response is quite different from the unconfined response, even with modest amounts of confining pressure. In the unconfined tests, except at very low impact speeds, the dynamic stress-strain curve rises to a peak followed by a rapid decrease almost to zero; no elastic recovery is seen at the end of the approximately 300 microsecond SHPB loading time, and the specimen is reduced to rubble. In the

confined tests, the specimen was always able to carry a significant amount of axial stress all the way to the end of the loading period, and an apparent elastic unloading (roughly parallel to the initial loading slope) was seen at the end of all 21 dynamic stress-strain curves, even when extensive damage was seen in the recovered specimens.

Intact specimens were recovered in 14 tests, although their lateral surfaces showed cracks. Five specimens had each been separated into two pieces by a diagonal crack, and two specimens showed fragmentation into more than two pieces. Ten of the 14 intact specimens showed approximately parallel lateral surface traces of a major diagonal crack similar to those in specimens which had been separated into two pieces. The diagonal surface cracks were inclined in the neighborhood of 30 degrees to the axial direction near the mid-length of the specimen, but at a larger angle near specimen ends, where end friction provided greater lateral constraint. These details of the final fracture into two pieces by a major diagonal crack are probably greatly dependent upon the size and end constraint conditions of the specimens. The initiation, propagation, and coalescence of cracks before they reach this final stage would be more indicative of the material response under confined loading, but this investigation did not include any measurements of these phenomena.

Only two of the dynamic stress-strain curves showed a peak stress followed only by strain softening, and these strain-softened at a much slower rate than in the unconfined tests, so that at the end of the SHPB loading time the stress was still more than 93 percent of the peak stress. Many of the stress-strain curves showed a first peak followed by a plateau or by a decreasing-stress region and then followed by another hardening region lasting to the end of the tests, where in most cases the final stress was higher than at the first peak. This second hardening region may be caused by the increasing lateral confining pressure during the test. For those cases where a major diagonal crack had formed, the increased hardening toward the end of the test may also be related to the propagation of the crack into the end regions of the specimen, where there is additional confinement caused by the end friction. Confirmation of these conjectures might be made by using a pressure cell with greater initial air space, so that the pressure would not increase so much during the test, and by reducing the end friction constraint.

The test results show a significant increase of strength with confining pressure. They also indicate that during the initial hardening regime before a peak or plateau is reached in the stress-strain curve, the hardening rate (slope of the stress-strain curve) increases with confining pressure, while the rate sensitivity decreases as the confining pressure increases. Some rate sensitivity is still present, however, except possibly in the highest pressure group.

SECTION V

RECOMMENDATIONS

A. PRESSURE CELL AND EXPERIMENTAL TECHNIQUE

The air volume space between the specimen and the chamber wall should be increased to allow the development of more "accumulator" type action when air is intentionally trapped in the chamber prior to pressurization. Even with the fairly small space available in the current design, lateral confinement pressure increases during the WES specimen tests have been limited to 20 to 80 percent. Doubling or tripling the space should allow even more effective smoothing of the pressure. Of course, additional buffering could also be accomplished by using an external accumulator, but the simplicity and proximity of the air-in-the-chamber method makes it the preferred approach.

The threaded end caps with their 8 thread per inch standard 60 degree threads require a considerable effort during tightening to compress the O-ring adequately. Also, it is somewhat awkward to immobilize the chamber during the tightening and loosening processes. The use of finer-pitch threads, say 12 threads per inch, should decrease the tightening torque to an acceptable level. Excessively fine threads should be avoided because of the danger of cross threading and stripping. The incorporation of spanner wrench slots into the chamber body, perhaps adjacent to the threaded section on each end, should result in more convenient assembly/disassembly. The wall thickness in these areas would have to be increased to allow for the slots.

The method for isolating the specimen from the pressurized water used in this study, although adequate, is considered to be unduly complicated and labor-intensive. With a sufficiently tough membrane material, it should be possible to eliminate the epoxy and aluminum tape application.

A chamber design to be used on a 2-inch-diameter SHPB could be easily adapted from the basic design provided here and incorporating the recommended changes. A somewhat shorter chamber (8 inches overall) could probably be used on existing equipment at AFESC.

B. RECOMMENDATIONS FOR FURTHER TESTING

An investigation of the internal crack distributions after various amounts of deformation is desirable. Since many of the confined specimens are recovered intact or in two pieces, they could be sectioned and micrographically examined to determine the crack distribution. A successful preliminary investigation of

this kind on unconfined specimens was reported in Reference 33 for which the tests were interrupted by a steel collar around the specimen in order to recover intact specimens. The amount of deformation in the confined tests can be controlled by varying the impact speed. The amount of deformation could also be controlled by varying the loading time by changing the length of the striker bar of the SHPB system, but this latter procedure would be time consuming and labor intensive.

Some indications of the timing of the major crack development might be obtained from strain gages and/or crack gages mounted on the lateral surface. Use of one or more circumferential strain gages would also give a transient record of the lateral expansion of the specimen.

The pressure rise during the test could be reduced even more by a modified design with a larger initial air volume in the pressure cell.

Increasing the magnitude of the static axial preload, so that the initial confinement state is more nearly hydrostatic, might also seem desirable. To achieve an initial hydrostatic state for the 3-inch (76.2-mm) diameter specimen at the highest level of lateral pressure used in these tests would, however, require an axial preload force of more than 10,000 lb (44.5 kN), which would require major changes in the preload procedure. The simple system used in these tests was designed only to provide sufficient preload to hold the specimen in place and to prevent the latex membrane from being forced into the bar/specimen interfaces when the lateral pressurization was applied. Axial preloads used were only 500 to 600 lb (2.22 to 2.67 kN), as shown in Tables A-1 to A-5. Because both the lateral pressure and the axial stress are monitored during the dynamic event, it is possible to determine the point early in the rise time of the dynamic axial loading at which the stress state becomes hydrostatic and to reference the subsequent response to the hydrostatic state so that there should be no need for static preloading to the hydrostatic state.

REFERENCES

1. D. McHenry and J. J. Shideler, "Review of Data on Effect of Speed in Mechanical Testing of Concrete," ASTM STP 185, 72-82, 1956.

2. D. Watstein, "Effect of Straining Rate on the Compressive Strength and Elastic Properties of Concrete," ACI Journal, 24, 729-744, 1953.

3. W. Goldsmith, M. Polivka and T. Yang, "Dynamic Behavior of Concrete," Experimental Mechanics, 66, 65-69, 1966.

4. W. Goldsmith, V. H. Kenner and T. E. Ricketts, "Dynamic Loading of Several Concrete-Like Mixtures," Proc. ASCE, J. Structural Division, 94, ST7, 1803-1827, 1968.

5. D. L. Birkimer and R. Lindemann, "Dynamic Tensile Strength of Concrete Materials," ACI Journal, Proc., 68 , 47-49, and Supplement No. 68-8, 1971.

6. G. R. Griner, "Dynamic Properties of Concrete," Master's Thesis, University of Florida, 1974.

7. G. R. Griner, R. L. Sierakowski and C. A. Ross, Bulletin No. 45, The Shock and Vibration Information Center, NRL, Washington D.C., June 1974.

8. R. L. Sierakowski, L. E. Malvern, J. A. Collins, J. E. Milton and C. A. Ross, "Penetration Impact Studies of Soil/Concrete," Final Report, AFOSR Grant No. 77-3029 and AFAL TR-78-9, University of Florida, Gainesville, Florida, 109-110, November 30, 1977.

9. H. E. Read and C. J. Maiden, "The Dynamic Behavior of Concrete," Topical Report 3 SR-707, Systems, Science and Software, La Jolla, California, August 1971.

10. V. G. Gregson, "A Shock Wave Study of Fondu-Frye WA-1 and a Concrete," General Motors Materials and Structures Laboratory, Report MSL-70-30, 1971.

11. H. Green, "Impact Strength of Concrete," Institution of Civil Engineers, Proc., 28, 361-396, 1964.

12. B. P. Hughes and R. Gregory, "The Impact Strength of Concrete Using Green's Ballistic Pendulum," Institution of Civil Engineers, Proc., 81, 731-740, 1968.

13. B. L. Atchley and H. L. Furr, "Strength and Energy Absorption Capabilities of Plain Concrete Under Dynamic and Static Loading," ACI Journal, 745-756, November 1967.

14. R. H. Seabold, "Dynamic Shear Strength of Reinforced Concrete Beams" - Part III, Technical Report R 695, Naval Civil Engineering Lab, Port Hueneme, California, September 1970.

15. B. P. Hughes and R. Gregory, "Concrete Subjected to High Rates of Loading in Compression," Magazine of Concrete Research, 24, 25-36, 1972.

16. B. P. Hughes and A. J. Watson, "Compressive Strength and Ultimate Strain of Concrete Under Impact Loading," Magazine of Concrete Research, 30, 189-199, 1978.

17. H. Kolsky, "An Investigation of the Mechanical Properties of Materials at Very High Rates of Loading," Proc. Phys. Soc. (London) Ser. B., 62, 676-704, 1949.

18. U. S. Lindholm, "Some Experiments with the Split Hopkinson's Pressure Bar," J. Mech. Phys. Solids, 12, 317-335, 1964.

19. U. S. Lindholm and L. M. Yeakley, "High Strain-rate Testing: Tension and Compression," Experimental Mechanics, 8, 1-9, 1968.

20. T. Nicholas, "Material Behavior at High Strain Rates," in Impact Dynamics, eds. Zukas, J. A. et al. (Wiley, New York 1982), 277-332.

21. L. D. Bertholf and C. H. Karnes, "Two-dimensional analysis of the Split Hopkinson Pressure Bar System," Journal of the Mechanics & Physics of Solids, 23, 1-19, 1975.

22. B. Lundberg, "A Split Hopkinson Bar Study of Energy Absorption in Dynamic Rock Fragmentation," Int. J. Rock Mech. & Mining Sci. & Geomech. Abstr., 13, 187-197, 1976.

23. J. Bhargava and A. Rehnström, "Dynamic Strength of Polymer Modified and Fiber-Reinforced Concretes," Cement and Concrete Research 7, 199-208, 1977.

24. T. Tang, L. E. Malvern and D. A. Jenkins, "Dynamic Compressive Testing of Concrete and Mortar," Engineering Mechanics in Civil Engineering, eds. Boresi, A. P. and Chong, K. P., (ASCE, New York, 1984), 663-666.

25. L. E. Malvern, D. A. Jenkins, T. Tang and C. A. Ross, "Dynamic Compressive Testing of Concrete," Proc. Second Symposium on the Interaction of Non-Nuclear Munitions with Structures, Panama City Beach, Florida, April 15-19, 1985, pp. 194-199.

26. L. E. Malvern, T. Tang, D. A. Jenkins and J. C. Gong, "Dynamic Compressive Strength of Cementitious Materials,", Materials Research Society, Symposium Proceedings, Vol. 64, 119-138, 1986.

27. L. E. Malvern, D. A. Jenkins, E. Jerome and J. C. Gong, Dispersion Correction for Split-Hopkinson Pressure Bar Data, Final Report No. ESL-TR-88-04, Air Force Engineering and Services Center, Tyndall AFB, Florida.

28. J. C. Gong and L. E. Malvern, "Dispersion Investigation in the Split Hopkinson Pressure Bar," accepted (1989) for publication in Journal of Engineering Materials and Technology, ASME.

29. C. W. Felice, The Response of Soil to Impulse Loads Using the Split-Hopkinson's Pressure Bar Technique, Ph. D. Dissertation, The University of Utah, 1985.

30. P. S. Follansbee and C. Frantz, "Wave Propagation in the Split Hopkinson Pressure Bar," ASME Journal of Engineering Materials and Technology, 105, 61-66, 1983.

31. H. A. Kormeling, A. J. Zielinski and H. W. Reinhardt, "Experiments on Concrete Under Single and Repeated Impact Loading," Report No. 5-80-3, Delft University of Technology, Stevin Laboratory, May 1980.

32. C. A. Ross, Split-Hopkinson Pressure Bar Tests, ESL-TR-88-82, Air Force Engineering and Services Center, Tyndall AFB, Fl., September 1988.

33. L. E. Malvern, D. A. Jenkins, T. Tang and J. C. Gong, "Dynamic Testing of Concrete with the Split Hopkinson Pressure Bar," Proc., Fourth International Symposium on the Interaction of Non-nuclear Munitions with structures, Panama City Beach, FL., April 17-21, 1989, pp. 296-301.

34. C. A. Ross, S. T. Kuennen and W. S. Strickland, "High Strain Rate Effects on Tensile Strength of Concrete," ibid 302-308.

35. J. W. Tedesco, C. A. Ross, R. M. Brunair, "Inelastic Analysis of the Dynamic Split Cylinder Test," ibid 309-314.

36. W. Suaris and S. P. Shah, "Mechanical Properties of Materials Subject to Impact," RILEM-CEB-IABSE-Interassociation Symposium on Concrete Structures Under Impact and Impulsive Loading, 33-62, Berlin, 1982.

37. G. C. Hoff, "Selected Bibliography on Fiber-Reinforced Cement and Concrete, Supplement No. 2," Miscellaneous paper C-76-6, U. S. Army Waterways Experiment Station, Vicksburg, Mississippi, 1979.

38. L. A. Glenn and W. Janach, "Failure of Granite Cylinders Under Impact Loading," International Journal of Fracture, 13, 301-317, 1977.

39. C. Young and C. N. Powell, "Lateral Inertia Effects on Rock Failure in Split Hopkinson-Bar Experiments," 20th U. S. Symposium on Rock Mechanics, 1979.

40. D. W. Hobbs, "Failure Criteria for Concrete", Chapter 10 of Handbook of Structural Concrete, Pitman Books Ltd., 1983.

41. K. H. Gerstle et al., "Behavior of concrete under Multiaxial Stress States," Journal of the Engineering Mechanics Division, ASCE, vol. 106, EM6, pp. 1383-1403, 1980.

42. R. Palaniswamy and S. P. Shah, "Fracture and Stress-Strain Relationship of Concrete under Triaxial Compression," Journal of the Structural Division, ASCE, Vol. 100, ST5, pp. 901-916, 1974.

43. J. Takeda, H. Tachikawa and K. Fujimoto, Proceedings of the Symposium on the Mechanical Behavior of Materials, Kyoto, August 21-24, Vol. II, 479-486, 1984.

44. H. Yamaguchi and K. Fujmoto, "Strain Rate Effect on Stress-Strain Relationships of Concrete," Proc., Fourth International Symposium on the Interaction of Non-nuclear Munitions with Structures, Panama City Beach, Fl., April 17-21, 1989, pp. 290-295.

45. J. K. Gran, Y. M. Gupta and A. L. Florence, "An Experimental Method to Study the Dynamic Tensile Failure of Brittle Geologic Materials," Mechanics of Materials, Vol. 6, 1987, pp. 113-125.

46. J. K. Gran, A. L. Florence and J. D. Colton, "Dynamic Triaxial Tests of High-Strength Concrete," Journal of Engineering Mechanics, ASCE, Vol. 115, 1989, pp. 891-904.

47. R. J. Christensen, S. R. Swanson and W. S. Brown, "Split-Hopkinson-Bar Tests on Rock Under Confining Pressure," Experimental Mechanics, 12, 508-513, 1972.

48. U. S. Lindholm, L. M. Yeakley and A. Nagy, "The Dynamic Strength and Fracture Properties of Dresser Basalt," Int. J. Rock. Mech. & Mining Sci. & Geomech. Abstracts, 11, 181-191, 1974.

49. J. C. Gong and L. E. Malvern, "Passively Confined Tests of Axial Dynamic Strength of Concrete," accepted (1989) for publication in Experimental Mechanics.

APPENDIX

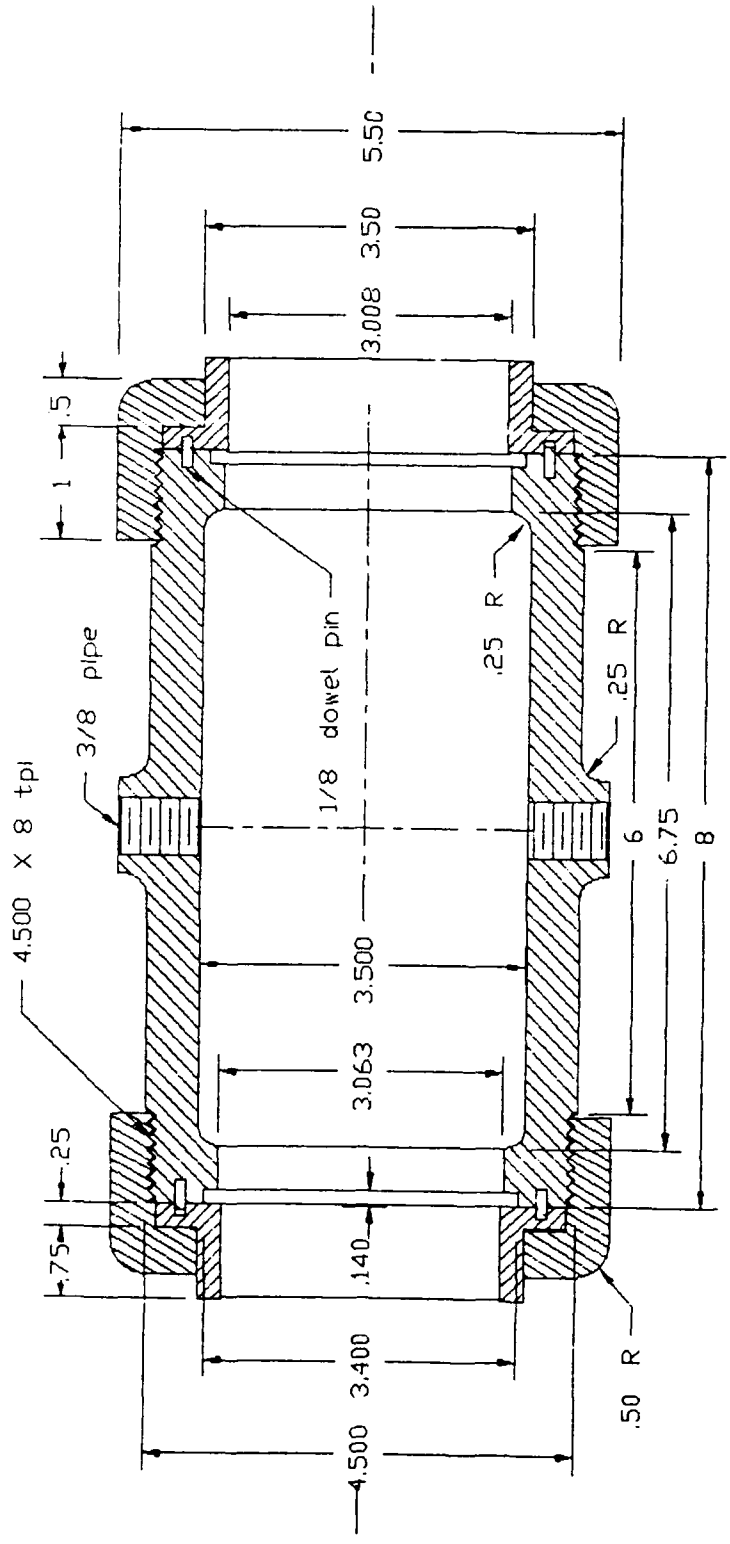

Figure A-1. Shop Drawing of Pressure Cell
(All Dimensions in Inches)

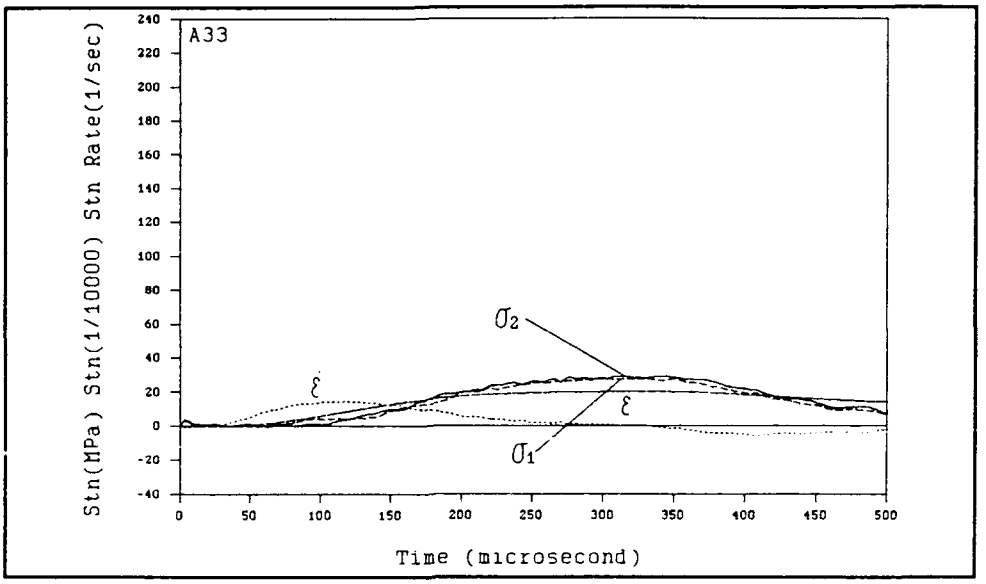

(a) Time Plots of Two Interface Stresses, Strain and Strain Rate.

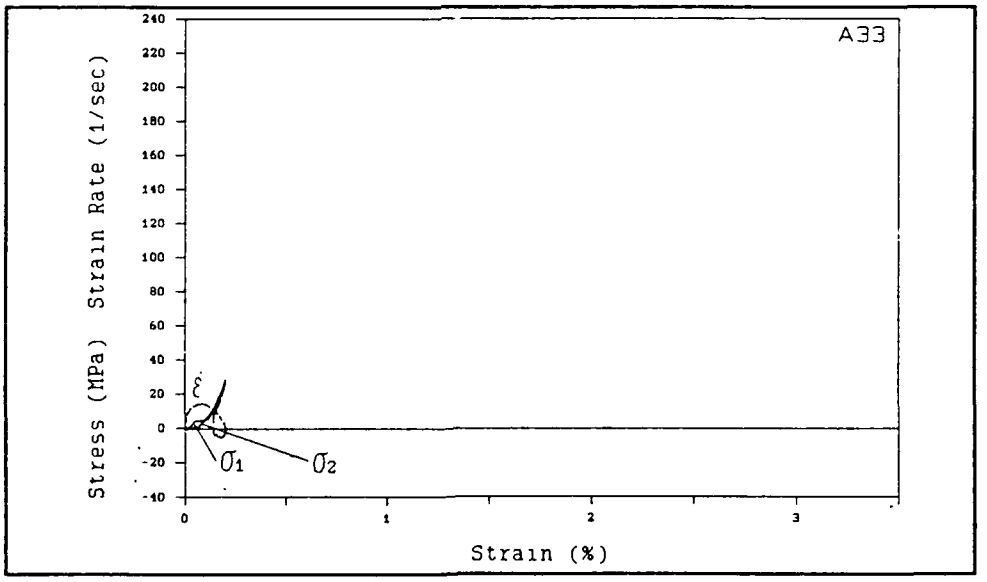

(b) Stress-Strain Curves and Strain Rate Versus Strain.

Figure A-2. Unconfined Test of Undamaged Specimen A33. Impact Speed 56.5 in/s (1.435 m/s).

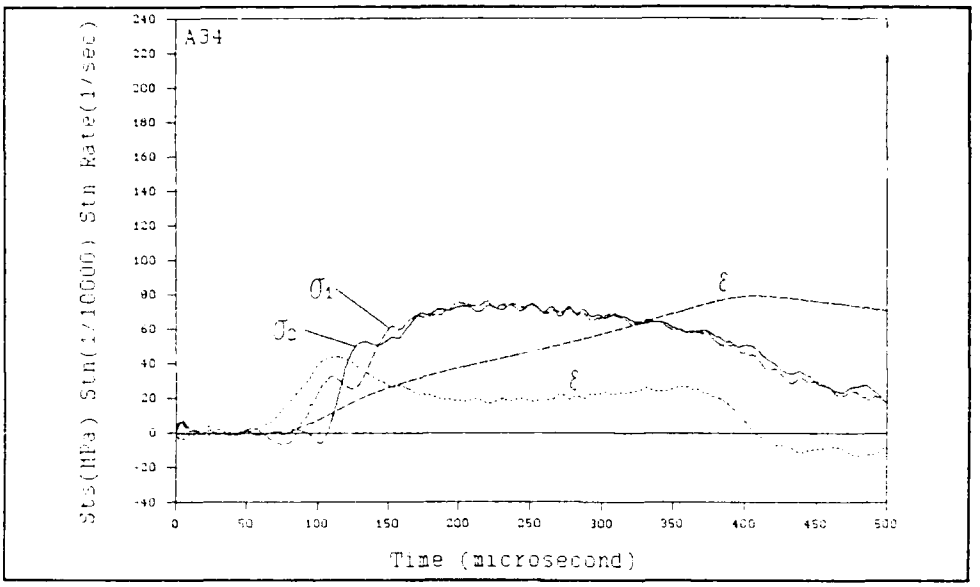

(a) Time Plots of Two Interface Stresses, Strain and Strain Rate.

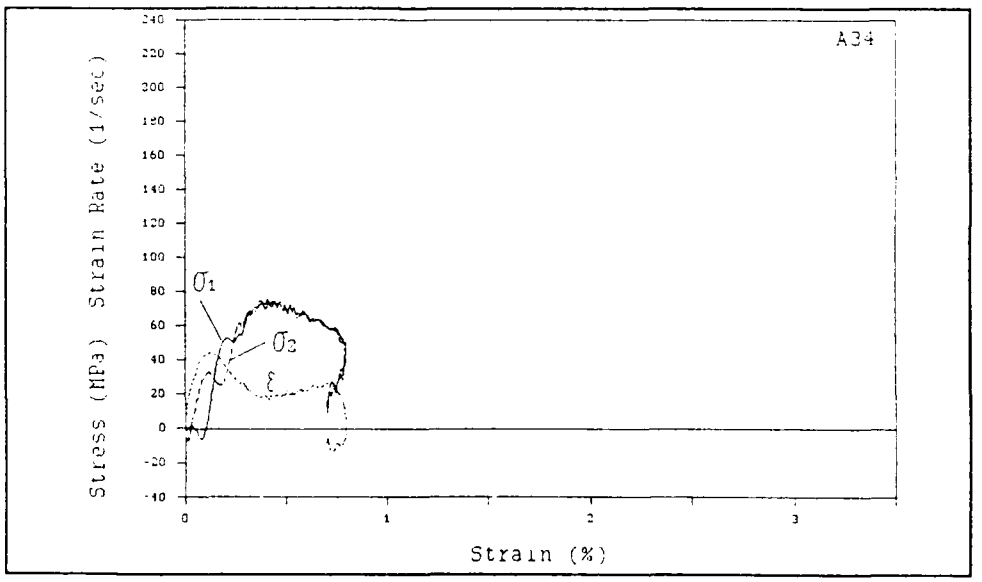

(b) Stress-Strain Curves and Strain Rate Versus Strain.

Figure A-3. Unconfined Test of Partially Intact Specimen A34. Impact Speed 200 in/s (5.08 m/s)

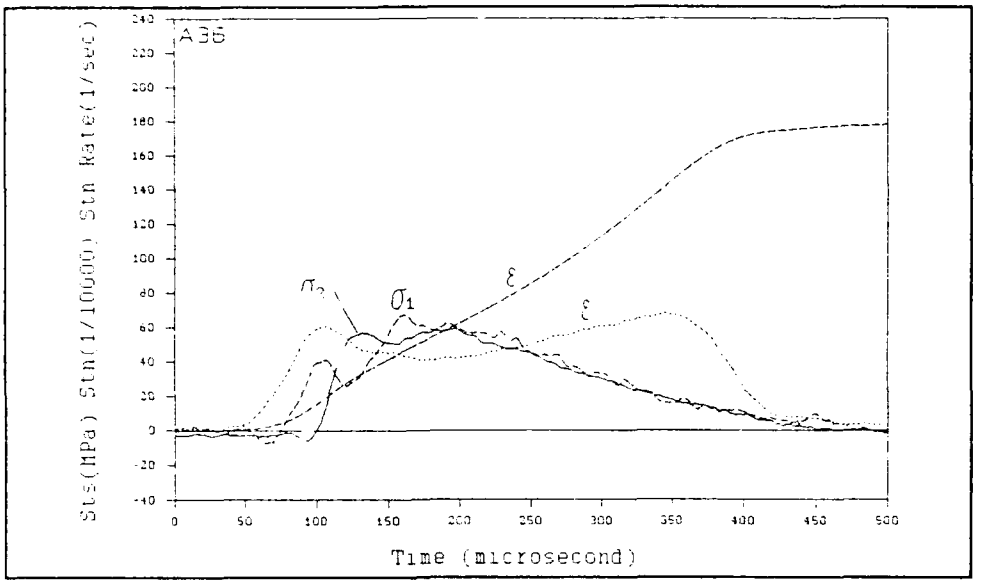

(a) Time Plots of Two Interface Stresses, Strain and Strain Rate.

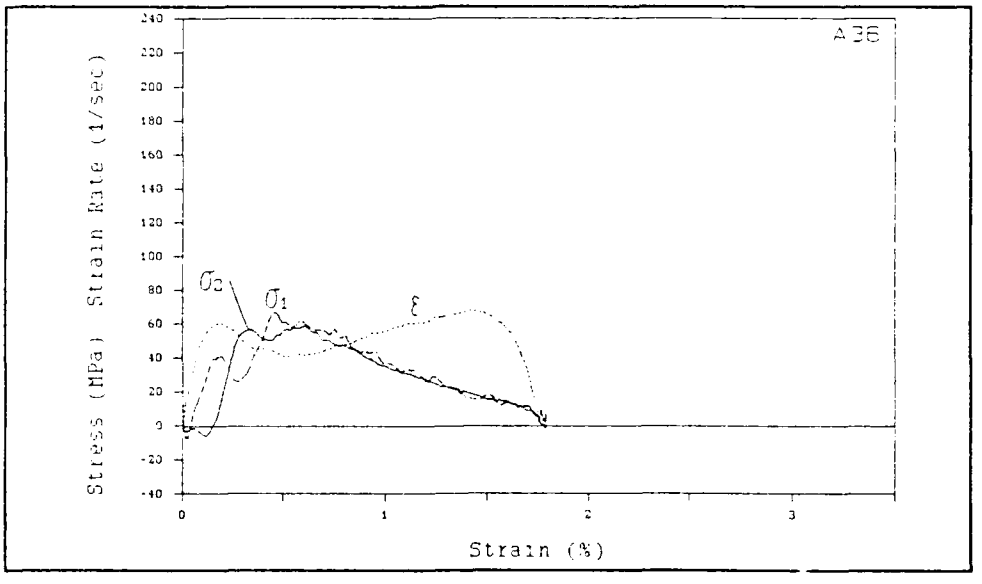

(b) Stress-Strain Curves and Strain Rate Versus Strain.

Figure A-4. Unconfined Test of Specimen A36. Impact Speed 242 in/s (6.15 m/s).

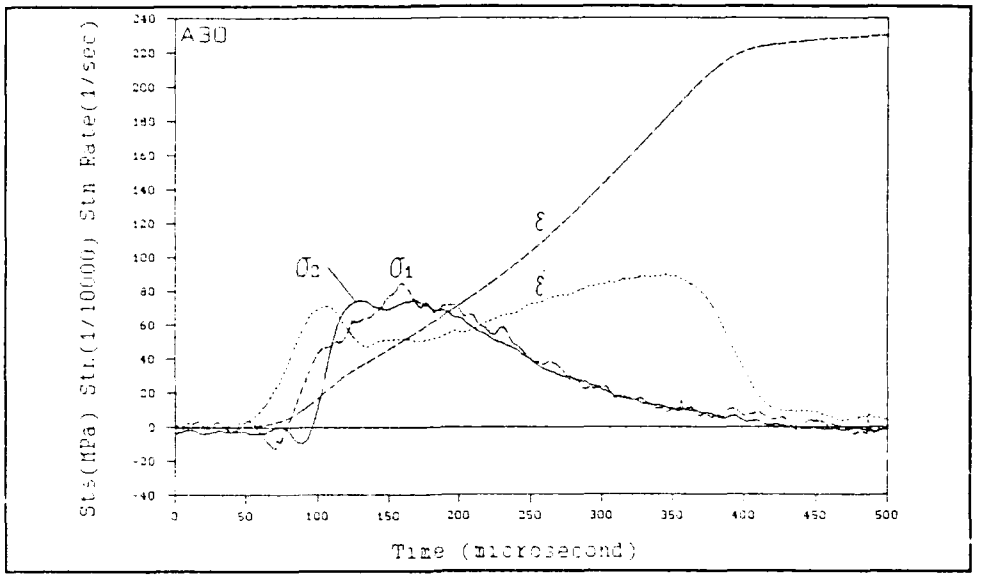

(a) Time Plots of Two Interface Stresses, Strain and Strain Rate.

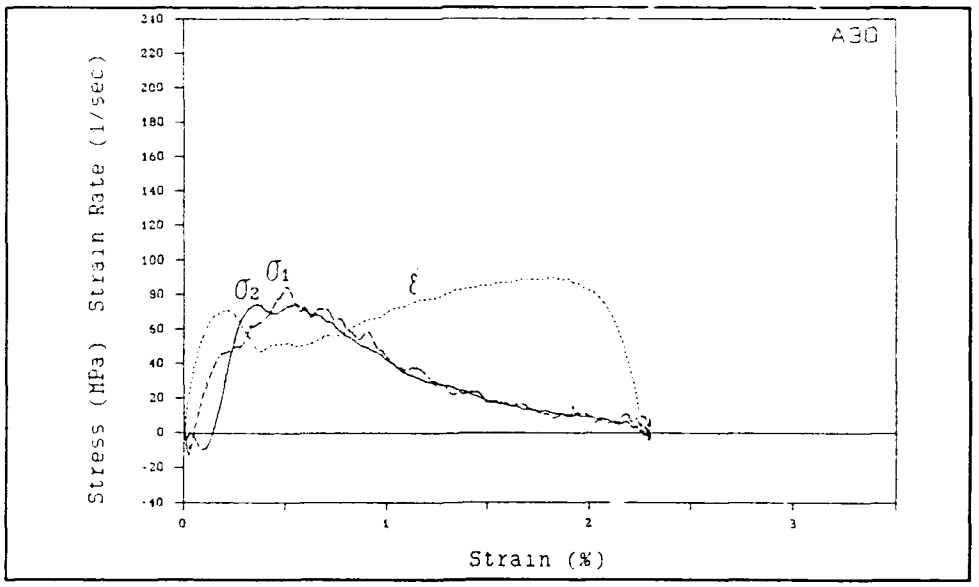

(b) Stress-Strain Curves and Strain Rate Versus Strain.

Figure A-5. Unconfined Test of Specimen A30. Impact Speed 300 in/s (7.62 m/s).

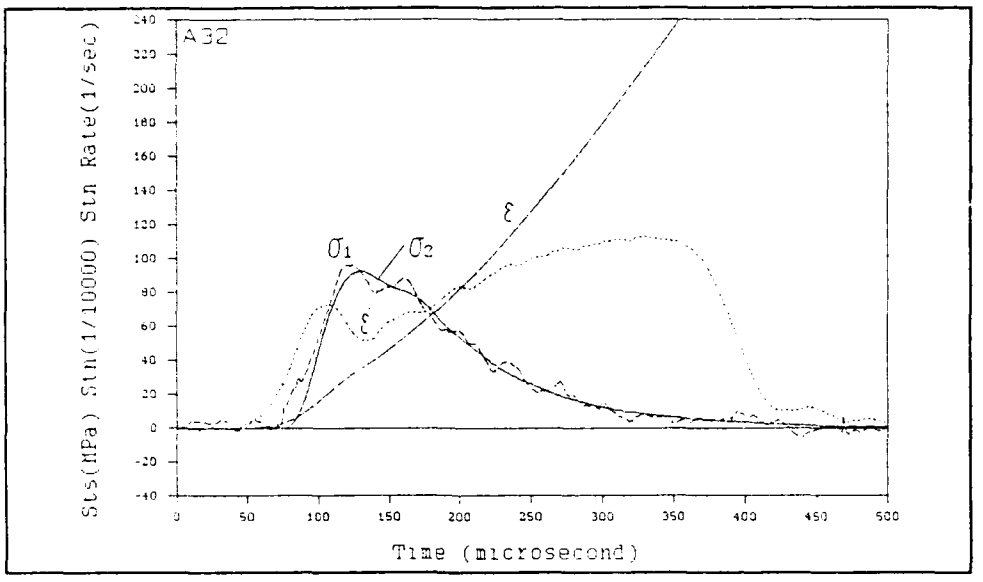

(a) Time Plots of Two Interface Stresses, Strain and Strain Rate.

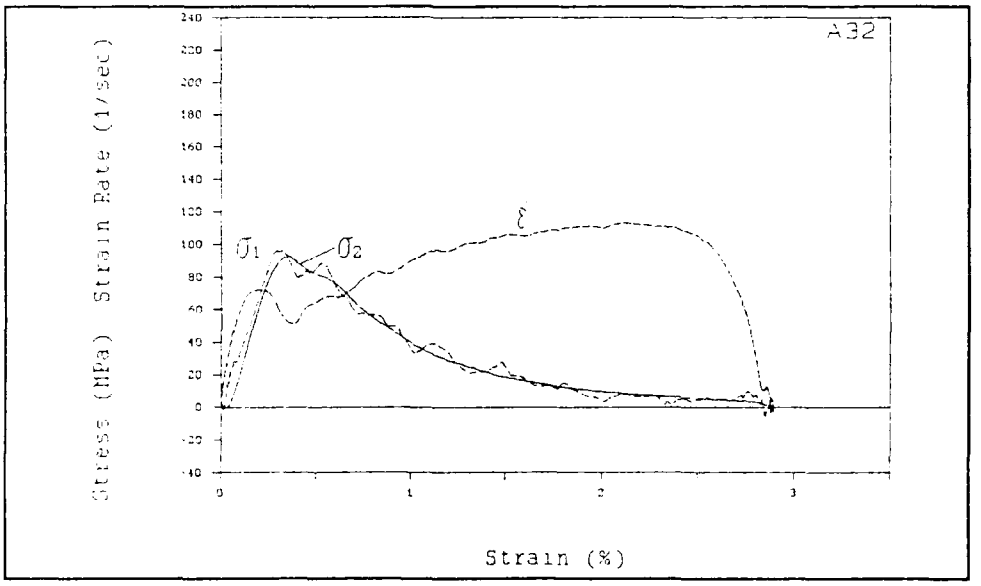

(b) Stress-Strain Curves and Strain Rate Versus Strain.

Figure A-6. Unconfined Test of Specimen A32. Impact Speed 352 in/s (8.94 m/s).

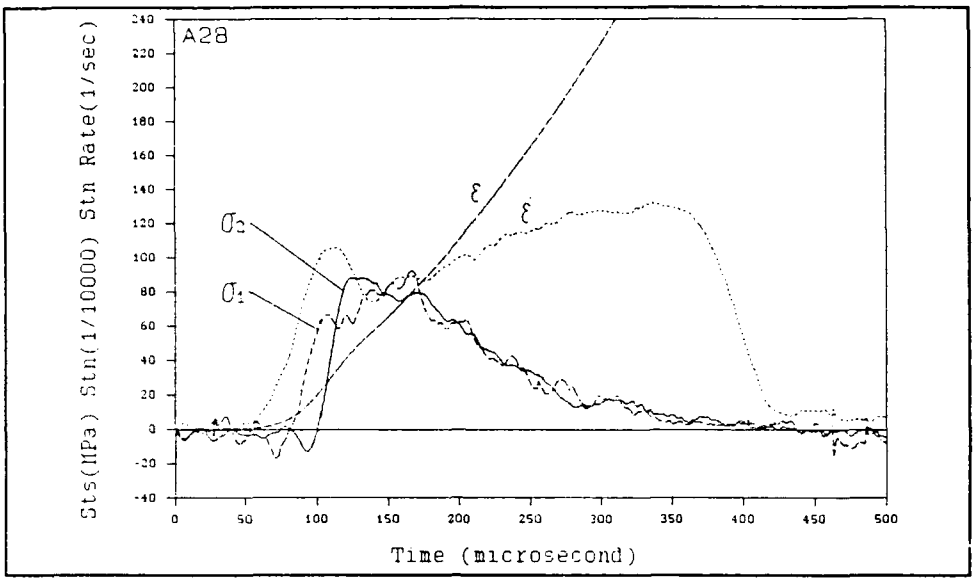

(a) Time Plots of Two Interface Stresses, Strain and Strain Rate.

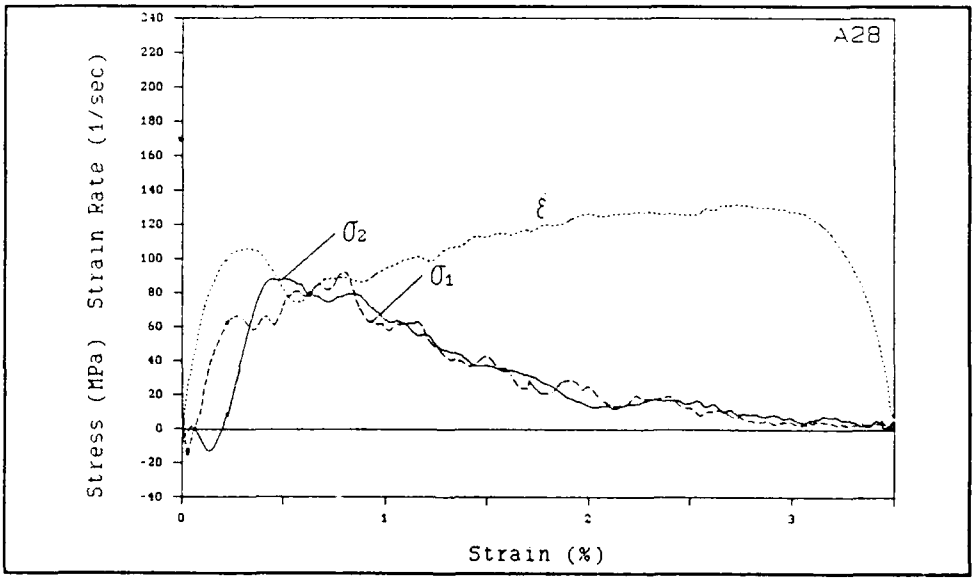

(b) Stress-Strain Curves and Strain Rate Versus Strain.

Figure A-7. Unconfined Test of Specimen A28. Impact Speed 412 in/s (10.46 m/s).

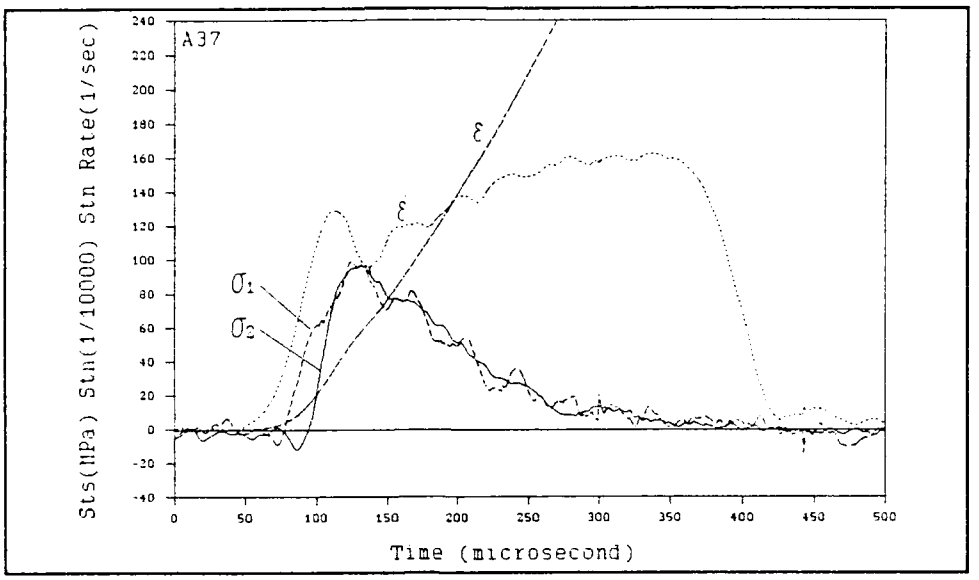

(a) Time Plots of Two Interface Stresses, Strain and Strain Rate.

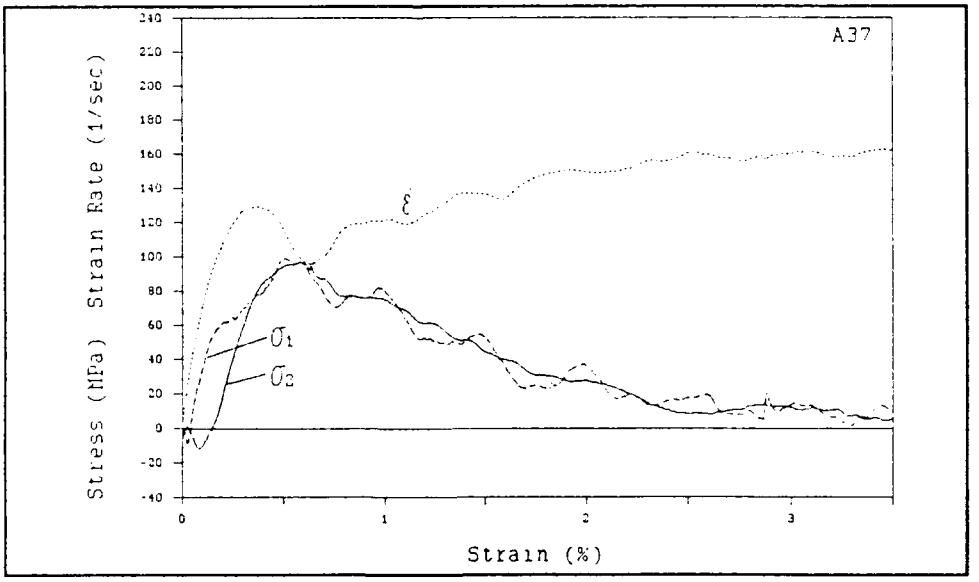

(b) Stress-Strain Curves and Strain Rate Versus Strain.

Figure A-8. Unconfined Test of Specimen A37. Impact Speed 502 in/s (12.75 m/s).

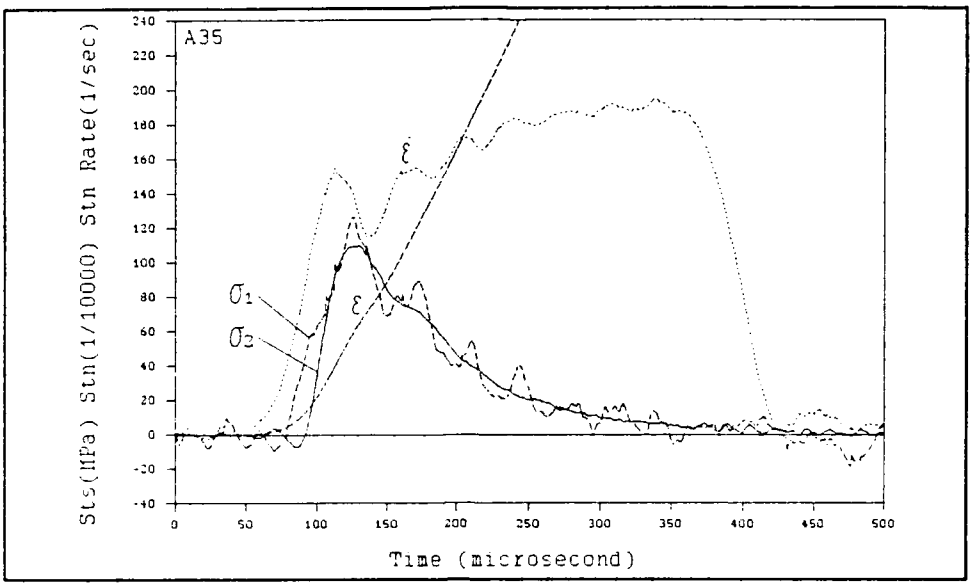

(a) Time Plots of Two Interface Stresses, Strain and Strain Rate.

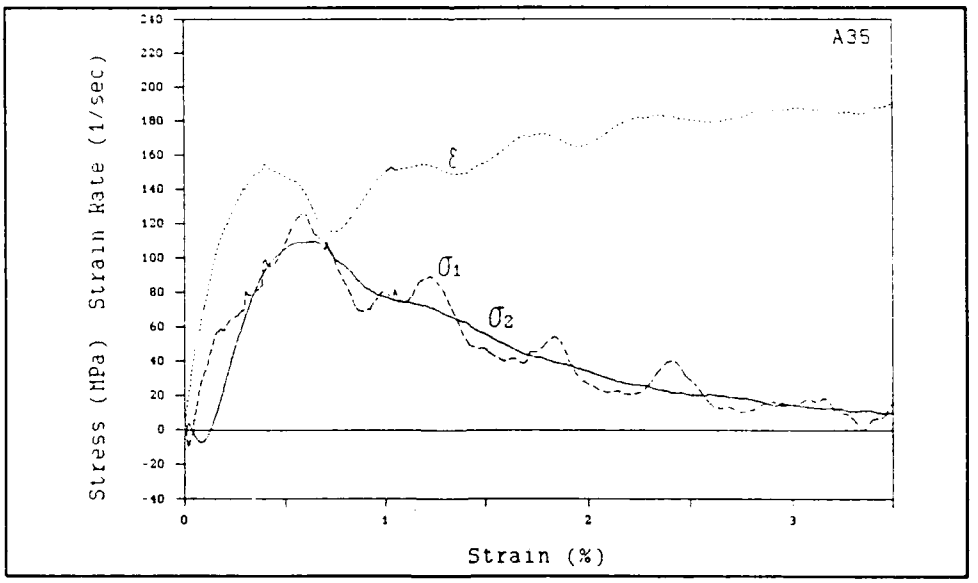

(b) Stress-Strain Curves and Strain Rate Versus Strain.

Figure A-9. Unconfined Test of Specimen A35. Impact Speed 585 in/s (14.86 m/s).

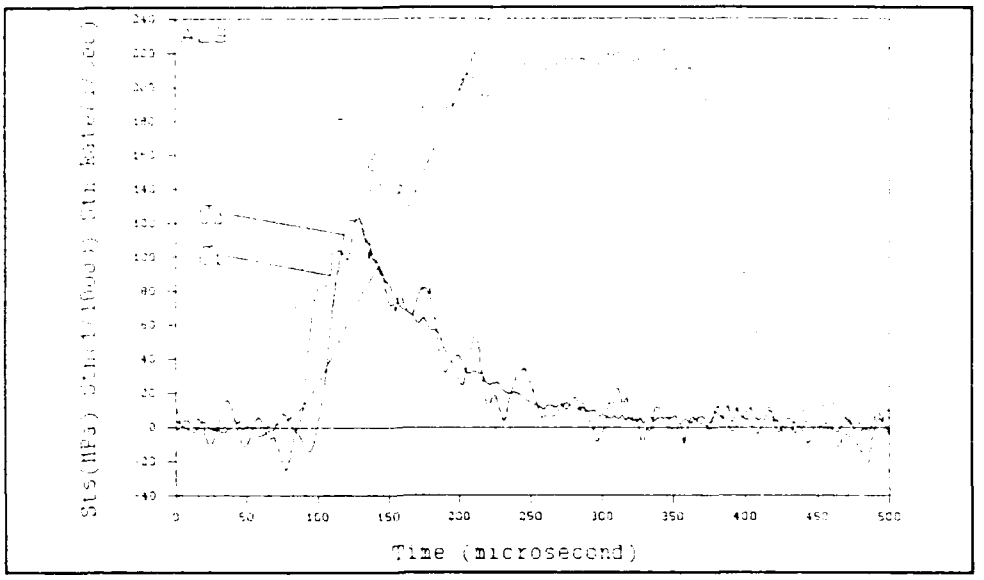

(a) Time Plots of Two Interface Stresses Strain and Strain Rate.

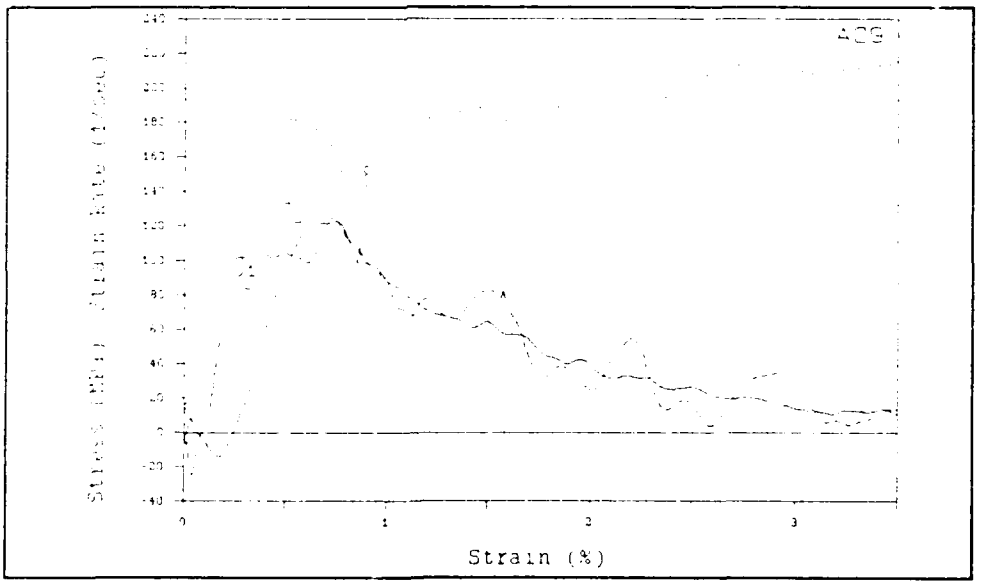

(b) Stress-Strain Curves and Strain Rate Versus Strain.

Figure A-10. Unconfined Test of Specimen A29. Impact Speed 666 in/s (16.92 m/s).

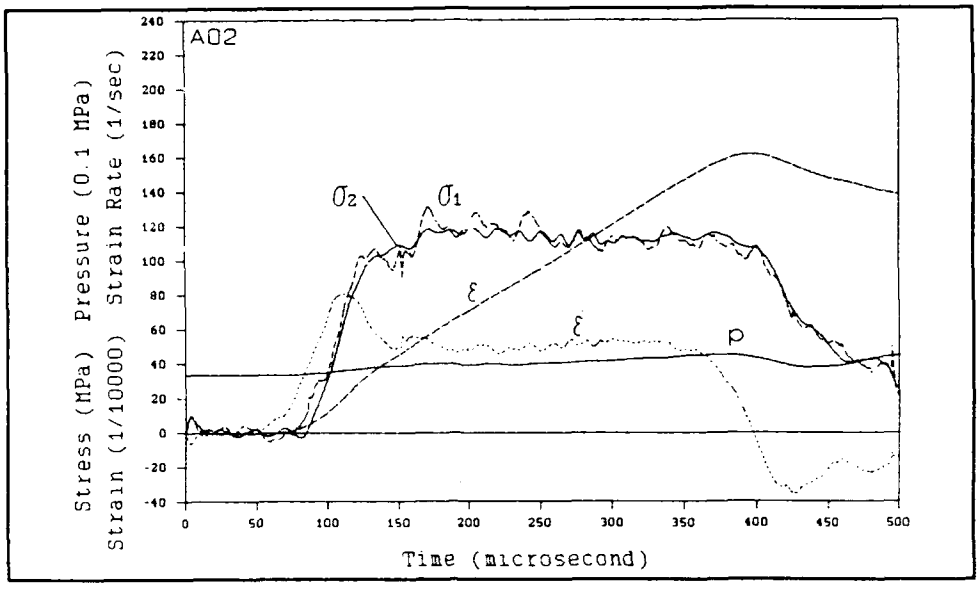

(a) Time Plots of Two Interface Stresses, Strain and Strain Rate.

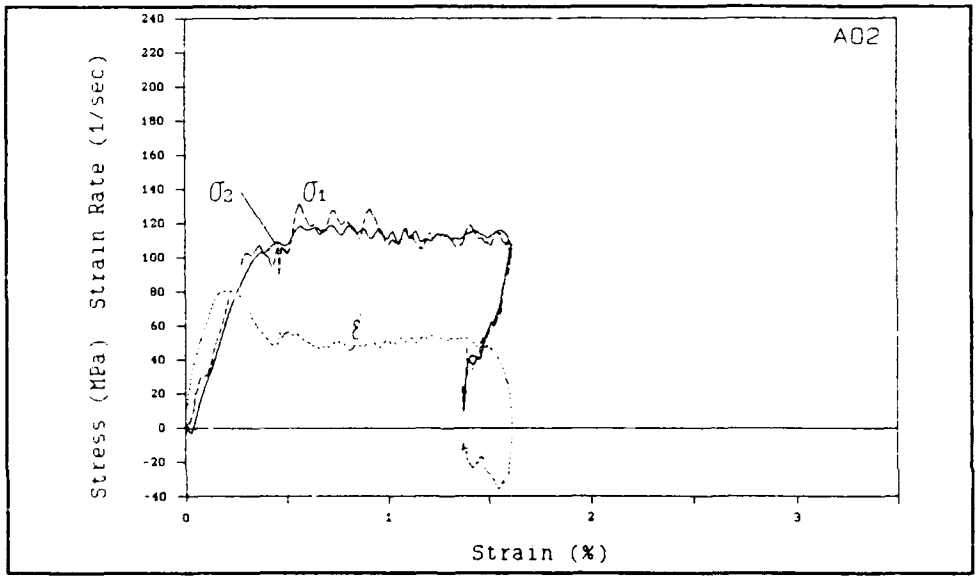

(b) Stress-Strain Curves and Strain Rate Versus Strain.

Figure A-11. Test of Specimen A02 with Initial Confining Pressure 3.35 MPa and Impact Speed 376 in/s (9.55 m/s).

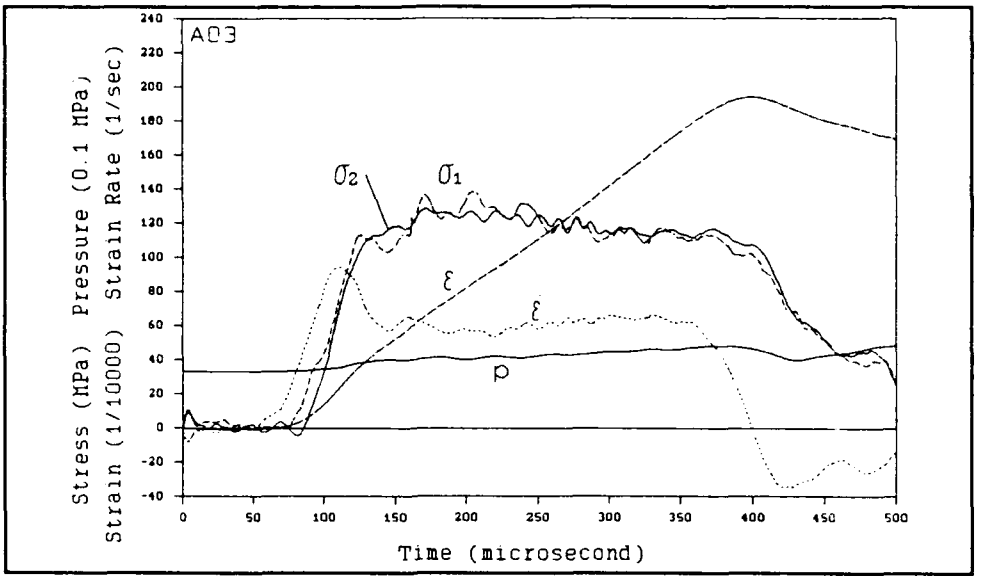

(a) Time Plots of Two Interface Stresses, Strain and Strain Rate.

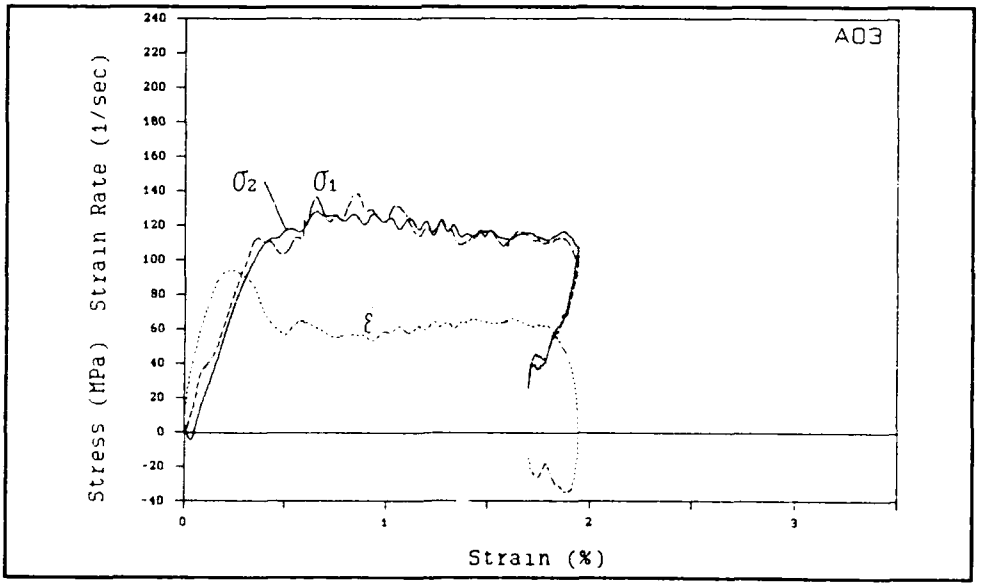

(b) Stress-Strain Curves and Strain Rate Versus Strain.

Figure A-12. Test of Specimen A03 with Initial Confining Pressure 3.32 MPa and Impact Speed 420 in/s (10.67 m/s).

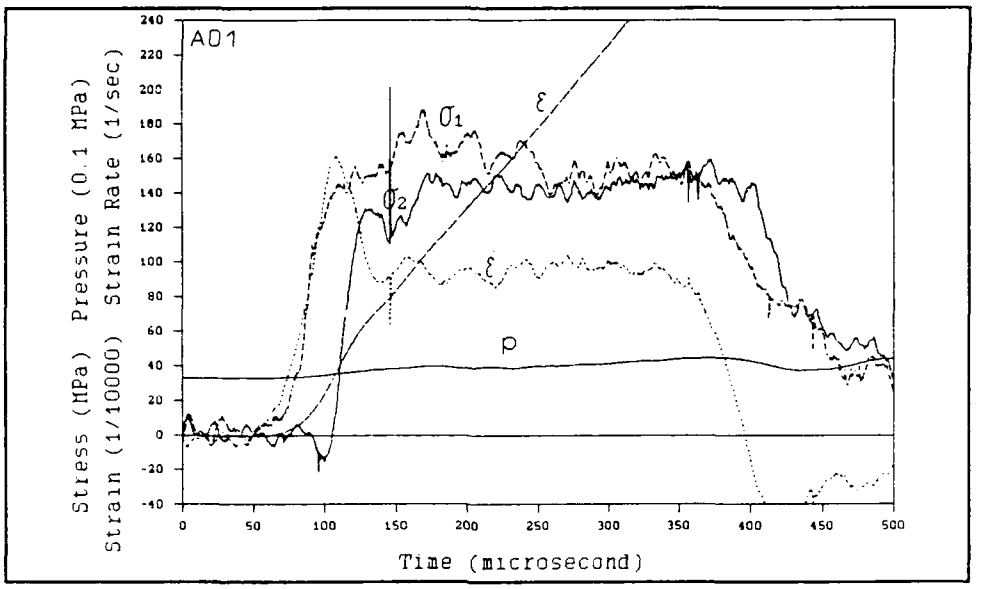

(a) Time Plots of Two Interface Stresses, Strain and Strain Rate.

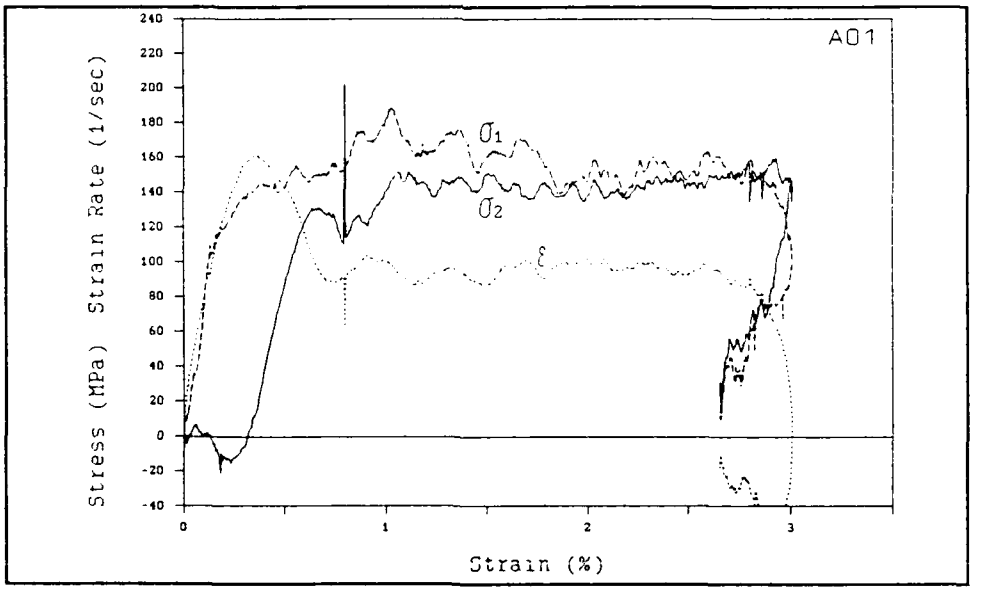

(b) Stress-Strain Curves and Strain Rate Versus Strain.

Figure A-13. Test of Specimen A01 with Initial Confining Pressure 3.32 MPa and Impact Speed 503 in/s (12.78 m/s).

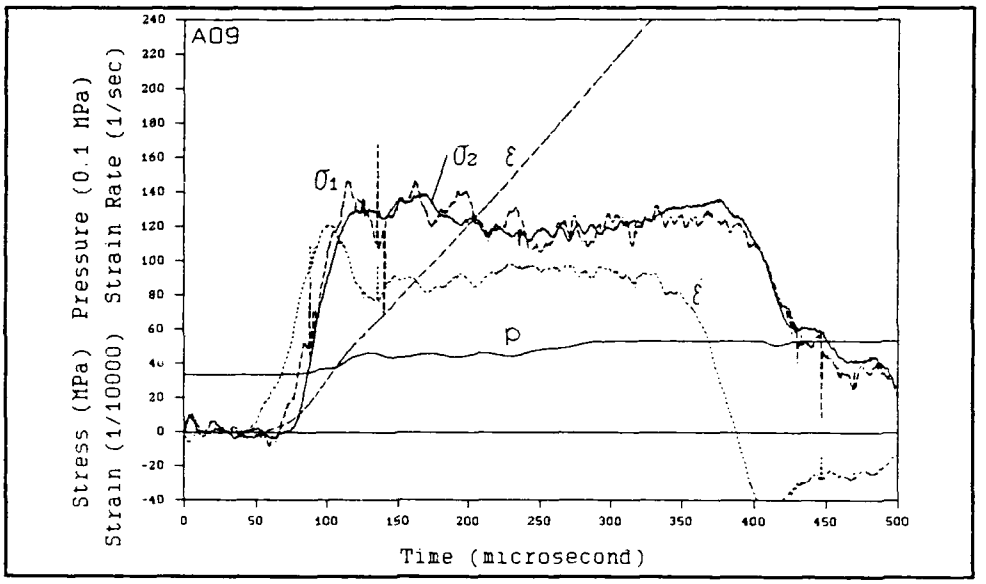

(a) Time Plots of Two Interface Stresses, Strain and Strain Rate.

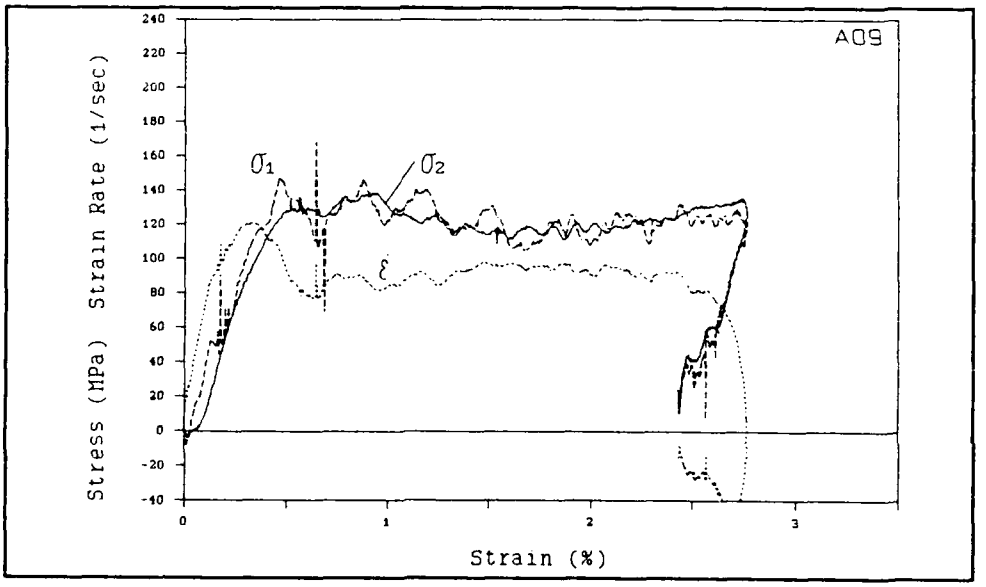

(b) Stress-Strain Curves and Strain Rate Versus Strain.

Figure A-14. Test of Specimen A09 with Initial Confining Pressure 3.36 MPa and Impact Speed 514 in/s (13.06 m/s).

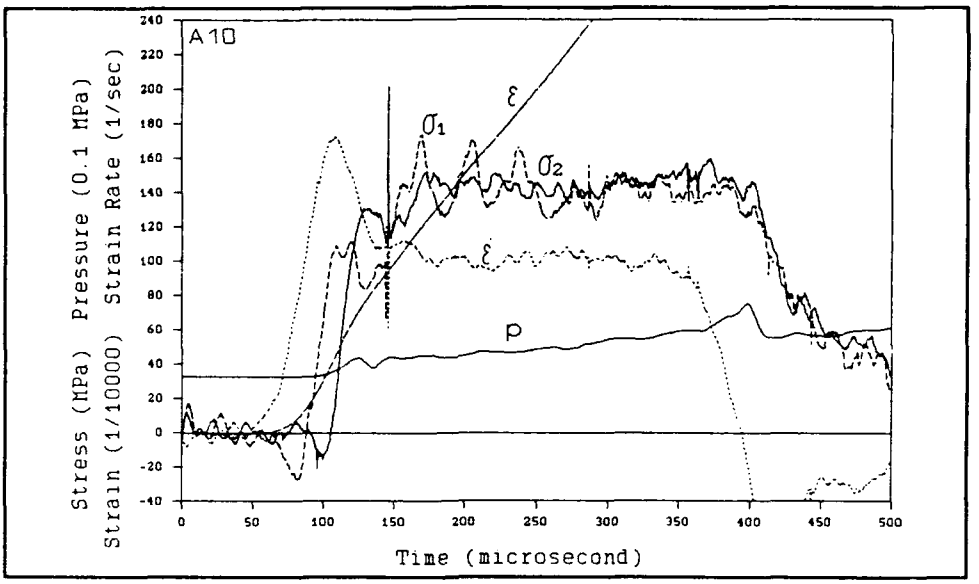

(a) Time Plots of Two Interface Stresses, Strain and Strain Rate.

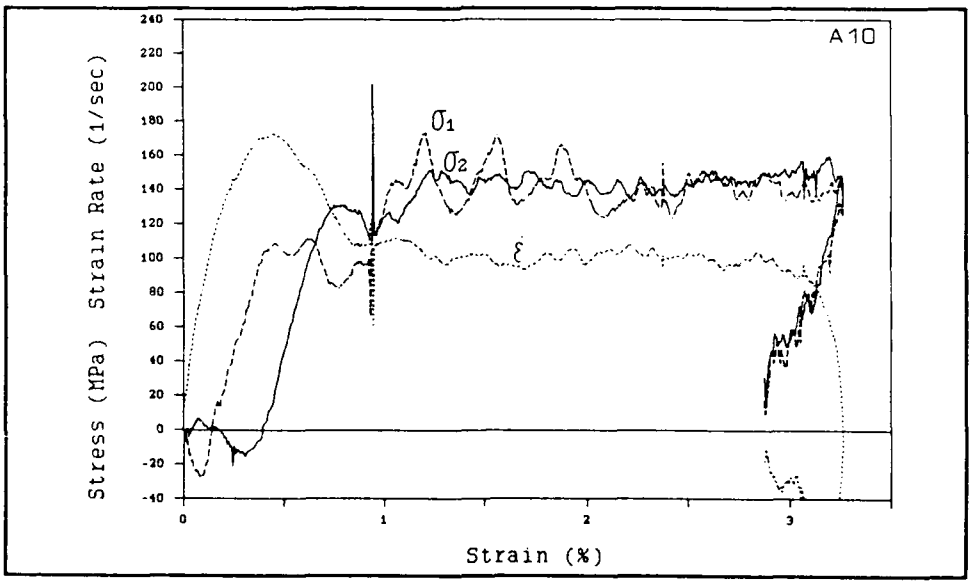

(b) Stress-Strain Curves and Strain Rate Versus Strain.

Figure A-15: Test of Specimen A10 with Initial Confining Pressure 3.26 MPa and Impact Speed 582 in/s (14.78 m/s).

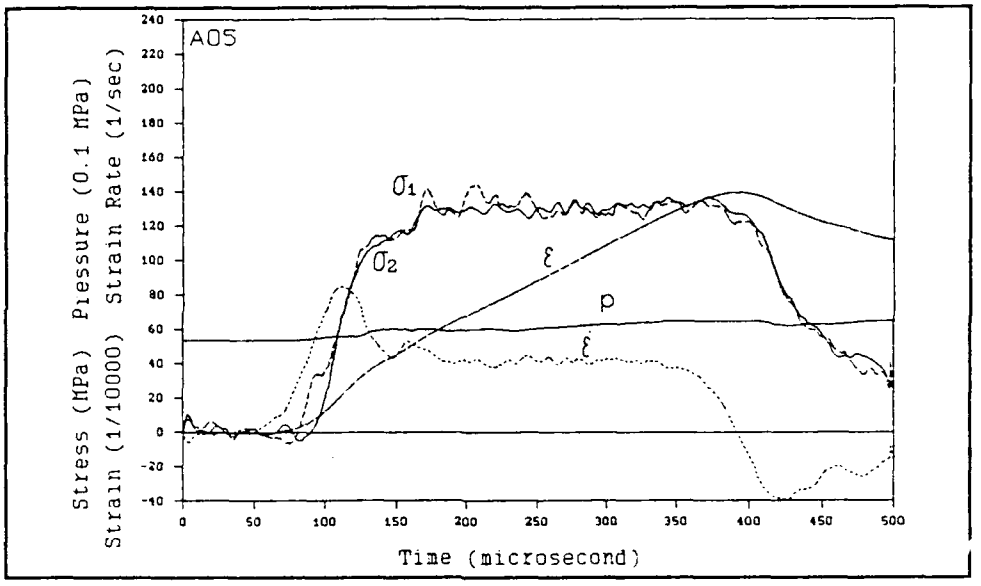

(a) Time Plots of Two Interface Stresses, Strain and Strain Rate.

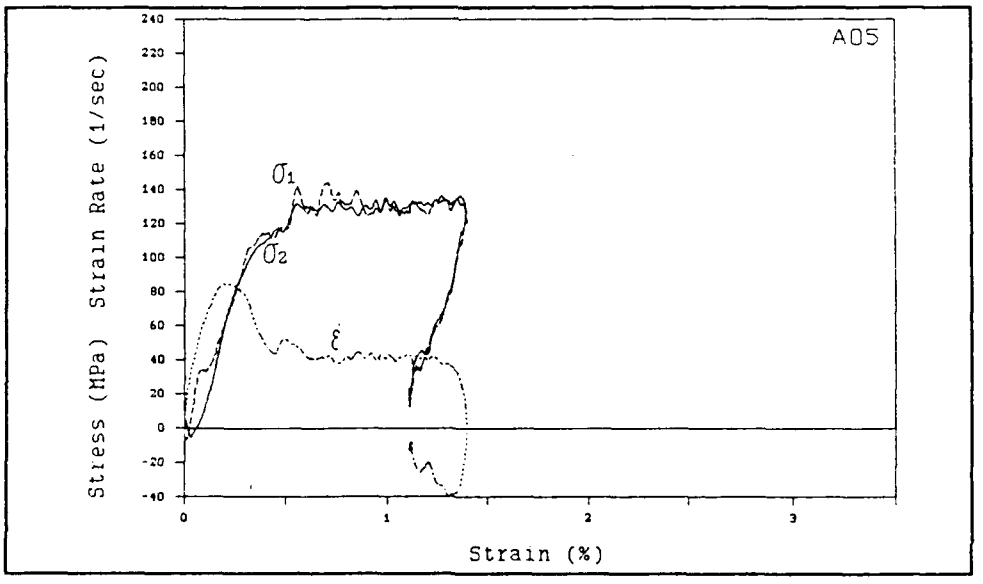

(b) Stress-Strain Curves and Strain Rate Versus Strain.

Figure A-16. Test of Specimen A05 with Initial Confining Pressure 5.34 MPa and Impact Speed 384 in/s (9.75 m/s).

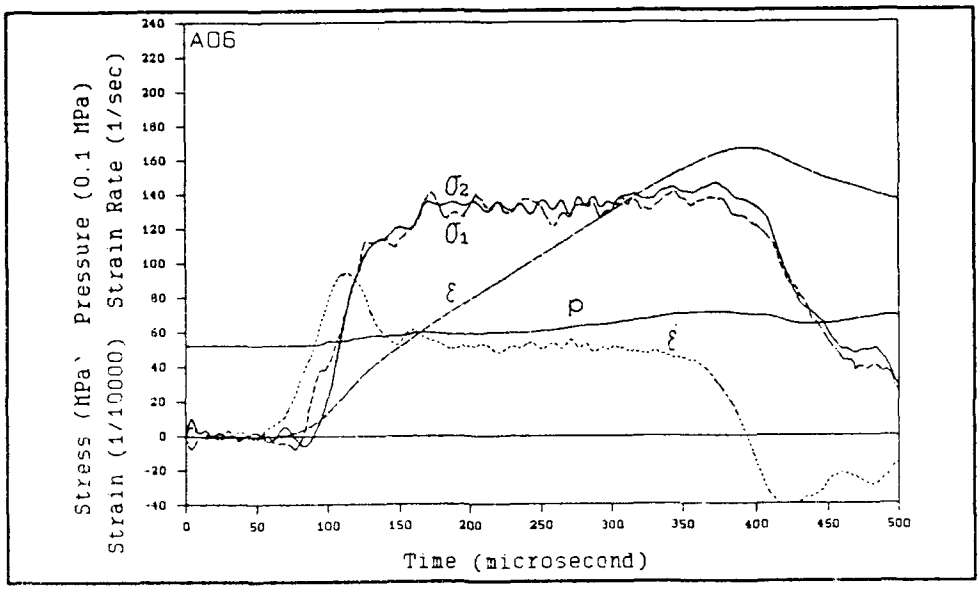

(a) Time Plots of Two Interface Stresses, Strain and Strain Rate.

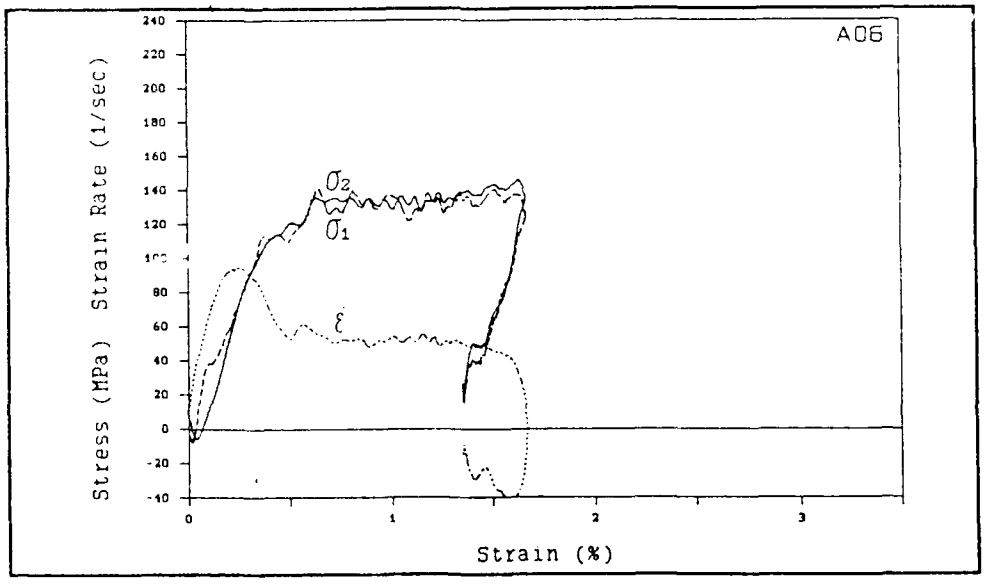

(b) Stress-Strain Curves and Strain Rate Versus Strain.

Figure A-17. Test of Specimen A06 with Initial Confining Pressure 5.19 MPa and Impact Speed 417 in/s (10.59 m/s).

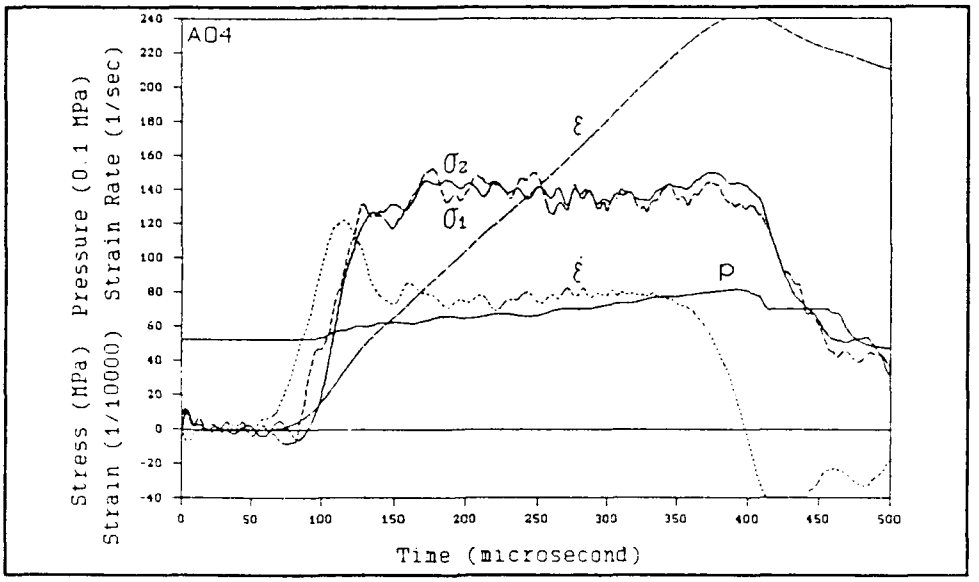

(a) Time Plots of Two Interface Stresses, Strain and Strain Rate.

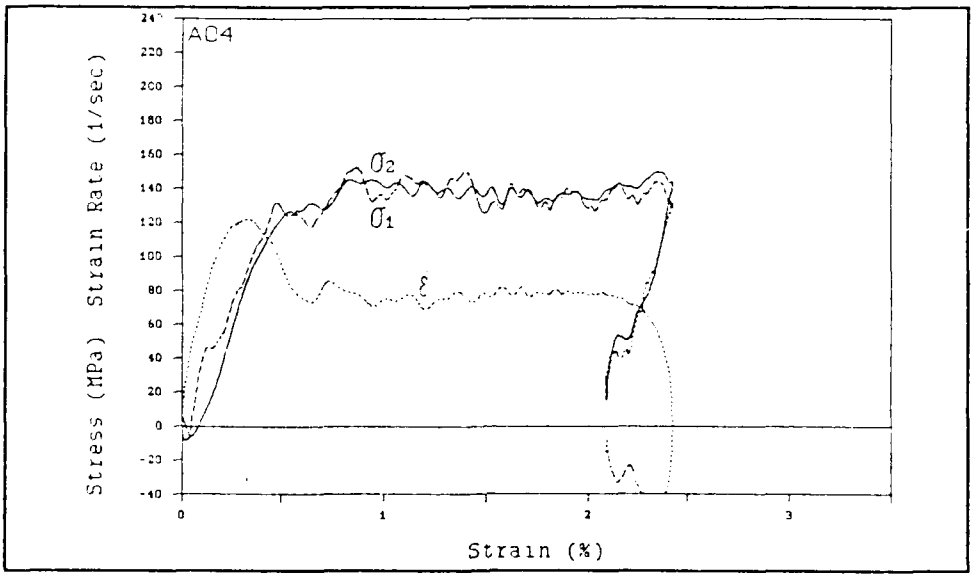

(b) Stress-Strain Curves and Strain Rate Versus Strain.

Figure A-18. Test of Specimen A04 with Initial Confining Pressure 5.23 MPa and Impact Speed 501 in/s (12.73 m/s).

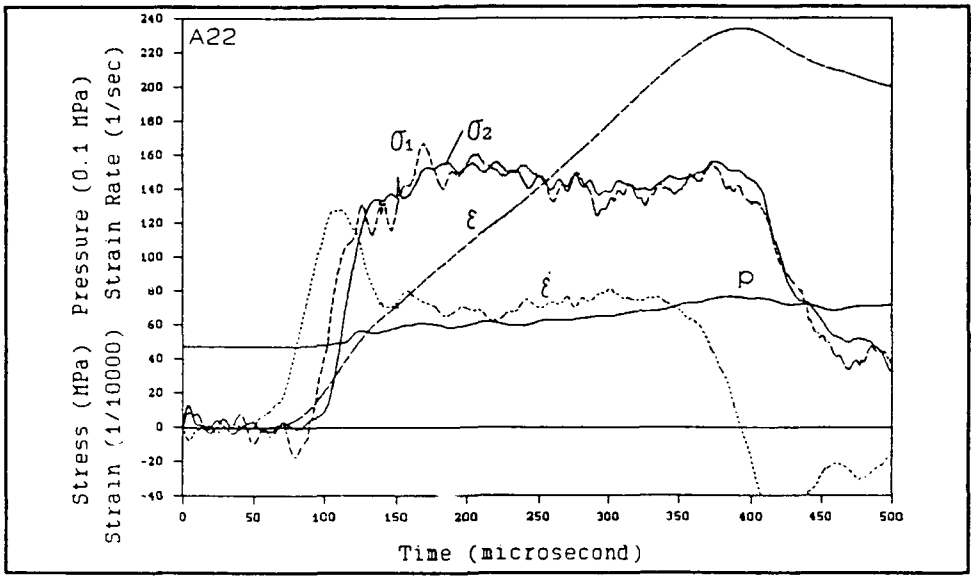

(a) Time Plots of Two Interface Stresses, Strain and Strain Rate.

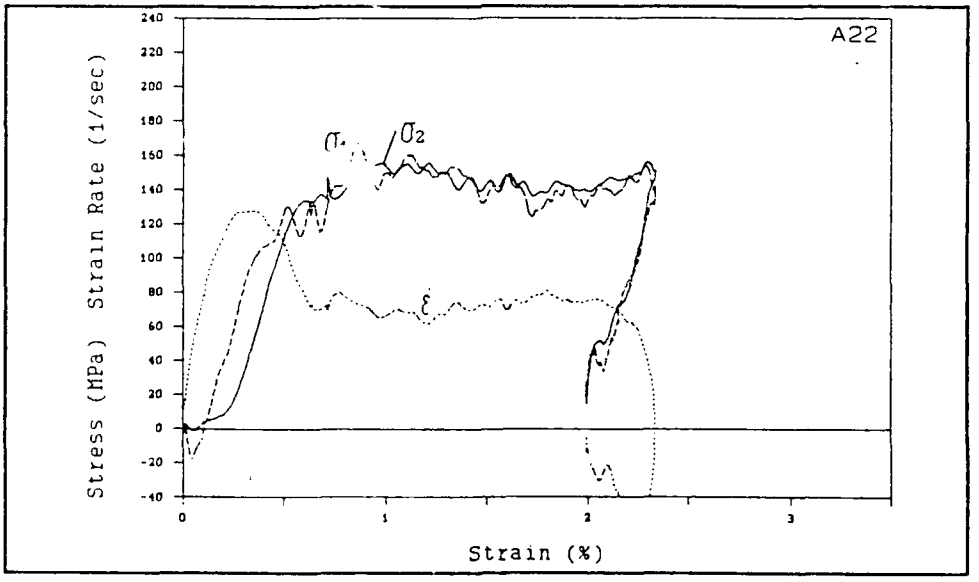

(b) Stress-Strain Curves and Strain Rate Versus Strain.

Figure A-19. Test of Specimen A22 with Initial Confining Pressure 4.73 MPa and Impact Speed 509 in/s (12.93 m/s).

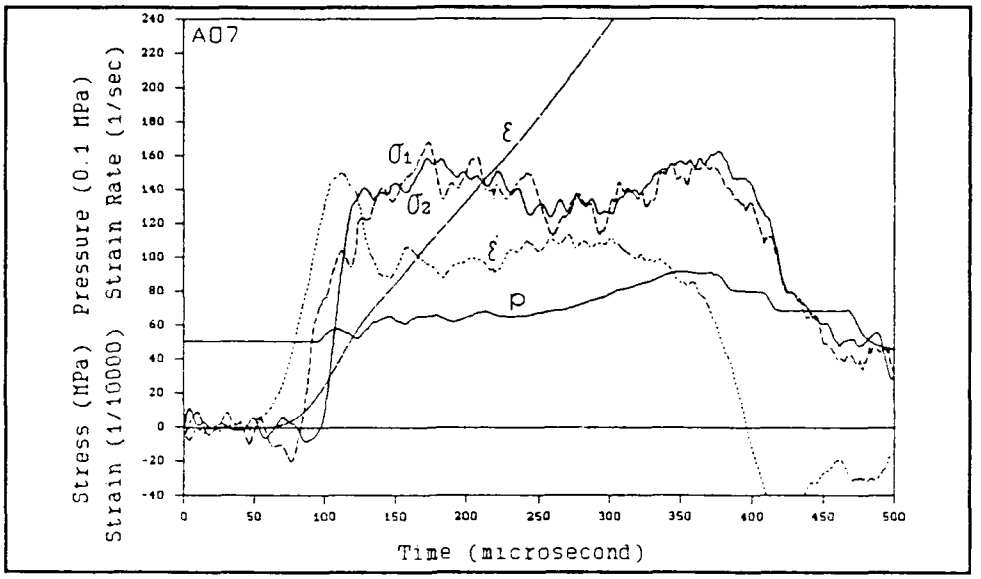

(a) Time Plots of Two Interface Stresses, Strain and Strain Rate.

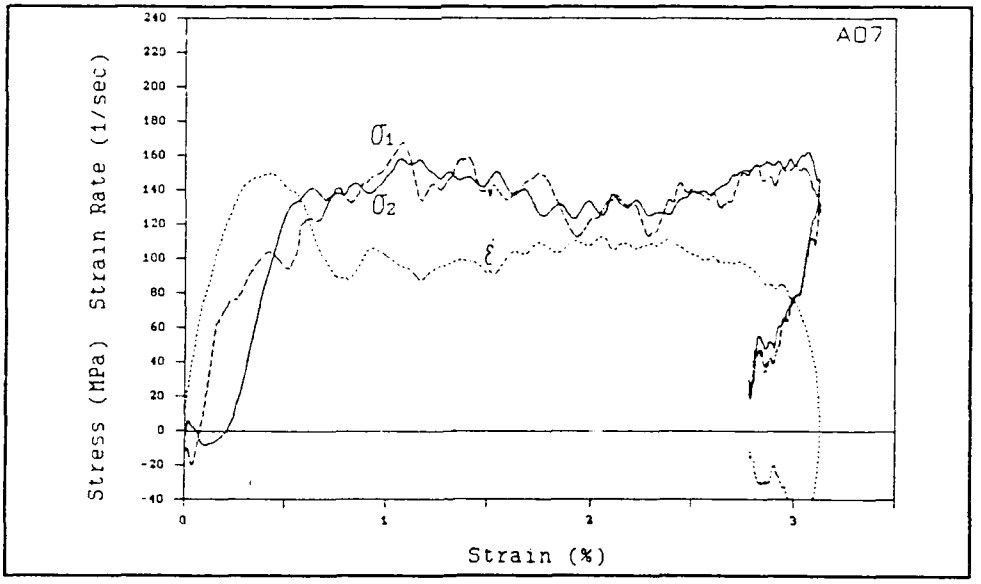

(b) Stress-Strain Curves and Strain Rate Versus Strain.

Figure A-20. Test of Specimen A07 with Initial Confining Pressure 5.03 MPa and Impact Speed 583 in/s (14.81 m/s).

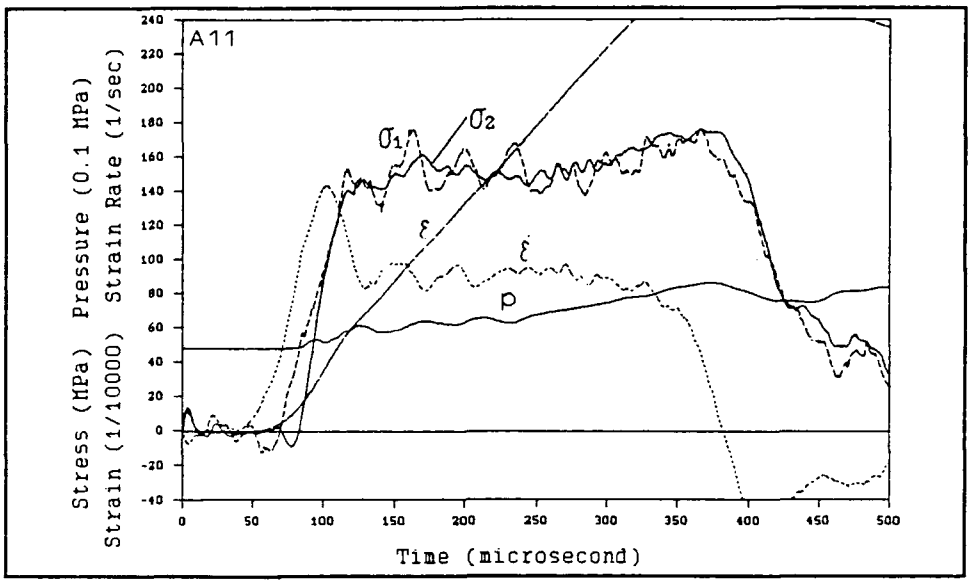

(a) Time Plots of Two Interface Stresses, Strain and Strain Rate.

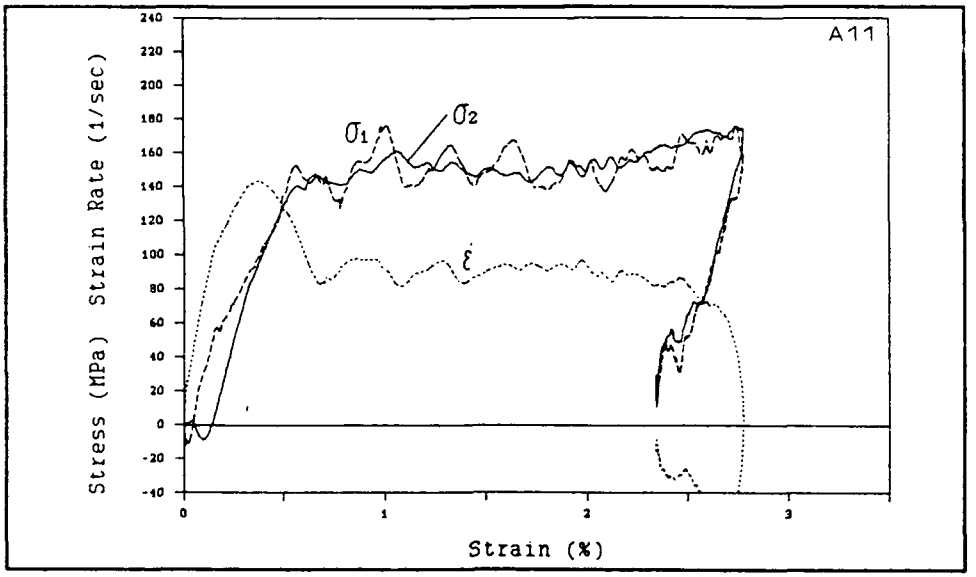

(b) Stress-Strain Curves and Strain Rate Versus Strain.

Figure A-21. Test of Specimen A11 with Initial Confining Pressure 4.81 MPa and Impact Speed 581 in/s (14.76 m/s).

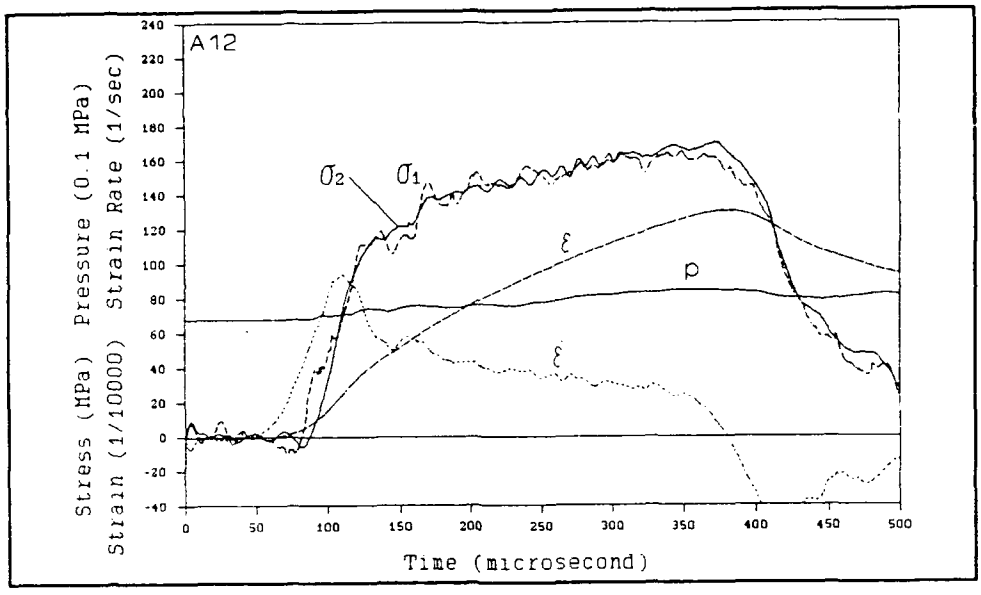

(a) Time Plots of Two Interface Stresses, Strain and Strain Rate.

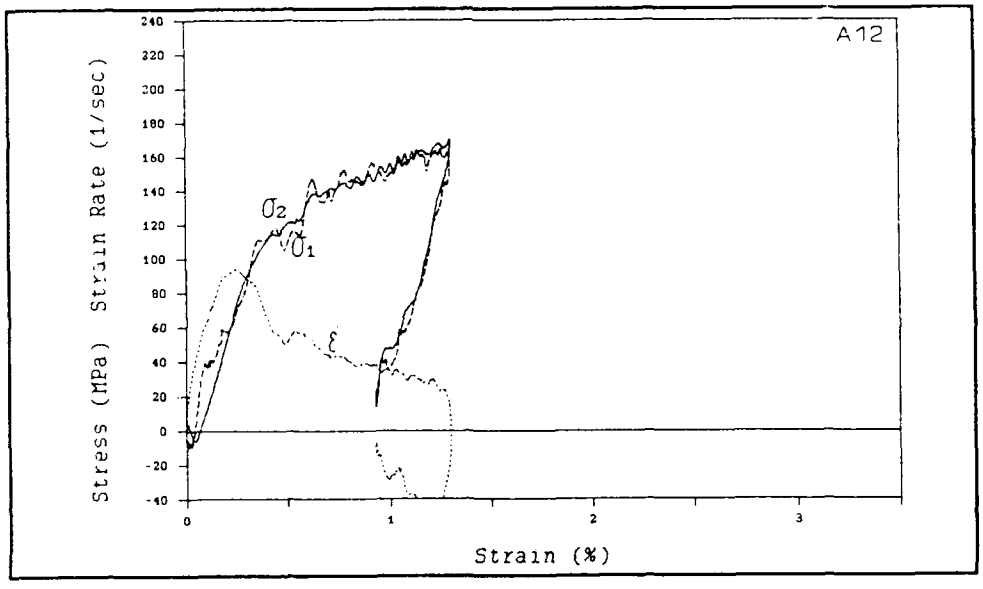

(b) Stress-Strain Curves and Strain Rate Versus Strain.

Figure A-22. Test of Specimen A12 with Initial Confining Pressure 6.81 MPa and Impact Speed 409 in/s (10.39 m/s).

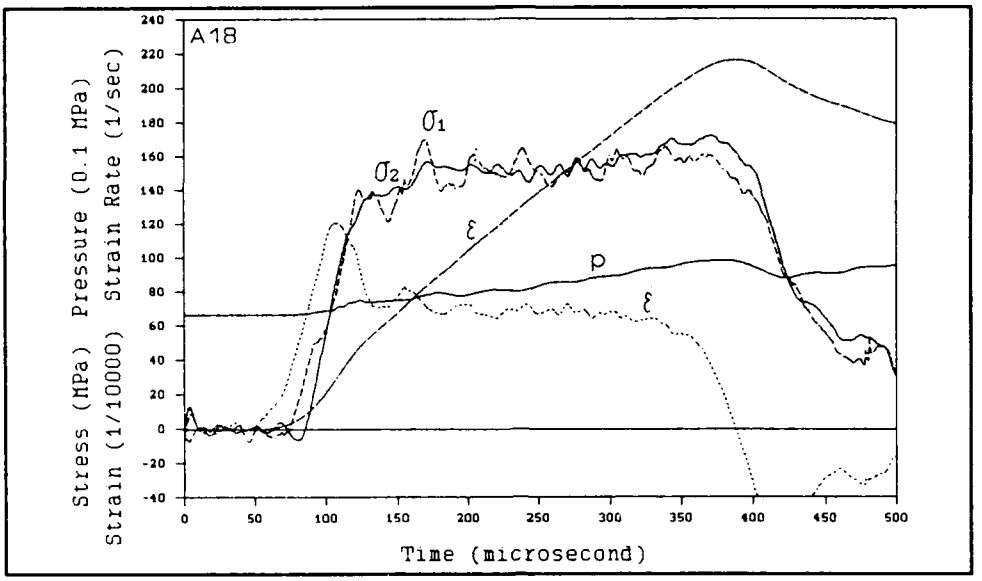

(a) Time Plots of Two Interface Stresses, Strain and Strain Rate.

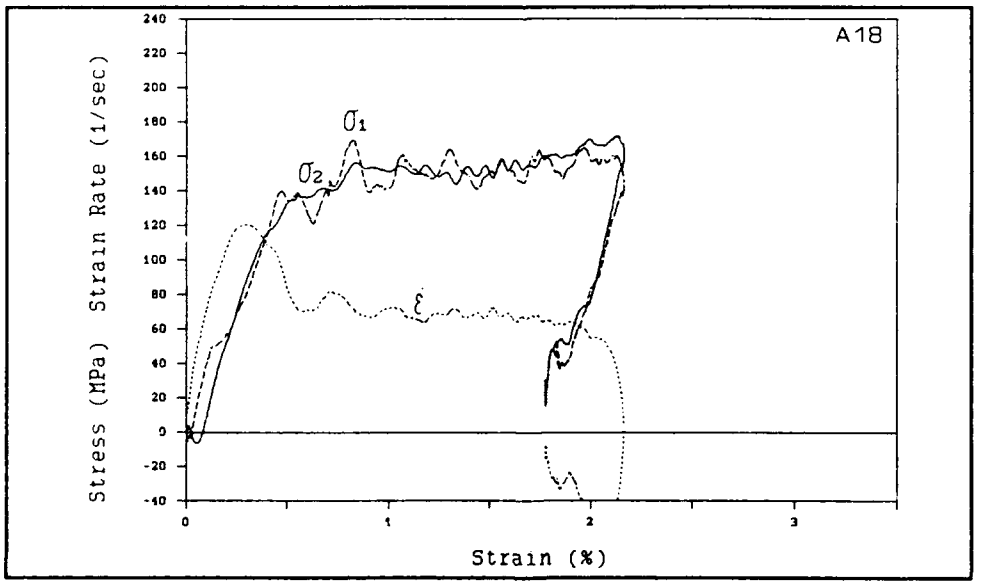

(b) Stress-Strain Curves and Strain Rate Versus Strain.

Figure A-23. Test of Specimen A18 with Initial Confining Pressure 6.64 MPa and Impact Speed 501 in/s (12.73 m/s).

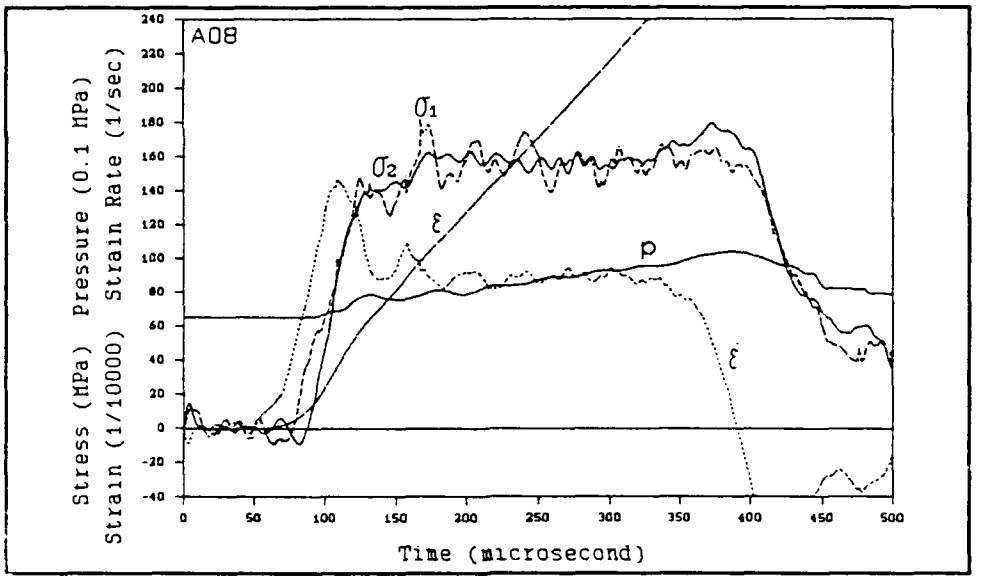

(a) Time Plots of Two Interface Stresses, Strain and Strain Rate.

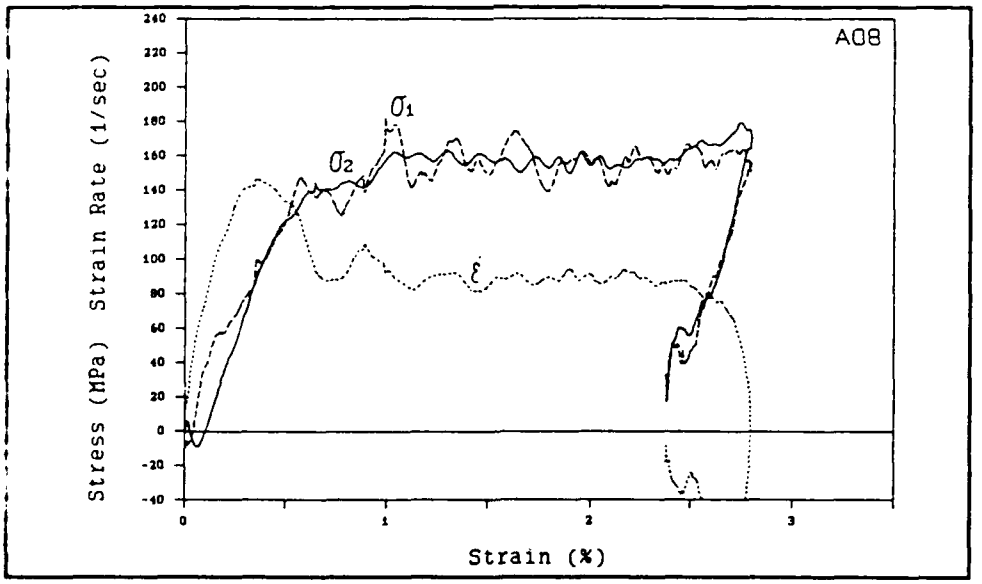

(b) Stress-Strain Curves and Strain Rate Versus Strain.

Figure A-24. Test of Specimen A08 with Initial Confining Pressure 6.52 MPa and Impact Speed 575 in/s (14.60 m/s).

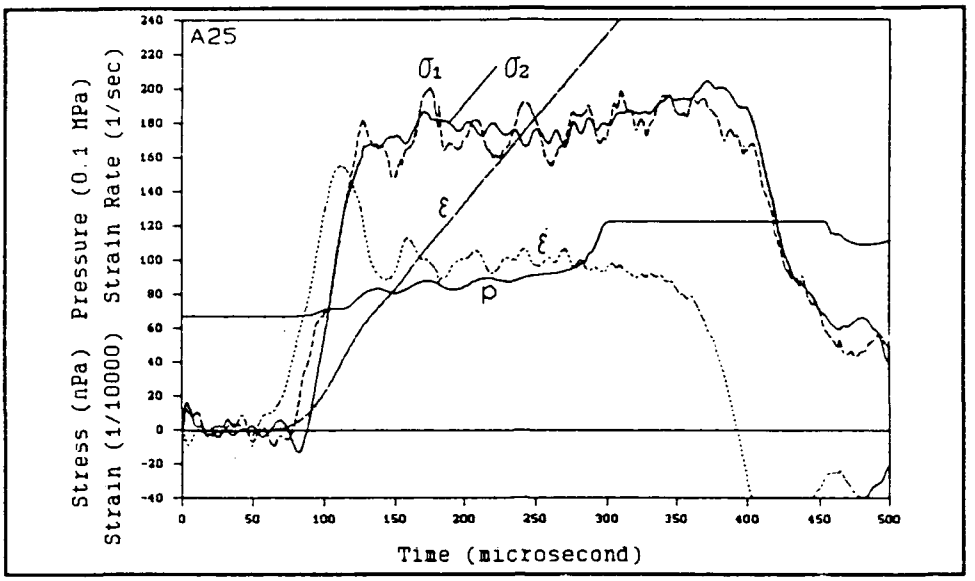

(a) Time Plots of Two Interface Stresses, Strain and Strain Rate.

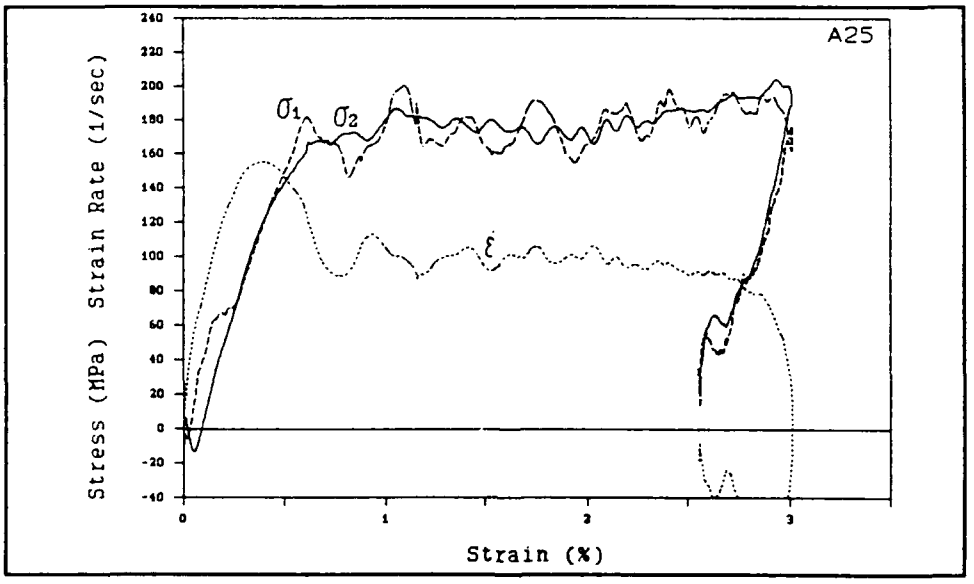

(b) Stress-Strain Curves and Strain Rate Versus Strain.

Figure A-25. Test of Specimen A25 with Initial Confining Pressure 6.72 MPa and Impact Speed 648 in/s (16.46 m/s).

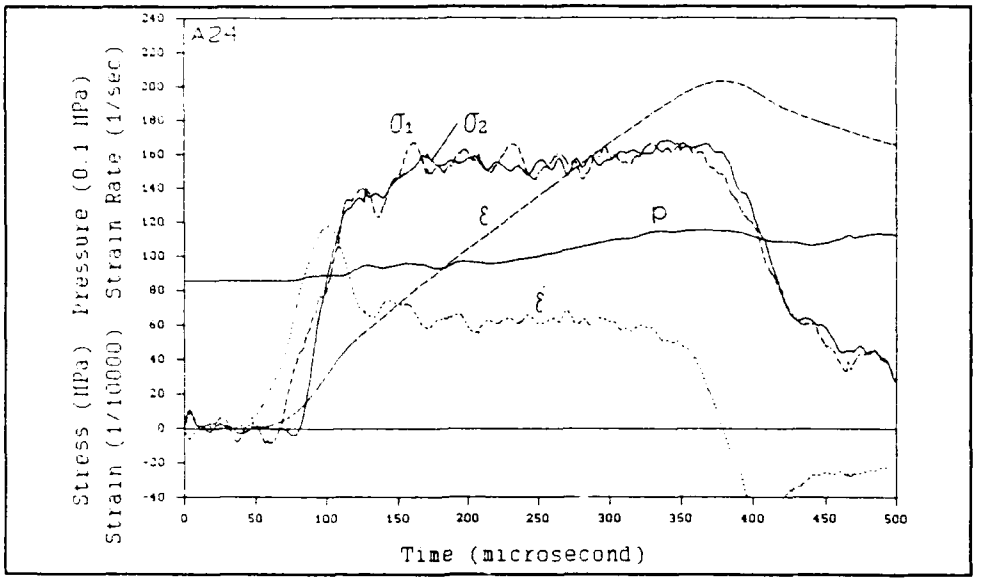

(a) Time Plots of Two Interface Stresses, Strain and Strain Rate.

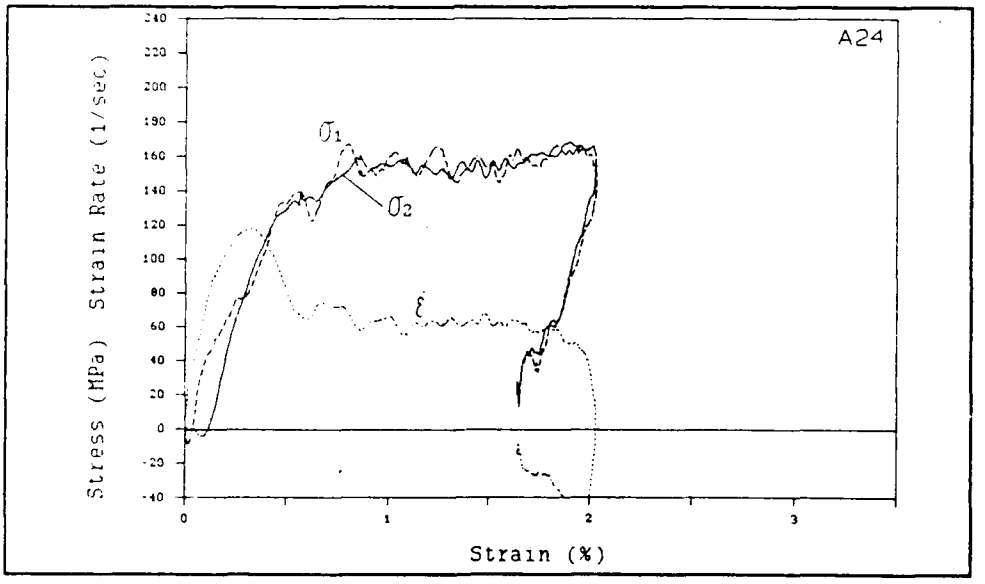

(b) Stress-Strain Curves and Strain Rate Versus Strain.

Figure A-26. Test of Specimen A24 with Initial Confining Pressure 8.55 MPa and Impact Speed 495 in/s (12.57 m/s).

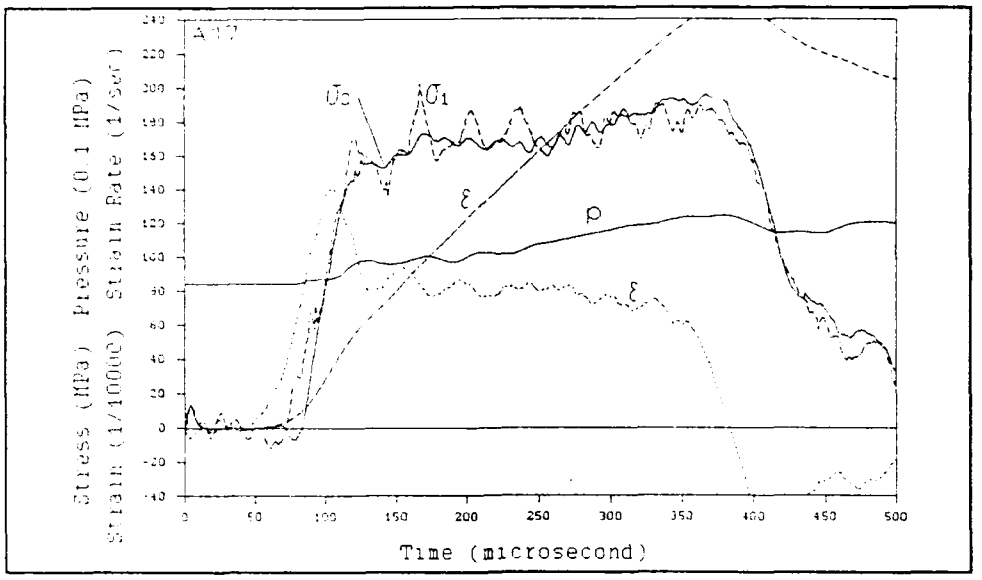

(a) Time Plots of Two Interface Stresses, Strain and Strain Rate.

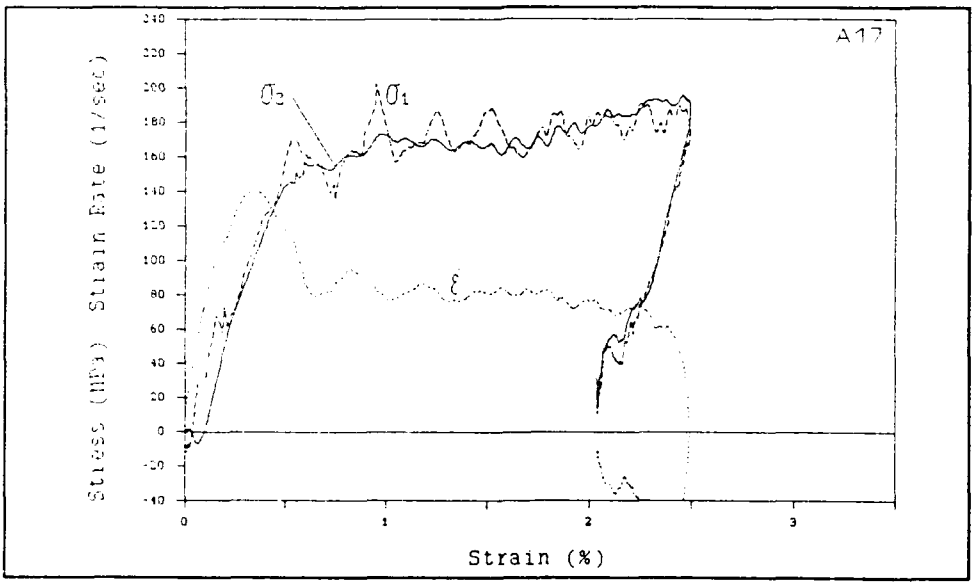

(b) Stress-Strain Curves and Strain Rate Versus Strain.

Figure A-27. Test of Specimen A17 with Initial Confining Pressure 8.41 MPa and Impact Speed 583 in/s (14.81 m/s).

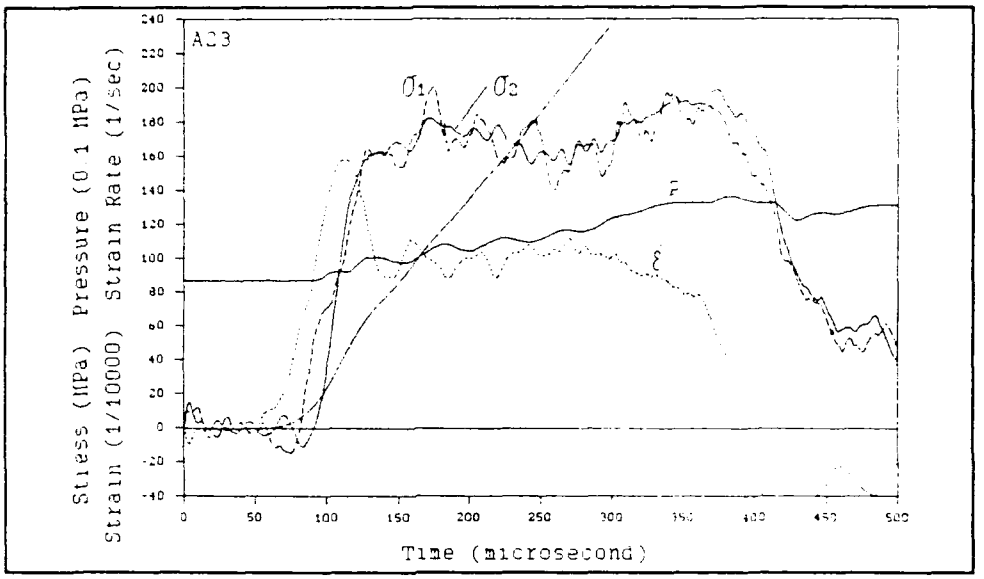

(a) Time Plots of Two Interface Stresses, Strain and Strain Rate.

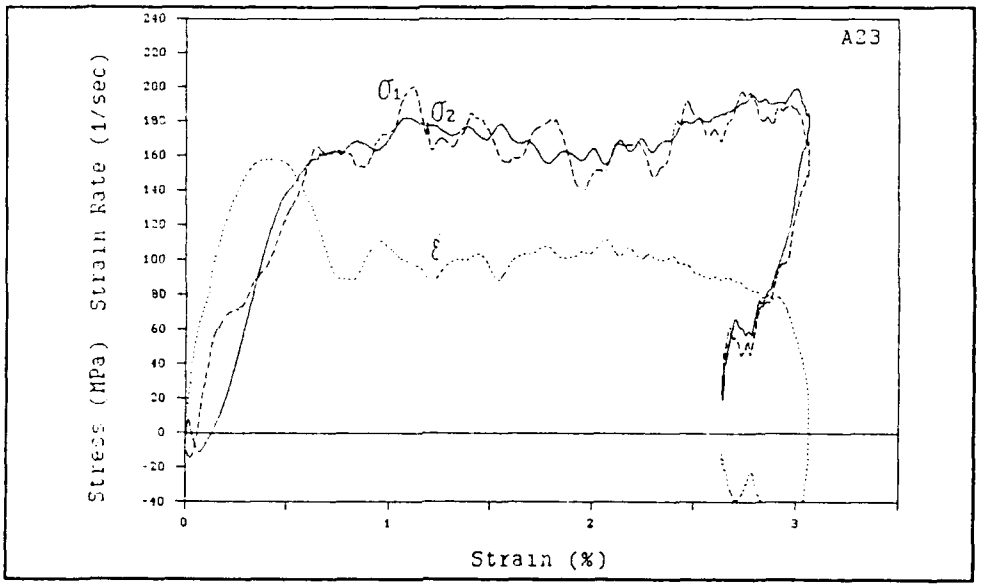

(b) Stress-Strain Curves and Strain Rate Versus Strain.

Figure A-28. Test of Specimen A23 with Initial Confining Pressure 8.69 MPa and Impact Speed 641 in/s (16.28 m/s).

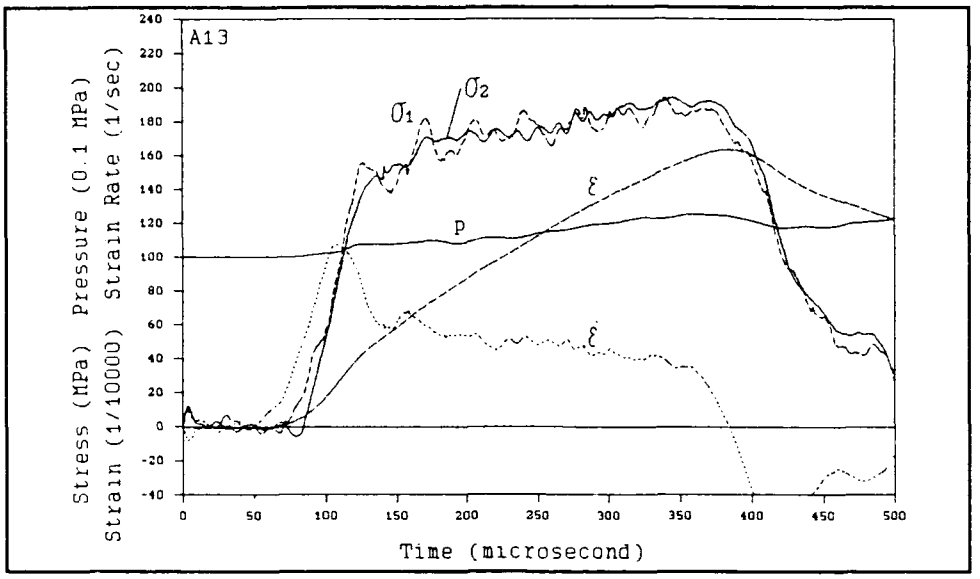

(a) Time Plots of Two Interface Stresses, Strain and Strain Rate.

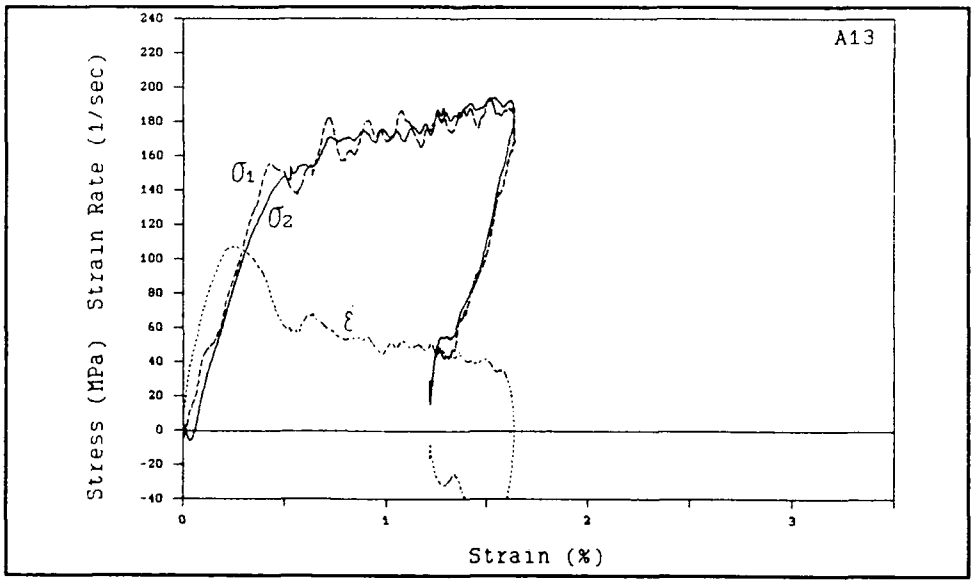

(b) Stress-Strain Curves and Strain Rate Versus Strain.

Figure A-29. Test of Specimen A13 with Initial Confining Pressure 10.0 MPa and Impact Speed 497 in/s (12.62 m/s).

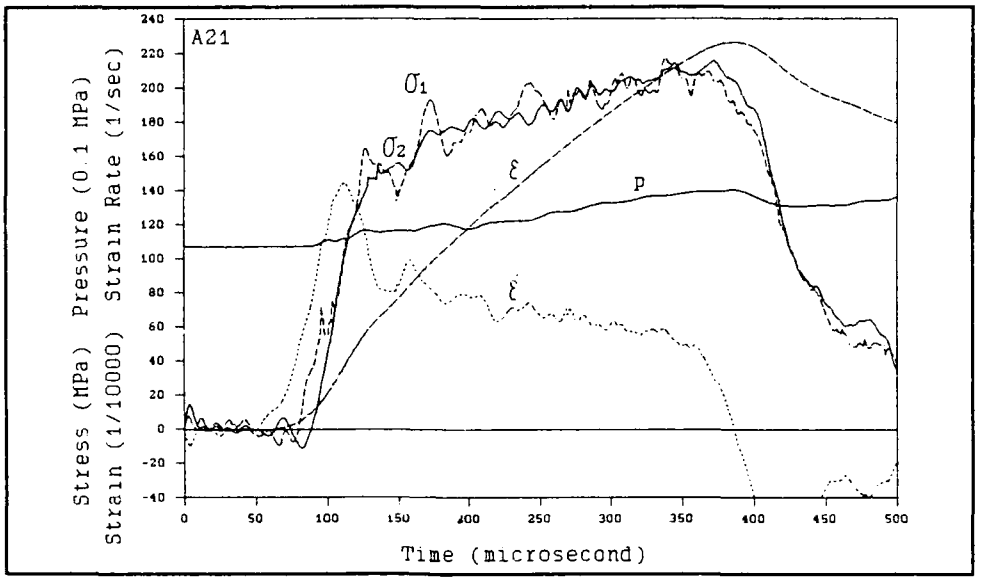

(a) Time Plots of Two Interface Stresses, Strain and Strain Rate.

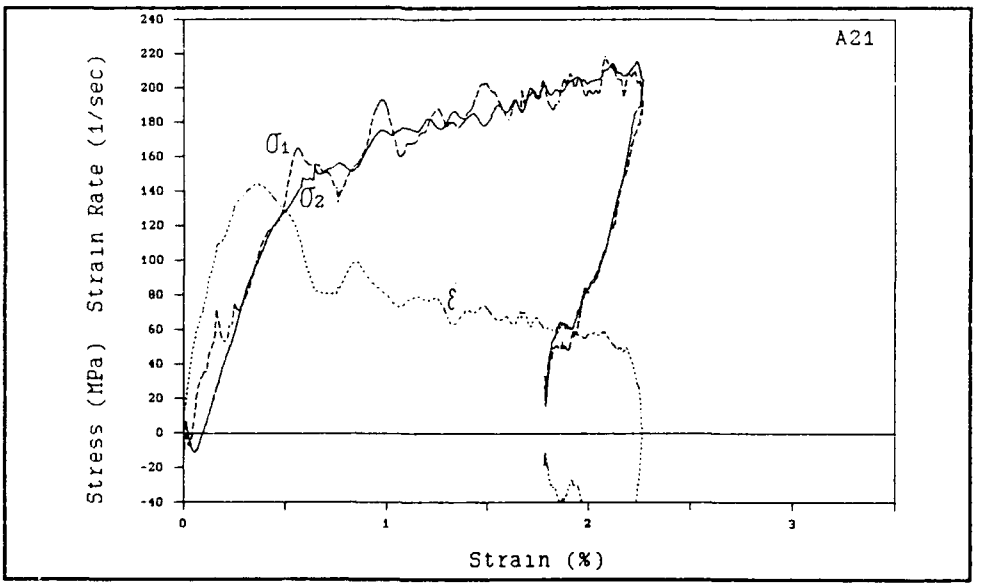

(b) Stress-Strain Curves and Strain Rate Versus Strain.

Figure A-30: Test of Specimen A21 with Initial Confining Pressure 10.7 MPa and Impact Speed 582 in/s (14.78 m/s).

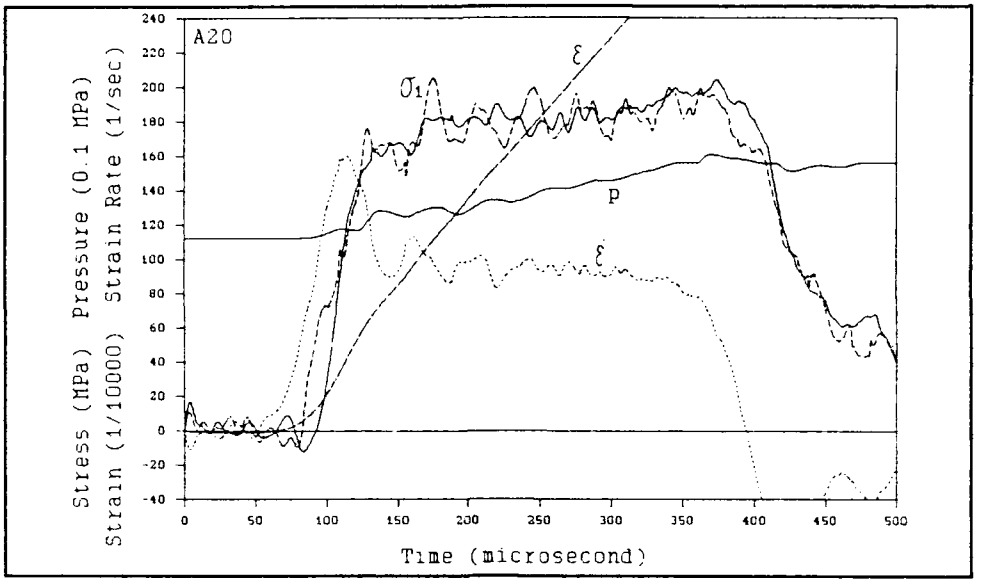

(a) Time Plots of Two Interface Stresses, Strain and Strain Rate.

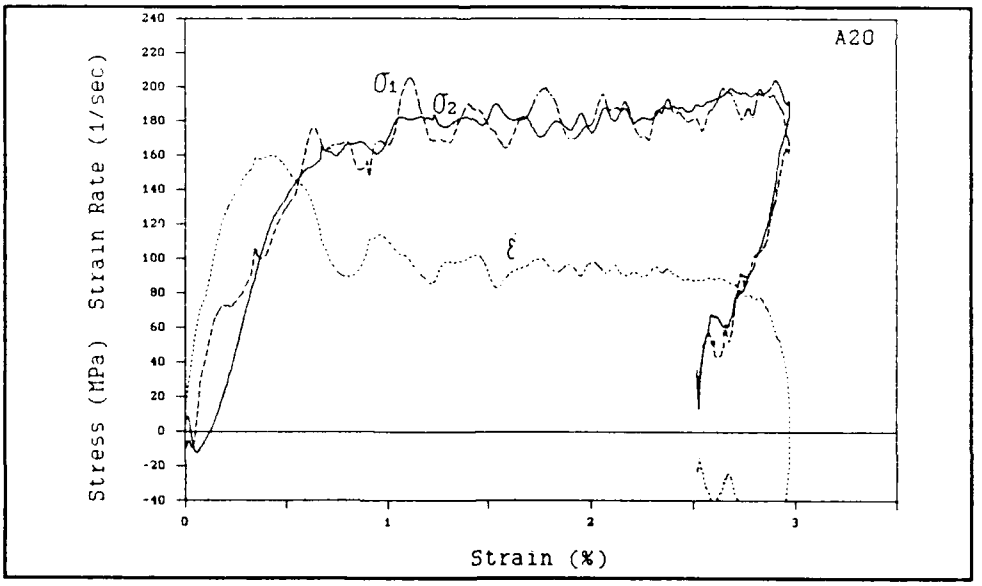

(b) Stress-Strain Curves and Strain Rate Versus Strain.

Figure A-31. Test of Specimen A20 with Initial Confining Pressure 11.2 MPa and Impact Speed 640 in/s (16.26 m/s).

TABLE A-1. CONFINED TEST OF GROUP 1 - Nominal Confining Pressure 500 psi (3.45 MPa)
Static Axial Preload 500 lb (2.22 kN)

Figure No.	Impact Speed (in/s)/ (m/s)	Lateral Pressure Start/End (MPa)	First Peak or Plateau			End of Loading		Damage Description
			Stress (MPa)	Strain Rate (s^{-1})	Strain per cent	Stress (MPa)	Strain Per Cent	
A-11	376/ 9.55	3.35/4.0	116	50	0.58	112	1.57	Short Cracks
A-12	420/ 10.66	3.32/4.0	124	59	0.65	116	1.94	Diagonal Crack not separated
A-13	503/ 12.78	3.32/4.4	144	92	1.09	150	2.80	Diagonal Crack separated
A-14	514/ 13.06	3.36/5.4	134	89	0.95	123	2.71	Diagonal Crack separated
A-15	582/ 14.78	3.26/5.9	147	100	1.23	150	3.27	Rubble

TABLE A-2. CONFINED TEST OF GROUP 2 - Nominal Confining Pressure 750 psi (5.17 MPa)
Static Axial Preload 500 lb (2.22 kN)

Figure No.	Impact Speed (in/s)/ (m/s)	Lateral Pressure Start/End (MPa)	First Peak or Plateau			End of Loading		Damage Description
			Stress (MPa)	Strain Rate (s^{-1})	Strain per cent	Stress (MPa)	Strain Per Cent	
A-16	384/ 9.75	5.34/6.4	130	40	0.55	132	1.38	Short Cracks
A-17	417/ 10.59	5.19/7.1	135	50	0.62	136	1.62	Long Cracks
A-18	501/ 12.73	5.23/7.8	139	76	0.83	141	2.75	Diagonal Crack not separated
A-19	509/ 12.93	4.73/7.7	153	68	0.97	151	2.74	Diagonal Crack not separated
A-20	583/ 14.81	5.03/9.0	155	95	1.07	151	3.06	Diagonal Crack separated
A-21	581/ 14.76	4.81/8.6	155	89	1.07	174	2.77	3 Large Pieces, many smaller fragments

TABLE A-3. CONFINED TEST OF GROUP 3 - Nominal Confining Pressure 1000 psi (6.90 MPa)
Static Axial Preload 500 lb (2.22 kN)

Figure No	Impact Speed (in/s)/ (m/s)	Lateral Pressure Start/End (MPa)	First Peak or Plateau Stress (MPa)	First Peak or Plateau Strain Rate (s^{-1})	First Peak or Plateau Strain per cent	End of Loading Stress (MPa)	End of Loading Strain Per Cent	Damage Description
A-22	409/ 10.39	6.81/8.4	No First Peak or Plateau			170	1.30	Long Cracks
A-23	501/ 12.73	6.64/9.7	158	86	0.86	170	2.24	Diagonal Crack not separated
A-24	575/ 14.60	6.52/10.3	153	71	1.03	162	2.75	Diagonal Crack not separated
A-25	648/ 16.46	6.72/—*	171	100	1.05	193	2.98	Diagonal Crack separated

* No record

TABLE A-4. CONFINED TEST OF GROUP 4 - Nominal Confining Pressure 1250 psi (8.62 MPa)
Static Axial Preload 600 lb (2.22 kN)

Figure No.	Impact Speed (in/s)/ (m/s)	Lateral Pressure Start/End (MPa)	First Peak or Plateau Stress (MPa)	First Peak or Plateau Strain Rate (s^{-1})	First Peak or Plateau Strain per cent	End of Loading Stress (MPa)	End of Loading Strain Per Cent	Damage Description
A-26	495/ 12.57	8.55/11.5	155	63	0.86	165	2.04	Diagonal Crack not separated
A-27	583/ 14.81	8.41/12.3	168	79	0.98	193	2.48	Diagonal Crack not separated
A-28	641/ 16.28	8.69/13.4	179	100	1.07	199	3.03	Diagonal Crack separated

TABLE A-5. CONFINED TEST OF GROUP 5 - Nominal Confining Pressure 1500 psi (10.34 MPa)
Static Axial Preload 600 lb (2.22 kN)

Figure No.	Impact Speed (in/s)/ (m/s)	Lateral Pressure Start/End (MPa)	First Peak or Plateau Stress (MPa)	First Peak or Plateau Strain Rate (s^{-1})	First Peak or Plateau Strain per cent	End of Loading Stress (MPa)	End of Loading Strain Per Cent	Damage Description
A-29	497/ 12.62	10.0/12.4	No First Peak or Plateau			192	1.63	Diagonal Crack not separated
A-30	582/ 14.78	10.7/13.9	176	76	0.97	214	2.26	Diagonal Crack not separated
A-31	640/ 16.6	11.2/16.1	179	96	1.06	195	2.96	Diagonal Crack separated

(The reverse of this page is blank.)